UCLouvain
University

Liver radioembolization : from dosimetry to clinical effects

Philippe d'Abadie, MD

Thesis submitted in fulfilment of the requirements for the degree of « docteur en sciences médicales » from UCLouvain

Promotor :	Prof. François Jamar Nuclear medicine department Cliniques universitaires Saint Luc, Université Catholique de Louvain
Co- promoter :	Prof. Renaud Lhommel Nuclear medicine department Cliniques universitaires Saint Luc, Université Catholique de Louvain
President of the Jury :	Prof. Isabelle Leclercq Institut de recherche expérimentale et clinique Pôle d'hépato-gastro-entérologie Université Catholique de Louvain
Secretary of the Jury :	Prof. Ivan Borbath Digestive oncology department Cliniques universitaires Saint Luc, Université Catholique de Louvain
Internal members :	Prof. Laurence Annet Radiology department Cliniques universitaires Saint Luc, Université Catholique de Louvain
	Doctor phys. Stephan Walrand Nuclear medicine department Cliniques universitaires Saint Luc, Université Catholique de Louvain
Invited members :	Prof. Etienne Garin Nuclear medicine department Cancer Institute Eugène Marquis, Rennes
	Prof. Chirstophe Deroose Nuclear medicine department University hospital Leuven

Remerciements- Acknowledgements

Cette thèse est le fruit d'une longue démarche scientifique et académique qui n'a été possible que grâce au soutien de nombreuses personnes à qui j'adresse ici mes sincères remerciements.

Mes premières pensées vont à mon promoteur, le professeur François Jamar, qui a été un mentor durant toutes ces années dans mon apprentissage de la recherche clinique. Il a été particulièrement attentif à la réussite de cette thèse, m'a fait partager sa rigueur scientifique, son sens critique et son savoir faire dans l'écriture d'un article scientifique. Son aide a aussi été déterminante dans l'élaboration du projet de recherche, dans le soutien logistique et administratif. Je lui adresse ma profonde gratitude.

Je remercie également le professeur Renaud Lhommel qui a initié le programme de radioembolisation et m'a fait confiance dès mes débuts dans le service pour réaliser les radioembolisations hépatiques et pour lancer les premiers travaux de recherche. Je le remercie également en sa qualité de chef de service de m'avoir accordé du temps protégé et d'avoir permis l'achat de logiciels performants d'analyse qui ont été indispensables à la réussite de cette thèse.

Ce travail n'aurait pas eu la même saveur sans le concours savant du docteur en physique Stephan Walrand. Il m'a aidé à analyser et interpréter les données avec beaucoup de clairvoyance, d'efficacité et d'originalité. Je lui suis très reconnaissant pour tout le savoir qu'il m'a fait partager durant ces années et de m'avoir communiqué sa logique scientifique et son esprit critique.

Mon intérêt pour la médecine nucléaire et pour la recherche clinique n'auraient certainement pas vu le jour si je n'avais pas rencontré le professeur Stanislas Pauwels. A mes débuts, le professeur Pauwels m'a appris les rouages du métier et m'a initié au raisonnement scientifique. Je lui rends ici un hommage sincère, moins d'un an après son décès.

Je remercie également mes autres collègues du service de médecine nucléaire pour leur soutien intellectuel et amical, en autres, le docteur en physique Michel Hesse et le Professeur Olivier Gheysens.

J'adresse ma profonde reconnaissance aux membres du jury. Je remercie particulièrement la présidente du jury, la professeure Isabelle Leclercq, qui m'a accompagné avec beaucoup de bienveillance durant ces années. Je remercie les professeurs Etienne Garin et Christophe Deroose de m'avoir fait l'immense honneur de leur présence. Je remercie les autres membres du jury interne pour leur soutien, la professeure Laurence Annet et le professeur Ivan Borbath.

J'adresse mon profond respect et ma gratitude aux autorités des Cliniques universitaires saint Luc et de l'université qui ont validé et financé ce doctorat. Je remercie particulièrement les membres de la commission du Fond de Recherche clinique des Cliniques universitaires Saint-Luc et les membres de la commission doctorale.

Enfin, permettez moi de remercier ma chère épouse, Alix, qui m'a soutenu durant toutes ces années. Elle a été particulièrement attentive à la réussite de ce doctorat, surtout dans les premières années.

Résumé

La radio-embolisation hépatique fait partie de l'arsenal thérapeutique des tumeurs hépatiques. Elle peut être utilisée avec des microsphères radioactives à base de verre ou de résine, qui diffèrent par leurs propriétés physico-chimiques et radioactives (1). Une imagerie post thérapeutique PET/CT ^{90}Y peut évaluer la dose à la tumeur et prédire le pronostic du patient (2, 3). Le PET/CT ^{90}Y peut aussi évaluer précisément la distribution hétérogène de la dose aux tumeurs en calculant un équivalent de dose uniforme (EDU) (4). L'EDU est fortement corrélé à la survie des patients et réunifie les niveaux de doses des microsphères en résine et en verre mais aussi avec ceux connus pour la radiothérapie externe (5, 6).

De plus, une imagerie pré-thérapeutique aux macro-agrégats d'albumine marqués (MAA) peut optimiser la planification de l'activité, en prédisant avec précision la dose au foie sain (7).

Par ailleurs, le ciblage tumoral peut être optimisé durant l'artériographie, en utilisant un cathéter spécifique appelé cathéter antireflux (8). Il permet d'augmenter de façon significative la dose absorbée à la tumeur, augmentant ainsi la probabilité de contrôle tumoral.

Abstract

Selective internal radiation therapy (SIRT) is part of the treatment strategy of liver tumors. SIRT can be performed using resin or glass microspheres, demonstrating different chemico-physical and radioactive properties (1). Post therapy imaging using ^{90}Y PET/CT can evaluate the deposition of the tumor-absorbed dose and predict the patient outcome (2, 3). ^{90}Y PET/CT can also precisely evaluate the heterogeneous distribution of the absorbed dose within the tumor by calculating a equivalent uniform dose (EUD) (4). Tumor EUD is strongly correlated with survival of patients and reunifies the absorbed doses between resin and glass microspheres as well as those from external radiation beam therapy (5, 6).

Moreover, pre-therapy imaging using ^{99m}Tc macroaggregated albumin (MAA) can optimize the activity planning, predicting with high accuracy the absorbed dose to the healthy liver (7).

Furthermore, the tumor targeting can be optimized using a specific catheter during the arteriography, named antireflux catheter (ARC) (8). Using ARC, the absorbed dose can be significantly increased in neuroendocrine and HCC tumors, hence, increasing the tumor control probability.

Biographie

1- d'Abadie P, Hesse M, Louppe A, Lhommel R, Walrand S, Jamar F. Microspheres used in liver radioembolization: from conception to clinical effects. Molecules 2021; 26: 3966
2- d'Abadie P, Walrand S, Hesse M, Annet L, Borbath I, Van den Eynde M, Lhommel R, Jamar F. Prediction of tumor response and patient outcome after radioembolization of hepatocellular carcinoma using 90Y-PET- computed tomography dosimetry. Nuclear Medicine Communications 2021; 42 747-754
3- d'Abadie P, Walrand S, Lhommel R, Hesse M, Borbath I., Jamar F. Optimization of the clinical effectiveness of radioembolization in hepatocellular carcinoma with dosimetry and patient-selection criteria.
4- Hesse M, d'Abadie P, Lhommel R, Jamar F, Walrand S. Yttrium-90 TOF-PET-Based EUD Predicts Response Post Liver Radioembolizations Using Recommended Manufacturer FDG Reconstruction Parameters. Frontiers in onology 2021; 11: 592529
5- d'Abadie P, Hesse M, Jamar F, Lhommel R, Walrand S. 90Y TOF-PET based EUD reunifies patient survival prediction in resin and glass microspheres radioembolization of HCC tumours. Physics in Medicine and Biology. 2018; 63: 245010
6- d'Abadie P, Walrand S, Hesse M, Borbath I, Lhommel R, Jamar F. EUD based ^{90}Y-TOF-PET post selective internal radionuclide therapy provides a similar TCP in HCC than observed in EBRT. Submitted.
7- d'Abadie P, Walrand S, Hesse M, Amini N, Lhommel R, Sawadogo K, Jamar F. Accurate non-tumoral 99mTc-MAA absorbed dose prediction to plan optimized activities in liver radioembolization using resin microspheres. Physica Medica. 2021; 89: 250-257
8- d'Abadie P, Walrand S, Goffette P, Amini N, van Maanen A, Lhommel R, Jamar F. Antireflux catheter improves tumor targeting in liver radioembolization with resin microspheres. Diagnostic and interventional radiology. 2021; 27: 768-773

Table of contents

List of abreviations **1**

1. Introduction **3**
1.1 Treatment planning 6
1.2 Physical and radionuclide properties of microspheres 12
1.3 Effects of microspheres at a voxel level: microdosimetry 13
1.4 Clinical applications 18
1.5 Effects of microspheres at a macroscopic level: clinical effects 22

2. Aims of the thesis **39**

3. Post therapy imaging using yttrium-90 PET-CT: prediction of tumor response and patient outcome **41**
3.1 Introduction 42
3.2 Material and methods 43
3.3 Results 48
3.4 Discussion 56

4. Post therapy imaging using yttrium-90 PET-CT: assessment of the microsphere distribution at a voxel level **65**
4.1 Introduction 66
4.2 Material and methods 66
4.3 Results 71
4.4 Discussion 74

5. EUD based ^{90}Y-TOF-PET post selective internal radionuclide therapy provides a similar TCP in HCC than observed in EBRT **85**
5.1 Introduction 86
5.2 Material and methods 87
5.3 Results 92
5.4 Discussion 94

6. ^{99m}Tc-MAA imaging to optimize the dose planning in radioembolization **103**
6.1 Introduction 104
6.2 Material and methods 105
6.3 Results 112
6.4 Discussion 124

7. Liver arteriography using an antireflux catheter : which impact on microsphere distribution ? **139**
7.1 Introduction 140
7.2 Material and methods 142
7.3 Results 148
7.4 Discussion 154

8. Perspectives **163**
8.1 Personalized dosimetry in SIRT: activity planning optimization with MAA SPECT/CT 163
8.2 Personalized dosimetry in SIRT: activity planning optimization with a scout dose 169
8.3 Optimization of tumor targeting 172
8.4 Patient selection: good candidates for SIRT 174

9. Summary and practical applications **185**

List of abbreviations

^{18} F : fluor-18
^{166}Ho : holmium-166
^{131}I : iodine-131
^{188}Re: rhenium-188
^{99m}Tc : technetium-99m
^{90}Y : yttrium 90
A : activity
ARC : antireflux catheter
BED : biologic effective dose
BSA : body surface area
C : counts
D : absorbed dose
DVH : dose -volume histogram
EHC : end-hole catheter
Equ. : equation
EUD : equivalent uniform dose
EBRT : external beam radiation therapy
f: fractional uptake
FDG: fluoro,2-deoxy glucose
FU: Follow-up
GBq : gigabecquerel
Gy : gray
HAI : hepatic arterial infusion
IQR : interquartile range
LSF : lung shunt fraction
M : mass
MAA : macro-aggregated albumin
MBq : megabecquerel
MC : Monte Carlo
MIRD : Medical Internal Radiation Dose
m RECIST : modified response evaluation criteria in solid tumors
NPP : negative predictive value
OS : overall survival
PFS : progression free survival
PLLA : poly-L-lactic acid
PPV : positive predictive value
RE : radioembolization
REILD : radioembolization induced liver disease
ROC : receiver operating characteristic

Se : sensitivity
Sp : specificity
SIRT : selective internal radiation therapy
SPECT/CT : single-photon emission computed tomography/computed tomography
TACE : transarterial chemoembolization
TCP : tumor control probability
TD : tumor dose
TLG : total lesion glycolysis
TLM : Total lesion metabolism
TOF : time of flight
T/NL : tumor to normal liver ratio
T/NTL : tumor to normal targeted liver uptake ratio
ICC : Intrahepatic cholangiocarcinoma
V : volume
VOI : volume of interest
WNLD : whole normal liver dose

1. Introduction [1]

Liver radioembolization (RE) or Selective Internal radiation therapy (SIRT) is commonly used for the treatment of hepatocellular carcinoma and secondary liver malignancies. This treatment is performed by injection of radioactive microspheres in the liver artery after transarterial catheterization. This catheterization could be more and less selective depending on the tumor localization(s)(Figure 1). Radioactive microspheres are trapped in the microvasculature (arterioles) of tumors and of the targeted liver parenchyma. Unlike the liver parenchyma which blood supply is mostly obtained by the portal vein, liver tumors are preferentially vascularized by the hepatic arteries. This preferential perfusion allows achieving a good tumor targeting of hypervascularized tumors with a limited irradiation of the non-tumoral liver (1). The objective is to deliver the highest dose to the tumor and the lowest to the normal targeted liver. The technique was initially developed using iodine-131 (^{131}I) Lipiodol, a radiolabeled ethiodized oil (2). After arterial administration, a large part of ^{131}I lipiodol stays in the liver (75%) and the remainder reaches the lungs (3). Due to the preferential liver arterial perfusion, liver tumors such as HCC demonstrated a preferential uptake compared to the healthy liver, ensuring a high irradiation of tumors and resulting in good clinical results (4). However, this

[1] Adapted from d'Abadie et al. Molecules, 2021 26, 3966

therapy suffers from several limitations. First, there are therapy radiation protection concerns due to the characteristics of ^{131}I. This radionuclide has a long half-life (8.04 days) and emits 1% of gamma radiation of high energy (0.364 MeV) (5). With a fixed injected activity of 2.2 GBq, the patient will stay in isolation at hospital during one week to limit the radiation exposure of environment (6). Second, due to the lung exposure, rare cases (2%) of serious diffuse infiltrative pneumopathies were reported (7). Thereafter, radiolabeled microspheres have emerged using yttrium-90 (^{90}Y) and holmium-166 (^{166}Ho). These radionuclides emit high energy beta radiations, resulting in high absorbed doses to tumors (in the range of 100 to 1000 Gy) (8). In comparison, the total dose to tumors is limited to a maximum of 70 Gy in external beam radiotherapy to avoid irreversible liver damage (9).

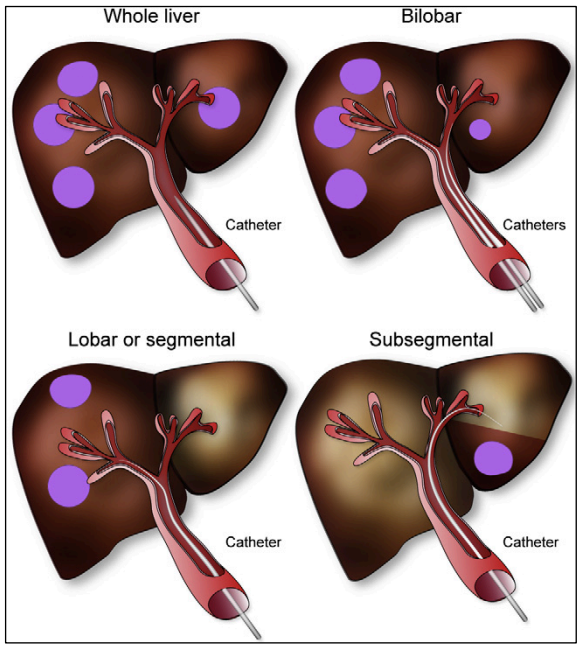

Figure 1: Liver microsphere distribution in liver radioembolisation is dependent on the arterial catheter position. Tumors are shown in purple and targeted liver in dark brown (adapted from Sangro et al. (10)).

Three types of microspheres are commercially available: ^{90}Y-resin microspheres (Sir-Spheres®, Sirtex Medical Ltd., Sydney, Australia), ^{90}Y-glass microspheres (Therasphere®, Boston Scientific, Boston, MA) and ^{166}Ho-poly-L-lactic acid (PLLA) microspheres (QuiremSpheres®, Quirem Medical B.V., Deventer, The Netherlands). SIR-Spheres®, TheraSphere® and QuiremSpheres® received European regulatory approval (CE mark) as Active Implantable Medical Devices (Council Directive 90/385/EEC) in October 2002, June 2006 and April 2015 respectively.

Other microspheres have been used but did not reach the level of marketing authorization in Europe, e.g., ^{188}Re-microspheres (11).

1.1 Treatment planning

A simulation of the treatment always precedes RE for evaluating its feasibility(12). This first procedure includes an arteriography with an accurate mapping of the liver arterial anatomy and the arterial branches of the tumor(s). Coil embolization(s) of some arterial branches is sometimes performed to avoid the risk of microsphere deposition in the digestive tract during the treatment phase. Finally, a diagnostic radiopharmaceutical agent, technetium-99m macroaggregated albumin (MAA), is injected in the arterial territory of the targeted tumors, simulating the injection of radioactive microspheres. Nuclear imaging with abdominal single photon emission computed tomography combined with X-ray computed tomography (SPECT/CT) follows this arteriography for evaluating the MAA distribution. MAA imaging permits to confirm the good targeting of the tumor(s), rule out extrahepatic abdominal uptake and significant shunting to lungs (calculation of the lung shunt fraction [LSF]): tumor arteriovenous shunts can form pathways for radioactive microspheres into the systemic circulation that are further trapped in the lung capillaries. The treatment is relatively contraindicated if the LSF is higher than 20% or when the lung dose is higher than 30 Gy (13). A significant radiation exposure of the lungs may induce radiation pneumonitis and fibrosis (14).

A specific amount of radioactive microspheres is injected into the liver arteries during the RE procedure and is characterized by the (radioactive) activity. This activity induces a radiation energy deposition in the liver defined by the absorbed dose. Based on the Medical Internal Radiation Dose (MIRD) formalism, the absorbed dose is defined as follows:

$$D\ (Gy) = \frac{A(GBq).k}{M(kg)} \quad (1)$$

With A the activity, M, the irradiated liver mass and k the conversion factor which is 50 J/GBq for ^{90}Y and 16 J/GBq for ^{166}Ho (15-17). The mass is derived from the volume that can be measured by medical imaging, multiplied by a density factor of 1.03 (18).

The absorbed dose represents the energy absorbed from ionizing radiation per unit mass of tissue. This emitted energy per unit mass depends on the quantity of radioactivity (defined by the activity A) and depends also on the properties of the radionuclide and it biodistribution (simplified by the factor k in equation (1)). More precisely, the absorbed dose for a source localized in a single tissue depends on the residence time of the radionuclide in the tissue (defined with the effective half-life) and depends on the properties of the energy deposition (mean energy per radionuclide, distance of energy deposition from the source)(19).

The methods for activity planning, as recommended by the manufacturers differ between the different types of microspheres and are summarized in table 1 (20-22).

Table 1: Usual recommended method for activity planning

Microsphere type	
^{90}Y-Resin $(BSA\ method)^{*}$	$A(GBq) = (BSA - 0.2) + \frac{Volume\ _{tumor}}{Volume_{tumor} + Volume_{normal\ (targeted)\ liver}}$ (BSA: the body surface area in m^2)
^{90}Y-Glass (mono-$compartmental\ method)^{+}$	$A\ (GBq) = \frac{Dose\ _{liver}.Mass_{liver}}{50.(1 - LSF)}$ (Dose $_{(targeted)\ liver}$: 80-150 Gy)
^{166}Ho- PLLA (mono-$compartmental\ method$)	$A(GBq) = \frac{Dose_{liver}.Mass_{liver}}{16}$ (Dose $_{liver:}$ 60 Gy maximum$^{\circ}$)

* With a reduction of the activity when the lung shunt is higher than 10%$^{+}$With an additional correction for the remaining activity in the vial (1-2%) $^{\circ}$60 Gy refers to the dose limit to the whole liver, without the need for reduction if the treatment is lobar (23).

These usual methods are semi-empirical, based on the body surface area for resin microspheres and using a mono-compartmental model for glass and ^{166}Ho-PLLA

microspheres (17). Compared to ^{90}Y-resin microspheres, the administered activity is usually threefold for ^{166}Ho-PLLA and 2.5-fold for glass microspheres (24, 25). These methods do not provide accurate dosimetry that separately takes into account the dose deposition in tumors and in the normal liver parenchyma for a dose optimization.

With resin microspheres and the BSA method, patients with a small liver might be overdosed and others with a large liver underdosed(26). In addition, Kafrouni et al. demonstrated that the activity calculated with the BSA method was associated with a suboptimal absorbed dose to tumor and normal liver, under the usual cut-offs for tumor response and liver tolerance in hepatocellular carcinoma (HCC) patients (i.e. 120 Gy and 50 Gy) (27). Previous data also demonstrated that the delivered activity with the BSA method must be significantly reduced for patients with small liver (<1.5L) or with low tumor involvement (<5%) to avoid RE induced liver disease (REILD) (28, 29).

Using resin or glass microspheres, some centers have adopted a more scientific and personalized dosimetric method based on the MAA distribution in the tumor and the normal liver compartments known as the partition or multi-compartmental model(30). With this method, the absorbed dose to the tumor compartment, to the healthy liver compartment and to the lungs is simulated using MAA imaging. For a good reproducibility between the simulation of treatment (MAA injection) and the treatment (^{90}Y injection), both liver

arteriographies must be very similar, positioning the catheter tip in same position and orientation in the arterial tree and preventing hemodynamic changes (avoid vasospasm, slow injection rate of MAA particles, avoid injection of particles near an arterial bifurcation) (31).

The tumor to normal liver ratio (T/NL) is calculated with MAA SPECT images as follows:

$$T/_{NL} = \frac{A_T/_{M_T}}{A_{NL}/_{M_{NL}}}$$

with A_T and M_T the activity and the mass of the tumor and A_{NL} and M_{NL} the activity and the mass of the normal (targeted) liver. The volumes of interest (VOIs) could be first delineated using the diagnostic CT scan or MRI and afterwards co-registered with MAA SPECT images. The functional volumes can also be assessed directly with the MAA SPECT/CT with accuracy using an isocontour method (32, 33).

The activity is defined as a function of the doses simulated in the tumor and normal liver compartments using the MAA distribution and can be calculated as follows (17):

$$A\ (GBq) = D_{NL}\ (Gy).\frac{T/_{NL}\,.M_T\ (kg) + M_{NL}\ (kg)}{50.\,(1 - LSF)}$$

Where D_{NL} is the target dose to the normal liver. Using resin microspheres, this target dose to the normal liver is variable, between 40 Gy for the whole liver to more than 150 Gy for a segmental treatment. The absorbed dose to the tumor(s) must be at least 100 Gy for expecting clinical response(34). For glass microspheres, a similar approach was applied to HCC patients with a targeted tumor dose of at least 205 Gy and a healthy (targeted) liver dose of maximum 120 Gy (35, 36).

However, this multi-compartmental model assumes a perfect correlation between the MAA distribution and the real distribution of the ^{90}Y microspheres. This consideration is questionable and subject to debate. Indeed, some previous studies demonstrated heterogeneous results in the ability of MAA imaging to precisely determine the tumor doses (37-44). This can be explained by several factors, in particular the fact that MAA particles have a smaller mean size (15 μm versus 25-32 μm for microspheres, with a larger range of size distribution from 10 to 60 μm), a lower density, a random shape and are injected in lower number as compared to the radioactive microspheres (41, 45, 46).

To the contrary of resin and glass microspheres, PLLA microspheres can also be used as scout dose during this workup phase. This scout dose (maximum 250 MBq ^{166}Ho) substitutes MAA without radiation-induced toxicity (47). Using identical particles between the workup and the treatment permits to predict with more

accuracy the liver distribution and especially the tumor doses (44). Moreover, the scout dose of PLLA microspheres seems to better estimate the lung shunt fraction as compared to MAA imaging (48).

1.2 Physical and radionuclide properties of microspheres

^{90}Y-resin microspheres, ^{90}Y-glass microspheres and ^{166}Ho-PLLA microspheres have different physico-chemical characteristics. Table 2 summarizes the main physical characteristics of ^{90}Y and ^{166}Ho radionuclides.

Both emit beta particles of high energy with a similar mean range of 2.5 mm. More than 90% of the radiation are delivered during the first 11 days for ^{90}Y (half-life: 2.7 days) and in only 4 days for ^{166}Ho (half-life: 1.1 day) (49, 50).

Table 2: Physical characteristics of radionuclides

Radionuclide	Labeled microspheres	Half-life	Beta emission (E. max)	Range of beta radiation	Other emissions
Yttrium-90 (^{90}Y)	Resin or glass	2.7 days	2.28 MeV	Mean : 2.5mm (Max : 11mm)	Positron (32. 10^{-6})
Holmium-166 (^{166}Ho)	PLLA	1.1 day	1.77 MeV (49%), 1.86 MeV (50%)	Mean :2.5 mm (Max :8.7mm)	Gamma (6.7%,82 keV)

Table 3: Structural characteristics of radioactive microspheres

Microspheres	Diameter (mean)	Density	Approximative number of micro-spheres per GBq*	Activity per microsphere
^{90}Y-Resin	32 μm	1.6 g/ml	13. 10^6	50 Bq
^{90}Y-Glass	25 μm	3.3 g/ml	0.4. 10^6	2500 Bq
^{166}Ho- PLLA	30 μm	1.4 g/ml	10. 10^6	450 Bq

*On the day of calibration (approximately). PLLA: poly-(L-lactic-acid)

The specific activity per sphere is respectively 50 and 5 times higher for glass microspheres as compared to resin and PLLA microspheres. The number of microspheres also differs between formulations: approximately 10 million for PLLA, 40 million for resin and only 4 million for glass microspheres (for a 3 GBq activity at the time of treatment).

1.3 Effects of microspheres at a voxel level

Due to their structural differences (Table 3), these microspheres have a different distribution into the liver at the sub centimeter level, which results in major variations in local absorbed doses.

Investigations of the local deposition of microspheres can be investigated in vivo by imaging (SPECT, PET and MRI) or simulated by computational models or by in

vitro artificial models of the hepatic arterial system. An excellent agreement was recently demonstrated between the deposition of microspheres simulated with a computational model and the real distribution observed in patients with ^{90}Y PET/CT (51). Especially, time of flight (TOF)-PET systems have the ability to capture with accuracy the distribution of the microspheres (52, 53). Contrarily to external radiotherapy, the absorbed dose distribution is heterogeneous in RE, resulting from a heterogeneous microsphere distribution at a voxel level (54, 55). Heterogeneity pattern in the activity distribution post radioembolization were evidenced by independent modalities: ex vivo microscopy analysis of liver tissue resection (55), microCT using glass microspheres (56), ^{166}Ho loaded spheres with MRI imaging (57) and Monte Carlo simulations of spheres transport in the hepatic arterial tree (52, 58).

^{90}Y-resin, ^{90}Y-glass and ^{166}Ho-PLLA microspheres have similar diameters permitting to reach similarly the microvasculature of tumors. The higher density of glass microspheres (Table 3) does not have a significant impact on the microspheres distribution compared to resin microspheres, as demonstrated by an experimental in vitro model of the hepatic vasculature (59). However, Jernigan et al. investigated the effects of density and demonstrated a lower penetration of glass compared to resin microspheres in a surrogate hepatic arterial system (60). In their flow model, the distal penetration depth was significantly lower for glass

microspheres and could be theoretically responsible of a reduced coverage of the tumor.

The main differences between microspheres are the specific activity per sphere and the number of injected microspheres during a treatment. Especially, glass microspheres are highly radioactive (2.500 Bq) and in limited number compared to others. Using a computational model, Walrand et al. demonstrated an asymmetrical distribution of the microspheres in the arterial liver tree, resulting in a large nonuniformity in the microsphere deposition at a sub centimeter level, especially when the number of microspheres is limited (52). In an in vivo study in pigs, Pasciak et al. confirmed the correlation between the number of injected microspheres and the degree of homogeneity of the absorbed dose at a microscopic level (56). In this study, four pigs received lobar infusions of ^{90}Y glass microspheres with an activity reaching a similar target liver dose of 50 Gy. In each pig, the injected glass microspheres differ in specific activity and number (from 1.532 Bq/microsphere and 610 microspheres/ml of tissue to 70 Bq/microsphere and 15.555 microspheres/ml of tissue), as illustrated in Figure 2.

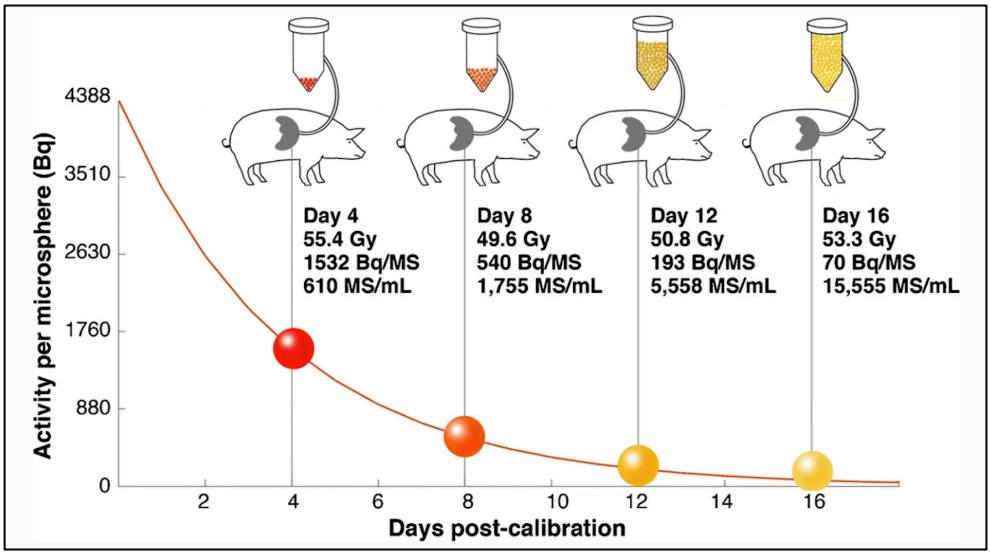

Figure 2: Amount of glass microspheres injected in pig livers as a function of time from microsphere calibration (4, 8, 12 or 16 days), resulting in spheres of different specific activity and concentrations (adapted from Pasciak et al. (56)).

The analysis of the microdosimetry data demonstrated important differences in absorbed doses deposition at a microscopic level. Each pig received the same average dose of 50 Gy but the distribution at a microscopic level was clearly different, very inhomogeneous when the number of microspheres was lower. The percentage of healthy liver receiving at least a potentially toxic dose of 40 Gy was only 24% for microspheres in relatively small number (e.g. 610 microspheres/ml of tissue) and important at 53% using more numerous microspheres (e.g. 15.555 microspheres/ml of tissue)). This effect is well illustrated in Figure 3.

Using microspheres in limited number induces a more heterogeneous liver distribution but also permits to be less toxic, avoiding to reach a toxic dose in a

large part of the normal liver. Using a Monte Carlo modeling, Pasciak et al. demonstrated also a similar behavior in tumors (61). The microsphere concentration was directly correlated with the tumor absorbed dose homogeneity.

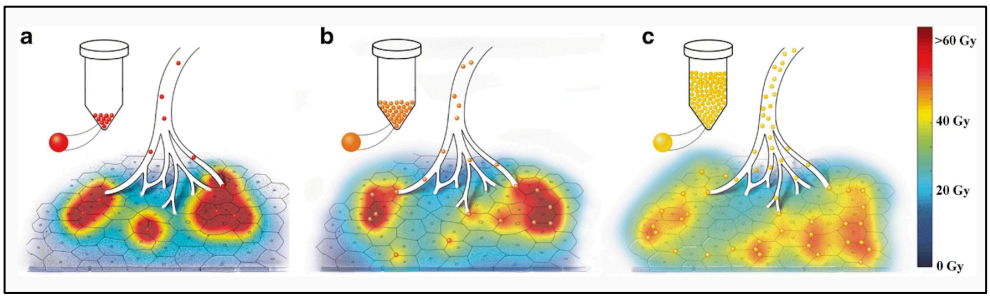

Figure 3: Artistic rendering of microscopic microsphere deposition at day 4 post-calibration (a), 8 post-calibration (b) and 12 post-calibration (c). Increased homogeneity of absorbed dose is apparent for glass microspheres injected at day 12 post-calibration (e.g., 193 Bq/microsphere, 5.558 microspheres/ ml). The proportion of the liver receiving a dose higher or equal to 40 Gy (red and yellow) was higher for glass microspheres injected at day 12 post-calibration (c). Adapted from Pasciak et al. (56).

In this model, no significant differences were observed for microsphere concentration in the range of 10.000-70.000 spheres/ml of tissue but apparent differences appear below 5.000 spheres/ml of tissue, resulting in more heterogeneous tumor dose distribution and risk of ineffectiveness. In this study, they also simulated the minimal dose deposited in 70% of the tumor (D70) and demonstrated a decrease up to 20% for the lowest microspheres concentration

(200 spheres/ml of tissue). Very interestingly, they also estimated the microsphere concentration in tumors receiving an absorbed dose of 100 Gy or 250 Gy with ^{90}Y- resin microspheres and ^{90}Y glass microspheres. For a tumor absorbed dose of 100 Gy with ^{90}Y resin microspheres, the microsphere density was largely above the critical concentration of 5.000 spheres/ml but came under the limit for ^{90}Y glass microspheres with a range between 820 and 18.600/ml. However, using a tumor-absorbed dose of 250 Gy, the microsphere concentration stayed optimum in a range between 2.050 and 46.500/ml for ^{90}Y glass microspheres. Therefore, by targeting a higher tumor absorbed dose (> 100 Gy) with ^{90}Y glass microspheres, the dose distribution at a microscopic level is more homogeneous, reaching an efficient dose deposition in a large part of the tumor.

^{90}Y- resin and^{166}Ho- PLLA microspheres could have an embolic effect because a high number of particles are injected in the liver arterial tree (Table 2). However, this effect may be very limited in particular because they have a very small size, permitting to reach the terminal microvasculature (62). Moreover, Bilbao et al. demonstrated no significant ischemic effect in pig liver models after injection of large quantities of non-radioactive resin microspheres (63). This is also explained by the unique dual blood supply of the normal liver, provided mainly by the portal vein.

1.4 Clinical applications

SIRT is part of the treatment strategy of primary liver malignancies and liver metastases (30).

The treatment options in HCC depend on the Barcelona clinic liver Cancer staging system (BCLC stage) (64). This classification takes into account the tumor characteristics (size, number of tumors, portal invasion or extra hepatic spread), the underlying liver function (Child-Pugh score) and the patient's performance status (Eastern cooperative oncology group [ECOG score]) (65). The BCLC stage accurately predicts the patient survival and help to determine the best treatment options. Recent recommendations of the European Society for Medical Oncology consider SIRT as an alternative treatment for BCLC stages A, B and C (66, 67). No randomized studies evaluated the interest of SIRT in BCLC A patients. However, a recent large retrospective study demonstrated that SIRT was efficient in unresectable solitary HCC alone or as neoadjuvant for bridging to a curative surgical approach (68). For intermediate HCC (BCLC B), transarterial chemoembolization (TACE) is recommended as first line therapy. However, previous prospective randomized studies demonstrated similar survival outcomes comparing TACE to SIRT (69). A randomized trial also demonstrated a better tumor control with SIRT compared to TACE (70). Considering the advanced stage (BCLC C), systemic therapies are often preferred using immunotherapy (atezolizumab plus bevacizumab) or targeted therapy (sorafenib, regorafenib…). Comparing SIRT to sorafenib, previous control randomized trials demonstrated

similar outcomes (71-73). The main results of the prospective and randomized studies in HCC are summarized in table 4. Moreover, the NEMESIS study computed the results of these three randomized trials, analyzing 1243 patients (73). This metanalysis confirmed that SIRT is non-inferior to sorafenib comparing OS (10.2 mo versus 9.2 mo; hazard ratio: 0.91 with CI 95% 0.78-1.05) and highlighted the better tolerance of SIRT (29% severe adverse events with SIRT versus 43% with sorafenib, $P < 0.01$).

Comparative studies did not demonstrate differences in response rates and patient outcome between resin and glass microspheres (74, 75). No data are currently available to evaluate the efficacy of PLLA microspheres in HCC. A disease control rate of 90% at 6 months was reported in a retrospective study enrolling only 9 patients BCLC B and C (76).

Table 4: Prospective and randomized studies in HCC

Studies	groups	Number of patients	BCLC score	Adverse events (≥ grade 3)	TRR	TTP (mo)	PFS (mo)	OS (mo)
Pitton et al. 2015 (77)	SIRT (resin)	12	B: 100%	NA	NA	12.4	6	19.7
	TACE	12	A: 8% B: 92%	NA	NA	11.2	7.2	26.3
Salem et al. 2016 (70)	SIRT (glass)	24	A: 75% B: 25%	NA	87%	> 26*	NA	18.6
	TACE	21	A: 81% B: 19%	NA	74%	4.8	NA	17.7
SARAH (71)	SIRT (resin)	237	C: 100%	41%	19%*	NA	4.1	9.9

	Sorafenib	222	C: 100%	63%*	12%	NA	3 .7	9.9
SIRveNIB (72)	SIRT (resin)	130	B: 61% C: 39%	28%	23 %*	6.1	6.3	8.8
	sorafenib	162	B: 54% C: 45%	51%*	2 %	5.4	5.2	10
SORAMIC (78)	SIRT (resin) + sorafenib	114	A: 4% B: 28% C: 68%	65%*	NA	NA	NA	14
	sorafenib	174	A: 2% B: 28% C: 70%	54%	NA	NA	NA	11.1

* Differences statistically significant (P < 0.05); NA: not available, TRR: tumor response rate; TTP: time to progression, PFS: progression free survival; OS: Overall survival

For advanced intrahepatic (liver dominant) cholangiocarcinoma (ICC), a treatment strategy including SIRT could be considered, performed alone or in combination with systemic chemotherapy (79). However, available literature is still insufficient to make strong recommendations (80). A recent phase 2 study using SIRT (glass microspheres) and concomitant first line chemotherapy demonstrated a high disease control rate with a tumor downstaging followed by a curative surgical approach in a significant number of patients (81).

For metastatic liver dominant colorectal cancer, SIRT should be considered for patients with a chemo-resistant disease (82). However, previous large randomized phase 3 trials failed to demonstrate superior overall survival (OS) and progression free survival (PFS) comparing a first line systemic chemotherapy +/- SIRT (83). However, the liver PFS and the technical resectability of liver metastases were significantly improved in the group treated with addition of SIRT (84, 85). A recent

phase 3 randomized trial studied also the addition of SIRT with a second line of chemotherapy for patients in progression after a first line of oxaliplatin or irinotecan. This study demonstrated a slight improvement of the liver and global PFS but no survival benefit (86). Similar survival rates were also shown using resin or glass microspheres in colorectal chemo-resistant metastases (87, 88). A phase 2 study in only 23 patients treated with holmium-166 microspheres in salvage therapy of colorectal liver metastases also demonstrated similar outcome (overall survival: 13.4 mo versus 8.3-15.2 mo with ^{90}Y-microspheres) (89, 90)

Liver metastases of neuroendocrine tumors can also be treated by SIRT. However, no randomized controlled trial demonstrated the efficacy of this treatment allowing strong recommendations (91). Nevertheless, a recent single-arm phase 2 study demonstrated the safety and the efficacy of one additional SIRT (PLLA microspheres) to a peptide receptor radionuclide therapy (92).

Clinical data (retrospective studies) demonstrated also a high disease control rate using SIRT in liver metastases from breast origin (93). Similarly to neuroendocrine tumors, no randomized controlled trials are available and there are still no recommendations in this indication (94).

1.5 Effects of microspheres at a macroscopic level: clinical effects

SIRT is usually well tolerated by patients. Severe adverse events are rare, including REILD (< 4%), gastrointestinal ulcer (< 5%) and radiation pneumonitis (<

1%) (62). These adverse events can be limited by a good selection of patients, excluding those with respectively advanced cirrhosis, a persistent MAA uptake in the digestive tract after repeated simulation arteriography and a significant lung shunt (> 20%).

Physical characteristics of the radioactive microspheres explain also their different toxicity and efficacy profiles. Regarding PLLA microspheres, more data are needed to evaluate and compare its efficiency and toxicity.

As far as toxicity is concerned, an excessive radiation dose to the healthy liver can induce a severe and potentially life-threatening complication, REILD with an incidence rate inferior to 4% (62). It is defined as a sinusoidal obstruction syndrome and a liver damage within 3 months after RE, in absence of tumor progression(95). This complication tends to occur especially when a large volume of liver parenchyma is exposed to radiation. Other risk factors include a recent exposure to chemotherapy and underlying cirrhosis (28). In external beam radiotherapy (EBRT), this complication occurs with a whole liver dose of 30-35 Gy (96). The tolerance is higher in RE, 40-50 Gy for resin microspheres and up to 90 Gy with glass microspheres (97-99). A study in pigs with administration of PLLA microspheres demonstrated no toxicity with absorbed doses over 100 Gy. In human studies in phase 1 and 2, the whole liver absorbed dose was limited to 60

Gy and was not associated with liver toxicity (89, 100). The homogeneity of the dose distribution explains the relative lower liver dose tolerability of external radiotherapy. To the contrary, a large heterogeneity of the dose distribution is a characteristic of RE, hence a relatively lower proportion of the liver parenchyma receives toxic doses (i.e. 30-35 Gy). As well described by Pasciak et al. (56), this liver dose heterogeneity is directly correlated with the number of microspheres injected in the liver. This characteristic could explain why the tolerable dose is significantly higher using glass microspheres with a reduced number of radioactive microspheres injected in the liver (table 3).

Another possible complication is the development of gastric/ duodenal ulcers, reported in 3.1% with resin microspheres and 0.1% with glass microspheres(101). A gastrointestinal deposition of microspheres leads to radiation induced ulcerations. It can occur when the liver arteries communicate with the digestive tract by collaterals or when the microsphere injection is administered in close digestive arteries such as the gastro duodenal artery or the right gastric artery (23). Prophylactic coil embolization of the hepato-splanchnic arteries or more distal injections of microspheres can be performed to prevent this complication (62). The main risk factor for gastro-duodenal ulceration is a stasis of the blood flow during the microsphere administration causing retrograde flux and extra-hepatic deposition(102). Due to the high number of injected microspheres (table 3), a potential stasis can occur during the administration of resin or PLLA

microspheres (103). With resin microspheres, an early stasis may occur in 20% of the procedures, resulting in an incomplete delivery of the prescribed activity and a suboptimal dose to tumors (104). Conversely, no evidence of flow stasis was demonstrated with glass microspheres, especially because a relatively small number of microspheres is injected (table 3) (105).

With regards to efficiency, tumor dosimetry is the predictive factor in SIRT. Previous data demonstrated a sigmoid relationship between the tumor absorbed dose and the radiological response (98, 106, 107). HCC patients treated with resin microspheres had better disease control and overall survival when tumor absorbed doses were above 100 Gy. Similarly, HCC patients treated with glass microspheres had also a better outcome with a tumor-absorbed dose of at least 205 Gy (108, 109). For colorectal metastases, a dose response relationship was also demonstrated with the three types of microspheres. A significant metabolic response was achieved with a tumor cut-off dose of 50-60 Gy with resin microspheres (110, 111), 139 Gy using glass microspheres (112) and 90 Gy using PLLA microspheres (113). The tumor dose distribution and its heterogeneity can be assessed with ^{90}Y PET/CT using dose-volume histograms (DVH). The tumor dose distribution showed predictive of the response to therapy. In 7 patients treated with resin microspheres for HCC tumors, Kao et al. demonstrated a complete radiological response when D70 was upper to 100 Gy (D70: minimal

dose to 70% of the tumor volume) and an incomplete response under this threshold (114). In 38 HCC patients treated with glass microspheres, D70 was also significantly higher in responders (median 140 Gy) compared to non-responders (median 24 Gy) (115). Figure 4 demonstrates an example of dose deposition after radioembolization (resin microspheres) of a large HCC. ^{90}Y PET, converted in a map of absorbed doses, demonstrated a good tumor targeting albeit an heterogenous distribution of the dose. A large part of the tumor received more than 100 Gy and a small part receiving a lower dose (< 50 Gy). The proportion of the tumor volume receiving a minimal absorbed dose can be detailed using a DVH (Figure 5).

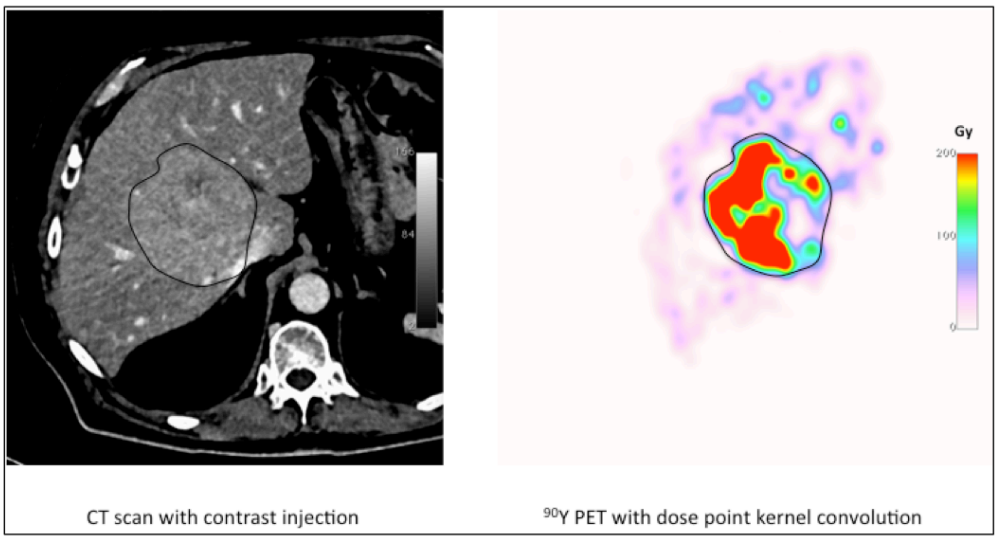

Figure 4: Tumor dose deposition after dose point kernel convolution of ^{90}Y PET. The tumor contours are delineated in black.

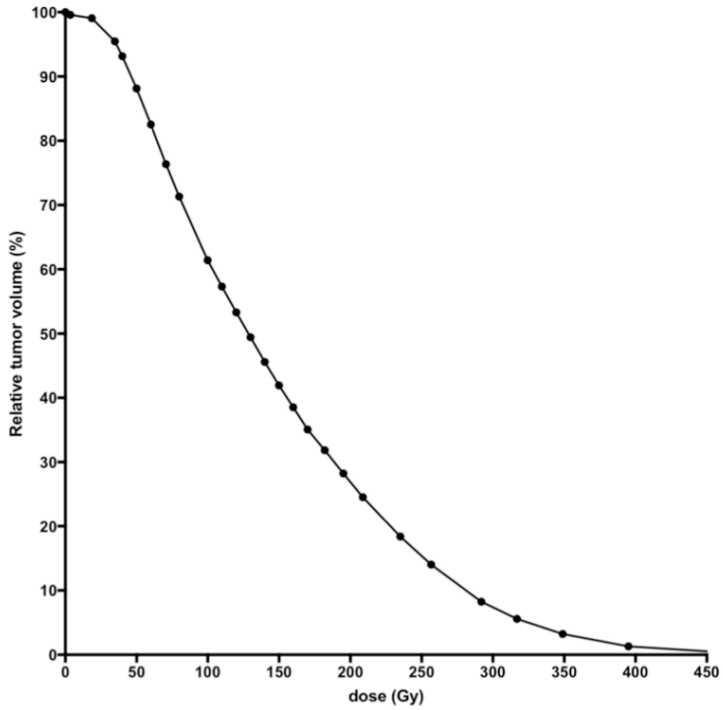

Figure 5: Dose volume histogram of the same tumor. In this case, 70% of the tumor volume (D70) received ca. 100 Gy.

References

1. Lewandowski RJ, Salem R. Yttrium-90 radioembolization of hepatocellular carcinoma and metastatic disease to the liver. Semin Intervent Radiol. 2006;23(1):64-72.

2. Giammarile F, Bodei L, Chiesa C, Flux G, Forrer F, Kraeber-Bodere F, et al. EANM procedure guideline for the treatment of liver cancer and liver metastases with intra-arterial radioactive compounds. Eur J Nucl Med Mol Imaging. 2011;38(7):1393-406.

3. Raoul JL, Bourguet P, Bretagne JF, Duvauferrier R, Coornaert S, Darnault P, et al. Hepatic artery injection of I-131-labeled lipiodol. Part I. Biodistribution study

results in patients with hepatocellular carcinoma and liver metastases. Radiology. 1988;168(2):541-5.
4. Lintia-Gaultier A, Perret C, Ansquer C, Eugene T, Kraeber-Bodere F, Frampas E. Intra-arterial injection of 131I-labeled Lipiodol for advanced hepatocellular carcinoma: a 7 years' experience. Nucl Med Commun. 2013;34(7):674-81.
5. Li R, Li D, Jia G, Li X, Sun G, Zuo C. Diagnostic Performance of Theranostic Radionuclides Used in Transarterial Radioembolization for Liver Cancer. Front Oncol. 2020;10:551622.
6. Ahmadzadehfar H, Sabet A, Wilhelm K, Biersack HJ, Risse J. Iodine-131-lipiodol therapy in hepatic tumours. Methods. 2011;55(3):246-52.
7. Lambert B, Van de Wiele C. Treatment of hepatocellular carcinoma by means of radiopharmaceuticals. Eur J Nucl Med Mol Imaging. 2005;32(8):980-9.
8. Kennedy AS, Nutting C, Coldwell D, Gaiser J, Drachenberg C. Pathologic response and microdosimetry of (90)Y microspheres in man: review of four explanted whole livers. Int J Radiat Oncol Biol Phys. 2004;60(5):1552-63.
9. Kennedy A. Radioembolization of hepatic tumors. J Gastrointest Oncol. 2014;5(3):178-89.
10. Sangro B, Inarrairaegui M, Bilbao JI. Radioembolization for hepatocellular carcinoma. J Hepatol. 2012;56(2):464-73.
11. Lambert B, Bacher K, Defreyne L. Rhenium-188 based radiopharmaceuticals for treatment of liver tumours. Q J Nucl Med Mol Imaging. 2009;53(3):305-10.
12. Gaba RC. Planning Arteriography for Yttrium-90 Microsphere Radioembolization. Semin Intervent Radiol. 2015;32(4):428-38.
13. Kennedy A, Nag S, Salem R, Murthy R, McEwan AJ, Nutting C, et al. Recommendations for radioembolization of hepatic malignancies using yttrium-90 microsphere brachytherapy: a consensus panel report from the radioembolization brachytherapy oncology consortium. Int J Radiat Oncol Biol Phys. 2007;68(1):13-23.
14. Arroyo-Hernandez M, Maldonado F, Lozano-Ruiz F, Munoz-Montano W, Nunez-Baez M, Arrieta O. Radiation-induced lung injury: current evidence. BMC Pulm Med. 2021;21(1):9.
15. Kim SP, Cohalan C, Kopek N, Enger SA. A guide to (90)Y radioembolization and its dosimetry. Phys Med. 2019;68:132-45.
16. Vente MA, Nijsen JF, de Wit TC, Seppenwoolde JH, Krijger GC, Seevinck PR, et al. Clinical effects of transcatheter hepatic arterial embolization with holmium-166 poly(L-lactic acid) microspheres in healthy pigs. Eur J Nucl Med Mol Imaging. 2008;35(7):1259-71.
17. Bastiaannet R, Kappadath SC, Kunnen B, Braat A, Lam M, de Jong H. The physics of radioembolization. EJNMMI Phys. 2018;5(1):22.

18. Kallini JR, Gabr A, Salem R, Lewandowski RJ. Transarterial Radioembolization with Yttrium-90 for the Treatment of Hepatocellular Carcinoma. Adv Ther. 2016;33(5):699-714.
19. Loevinger R BT, Watson E. MIRD PRIMER for absorbed dose calculation. The Society of Nuclear Medicine, Inc
. 1988:1-7.
20. SIR-Spheres. Instructions For Use. North Sydney, Australia: SIRTeX Medical Limited. 2019.
21. Therasphere. Instructions for use. 2021.
22. QuiremSpheres. Instruction for use. 2020.
.
23. Alsultan AA, Braat A, Smits MLJ, Barentsz MW, Bastiaannet R, Bruijnen RCG, et al. Current Status and Future Direction of Hepatic Radioembolisation. Clin Oncol (R Coll Radiol). 2021;33(2):106-16.
24. Smits ML, Nijsen JF, van den Bosch MA, Lam MG, Vente MA, Huijbregts JE, et al. Holmium-166 radioembolization for the treatment of patients with liver metastases: design of the phase I HEPAR trial. J Exp Clin Cancer Res. 2010;29:70.
25. James T, Hill J, Fahrbach T, Collins Z. Differences in Radiation Activity Between Glass and Resin 90Y Microspheres in Treating Unresectable Hepatic Cancer. Health Phys. 2017;112(3):300-4.
26. Lam MG, Louie JD, Abdelmaksoud MH, Fisher GA, Cho-Phan CD, Sze DY. Limitations of body surface area-based activity calculation for radioembolization of hepatic metastases in colorectal cancer. J Vasc Interv Radiol. 2014;25(7):1085-93.
27. Kafrouni M, Allimant C, Fourcade M, Vauclin S, Delicque J, Ilonca AD, et al. Retrospective Voxel-Based Dosimetry for Assessing the Ability of the Body-Surface-Area Model to Predict Delivered Dose and Radioembolization Outcome. J Nucl Med. 2018;59(8):1289-95.
28. Gil-Alzugaray B, Chopitea A, Inarrairaegui M, Bilbao JI, Rodriguez-Fraile M, Rodriguez J, et al. Prognostic factors and prevention of radioembolization-induced liver disease. Hepatology. 2013;57(3):1078-87.
29. Sangro B, Gil-Alzugaray B, Rodriguez J, Sola I, Martinez-Cuesta A, Viudez A, et al. Liver disease induced by radioembolization of liver tumors: description and possible risk factors. Cancer. 2008;112(7):1538-46.
30. Padia SA, Lewandowski RJ, Johnson GE, Sze DY, Ward TJ, Gaba RC, et al. Radioembolization of Hepatic Malignancies: Background, Quality Improvement Guidelines, and Future Directions. J Vasc Interv Radiol. 2017;28(1):1-15.
31. Garin E, Palard X, Rolland Y. Personalised Dosimetry in Radioembolisation for HCC: Impact on Clinical Outcome and on Trial Design. Cancers (Basel). 2020;12(6).

32. Garin E, Rolland Y, Lenoir L, Pracht M, Mesbah H, Poree P, et al. Utility of Quantitative Tc-MAA SPECT/CT for yttrium-Labelled Microsphere Treatment Planning: Calculating Vascularized Hepatic Volume and Dosimetric Approach. Int J Mol Imaging. 2011;2011:398051.
33. Garin E, Lenoir L, Rolland Y, Laffont S, Pracht M, Mesbah H, et al. Effectiveness of quantitative MAA SPECT/CT for the definition of vascularized hepatic volume and dosimetric approach: phantom validation and clinical preliminary results in patients with complex hepatic vascularization treated with yttrium-90-labeled microspheres. Nucl Med Commun. 2011;32(12):1245-55.
34. Levillain H, Bagni O, Deroose CM, Dieudonne A, Gnesin S, Grosser OS, et al. International recommendations for personalised selective internal radiation therapy of primary and metastatic liver diseases with yttrium-90 resin microspheres. Eur J Nucl Med Mol Imaging. 2021.
35. Garin E, Lenoir L, Rolland Y, Edeline J, Mesbah H, Laffont S, et al. Dosimetry based on 99mTc-macroaggregated albumin SPECT/CT accurately predicts tumor response and survival in hepatocellular carcinoma patients treated with 90Y-loaded glass microspheres: preliminary results. J Nucl Med. 2012;53(2):255-63.
36. Garin E, Rolland Y, Boucher E. Pre-therapeutic dosimetry evaluation and selective internal radiation therapy of hepatocellular carcinoma using yttrium-90-loaded microspheres. J Hepatol. 2013;58(5):1055-6.
37. Justin K. Mikell YKD, Dawn Owen. Transarterial radiombolization for hepatocellular carcinoma and hepatic metastases: Clinical aspects and dosimetry models. Seminars in radiation oncology. 2019;30:68-76.
38. Jadoul A, Bernard C, Lovinfosse P, Gerard L, Lilet H, Cornet O, et al. Comparative dosimetry between (99m)Tc-MAA SPECT/CT and (90)Y PET/CT in primary and metastatic liver tumors. Eur J Nucl Med Mol Imaging. 2020;47(4):828-37.
39. Kafrouni M, Allimant C, Fourcade M, Vauclin S, Guiu B, Mariano-Goulart D, et al. Analysis of differences between (99m)Tc-MAA SPECT- and (90)Y-microsphere PET-based dosimetry for hepatocellular carcinoma selective internal radiation therapy. EJNMMI Res. 2019;9(1):62.
40. Gnesin S, Canetti L, Adib S, Cherbuin N, Silva Monteiro M, Bize P, et al. Partition Model-Based 99mTc-MAA SPECT/CT Predictive Dosimetry Compared with 90Y TOF PET/CT Posttreatment Dosimetry in Radioembolization of Hepatocellular Carcinoma: A Quantitative Agreement Comparison. J Nucl Med. 2016;57(11):1672-8.
41. Wondergem M, Smits ML, Elschot M, de Jong HW, Verkooijen HM, van den Bosch MA, et al. 99mTc-macroaggregated albumin poorly predicts the intrahepatic distribution of 90Y resin microspheres in hepatic radioembolization. J Nucl Med. 2013;54(8):1294-301.

42. Ilhan H, Goritschan A, Paprottka P, Jakobs TF, Fendler WP, Todica A, et al. Predictive Value of 99mTc-MAA SPECT for 90Y-Labeled Resin Microsphere Distribution in Radioembolization of Primary and Secondary Hepatic Tumors. J Nucl Med. 2015;56(11):1654-60.
43. Haste P, Tann M, Persohn S, LaRoche T, Aaron V, Mauxion T, et al. Correlation of Technetium-99m Macroaggregated Albumin and Yttrium-90 Glass Microsphere Biodistribution in Hepatocellular Carcinoma: A Retrospective Review of Pretreatment Single Photon Emission CT and Posttreatment Positron Emission Tomography/CT. J Vasc Interv Radiol. 2017;28(5):722-30 e1.
44. Smits MLJ, Dassen MG, Prince JF, Braat A, Beijst C, Bruijnen RCG, et al. The superior predictive value of (166)Ho-scout compared with (99m)Tc-macroaggregated albumin prior to (166)Ho-microspheres radioembolization in patients with liver metastases. Eur J Nucl Med Mol Imaging. 2020;47(4):798-806.
45. Bult W, Vente MA, Zonnenberg BA, Van Het Schip AD, Nijsen JF. Microsphere radioembolization of liver malignancies: current developments. Q J Nucl Med Mol Imaging. 2009;53(3):325-35.
46. Al-Janabi MA, Yousif ZM, Kadim AH, Al-Salem AM. A new technique for the preparation of ready-to-use macroaggregated albumin (MAA) kits to be labelled with 99mTc for lung scanning. Int J Appl Radiat Isot. 1983;34(10):1473-8.
47. Braat A, Prince JF, van Rooij R, Bruijnen RCG, van den Bosch M, Lam M. Safety analysis of holmium-166 microsphere scout dose imaging during radioembolisation work-up: A cohort study. Eur Radiol. 2018;28(3):920-8.
48. Elschot M, Nijsen JF, Lam MG, Smits ML, Prince JF, Viergever MA, et al. ((9)(9)m)Tc-MAA overestimates the absorbed dose to the lungs in radioembolization: a quantitative evaluation in patients treated with (1)(6)(6)Ho-microspheres. Eur J Nucl Med Mol Imaging. 2014;41(10):1965-75.
49. Murthy R, Kamat P, Nunez R, Salem R. Radioembolization of yttrium-90 microspheres for hepatic malignancy. Semin Intervent Radiol. 2008;25(1):48-57.
50. Klaassen NJM, Arntz MJ, Gil Arranja A, Roosen J, Nijsen JFW. The various therapeutic applications of the medical isotope holmium-166: a narrative review. EJNMMI Radiopharm Chem. 2019;4(1):19.
51. Anton R, Antonana J, Aramburu J, Ezponda A, Prieto E, Andonegui A, et al. A proof-of-concept study of the in-vivo validation of a computational fluid dynamics model of personalized radioembolization. Sci Rep. 2021;11(1):3895.
52. Walrand S, Hesse M, Chiesa C, Lhommel R, Jamar F. The low hepatic toxicity per Gray of 90Y glass microspheres is linked to their transport in the arterial tree favoring a nonuniform trapping as observed in posttherapy PET imaging. J Nucl Med. 2014;55(1):135-40.
53. Pasciak AS, Bourgeois AC, McKinney JM, Chang TT, Osborne DR, Acuff SN, et al. Radioembolization and the Dynamic Role of (90)Y PET/CT. Front Oncol. 2014;4:38.

54. Hogberg J, Rizell M, Hultborn R, Svensson J, Henrikson O, Molne J, et al. Increased absorbed liver dose in Selective Internal Radiation Therapy (SIRT) correlates with increased sphere-cluster frequency and absorbed dose inhomogeneity. EJNMMI Phys. 2015;2(1):10.
55. Hogberg J, Rizell M, Hultborn R, Svensson J, Henrikson O, Molne J, et al. Heterogeneity of microsphere distribution in resected liver and tumour tissue following selective intrahepatic radiotherapy. EJNMMI Res. 2014;4(1):48.
56. Pasciak AS, Abiola G, Liddell RP, Crookston N, Besharati S, Donahue D, et al. The number of microspheres in Y90 radioembolization directly affects normal tissue radiation exposure. Eur J Nucl Med Mol Imaging. 2020;47(4):816-27.
57. van de Maat GH, Seevinck PR, Elschot M, Smits ML, de Leeuw H, van Het Schip AD, et al. MRI-based biodistribution assessment of holmium-166 poly(L-lactic acid) microspheres after radioembolisation. Eur Radiol. 2013;23(3):827-35.
58. Crookston NR, Fung GSK, Frey EC. Development of a Customizable Hepatic Arterial Tree and Particle Transport Model for Use in Treatment Planning. IEEE Trans Radiat Plasma Med Sci. 2019;3(1):31-7.
59. Caine M, McCafferty MS, McGhee S, Garcia P, Mullett WM, Zhang X, et al. Impact of Yttrium-90 Microsphere Density, Flow Dynamics, and Administration Technique on Spatial Distribution: Analysis Using an In Vitro Model. J Vasc Interv Radiol. 2017;28(2):260-8 e2.
60. Jernigan SR, Osborne JA, Mirek CJ, Buckner G. Selective internal radiation therapy: quantifying distal penetration and distribution of resin and glass microspheres in a surrogate arterial model. J Vasc Interv Radiol. 2015;26(6):897-904 e2.
61. Pasciak AS, Bourgeois AC, Bradley YC. A Microdosimetric Analysis of Absorbed Dose to Tumor as a Function of Number of Microspheres per Unit Volume in 90Y Radioembolization. J Nucl Med. 2016;57(7):1020-6.
62. Riaz A, Awais R, Salem R. Side effects of yttrium-90 radioembolization. Front Oncol. 2014;4:198.
63. Bilbao JI, de Martino A, de Luis E, Diaz-Dorronsoro L, Alonso-Burgos A, Martinez de la Cuesta A, et al. Biocompatibility, inflammatory response, and recannalization characteristics of nonradioactive resin microspheres: histological findings. Cardiovasc Intervent Radiol. 2009;32(4):727-36.
64. Reig M, Forner A, Rimola J, Ferrer-Fabrega J, Burrel M, Garcia-Criado A, et al. BCLC strategy for prognosis prediction and treatment recommendation Barcelona Clinic Liver Cancer (BCLC) staging system. The 2022 update. J Hepatol. 2021.
65. Couri T, Pillai A. Goals and targets for personalized therapy for HCC. Hepatol Int. 2019;13(2):125-37.

66. Vogel A, Martinelli E, clinicalguidelines@esmo.org EGCEa, Committee EG. Updated treatment recommendations for hepatocellular carcinoma (HCC) from the ESMO Clinical Practice Guidelines. Ann Oncol. 2021;32(6):801-5.
67. Lee JJX, Tai DW, Choo SP. Locoregional therapy in hepatocellular carcinoma: when to start and when to stop and when to revisit. ESMO Open. 2021;6(3):100129.
68. Salem R, Johnson GE, Kim E, Riaz A, Bishay V, Boucher E, et al. Yttrium-90 Radioembolization for the Treatment of Solitary, Unresectable HCC: The LEGACY Study. Hepatology. 2021.
69. Casadei Gardini A, Tamburini E, Inarrairaegui M, Frassineti GL, Sangro B. Radioembolization versus chemoembolization for unresectable hepatocellular carcinoma: a meta-analysis of randomized trials. Onco Targets Ther. 2018;11:7315-21.
70. Salem R, Gordon AC, Mouli S, Hickey R, Kallini J, Gabr A, et al. Y90 Radioembolization Significantly Prolongs Time to Progression Compared With Chemoembolization in Patients With Hepatocellular Carcinoma. Gastroenterology. 2016;151(6):1155-63 e2.
71. Vilgrain V, Pereira H, Assenat E, Guiu B, Ilonca AD, Pageaux GP, et al. Efficacy and safety of selective internal radiotherapy with yttrium-90 resin microspheres compared with sorafenib in locally advanced and inoperable hepatocellular carcinoma (SARAH): an open-label randomised controlled phase 3 trial. Lancet Oncol. 2017;18(12):1624-36.
72. Chow PKH, Gandhi M, Tan SB, Khin MW, Khasbazar A, Ong J, et al. SIRveNIB: Selective Internal Radiation Therapy Versus Sorafenib in Asia-Pacific Patients With Hepatocellular Carcinoma. J Clin Oncol. 2018;36(19):1913-21.
73. Venerito M, Pech M, Canbay A, Donghia R, Guerra V, Chatellier G, et al. NEMESIS: Noninferiority, Individual-Patient Metaanalysis of Selective Internal Radiation Therapy with (90)Y Resin Microspheres Versus Sorafenib in Advanced Hepatocellular Carcinoma. J Nucl Med. 2020;61(12):1736-42.
74. Biederman DM, Titano JJ, Tabori NE, Pierobon ES, Alshebeeb K, Schwartz M, et al. Outcomes of Radioembolization in the Treatment of Hepatocellular Carcinoma with Portal Vein Invasion: Resin versus Glass Microspheres. J Vasc Interv Radiol. 2016;27(6):812-21 e2.
75. Van Der Gucht A, Jreige M, Denys A, Blanc-Durand P, Boubaker A, Pomoni A, et al. Resin Versus Glass Microspheres for (90)Y Transarterial Radioembolization: Comparing Survival in Unresectable Hepatocellular Carcinoma Using Pretreatment Partition Model Dosimetry. J Nucl Med. 2017;58(8):1334-40.
76. Radosa CG, Radosa JC, Grosche-Schlee S, Zophel K, Plodeck V, Kuhn JP, et al. Holmium-166 Radioembolization in Hepatocellular Carcinoma: Feasibility and Safety of a New Treatment Option in Clinical Practice. Cardiovasc Intervent Radiol. 2019;42(3):405-12.

77. Pitton MB, Kloeckner R, Ruckes C, Wirth GM, Eichhorn W, Worns MA, et al. Randomized comparison of selective internal radiotherapy (SIRT) versus drug-eluting bead transarterial chemoembolization (DEB-TACE) for the treatment of hepatocellular carcinoma. Cardiovasc Intervent Radiol. 2015;38(2):352-60.
78. Ricke J, Klumpen HJ, Amthauer H, Bargellini I, Bartenstein P, de Toni EN, et al. Impact of combined selective internal radiation therapy and sorafenib on survival in advanced hepatocellular carcinoma. J Hepatol. 2019;71(6):1164-74.
79. Banales JM, Marin JJG, Lamarca A, Rodrigues PM, Khan SA, Roberts LR, et al. Cholangiocarcinoma 2020: the next horizon in mechanisms and management. Nat Rev Gastroenterol Hepatol. 2020;17(9):557-88.
80. Edeline J, Lamarca A, McNamara MG, Jacobs T, Hubner RA, Palmer D, et al. Locoregional therapies in patients with intrahepatic cholangiocarcinoma: A systematic review and pooled analysis. Cancer Treat Rev. 2021;99:102258.
81. Edeline J, Touchefeu Y, Guiu B, Farge O, Tougeron D, Baumgaertner I, et al. Radioembolization Plus Chemotherapy for First-line Treatment of Locally Advanced Intrahepatic Cholangiocarcinoma: A Phase 2 Clinical Trial. JAMA Oncol. 2020;6(1):51-9.
82. Van Cutsem E, Cervantes A, Adam R, Sobrero A, Van Krieken JH, Aderka D, et al. ESMO consensus guidelines for the management of patients with metastatic colorectal cancer. Ann Oncol. 2016;27(8):1386-422.
83. Wasan HS, Gibbs P, Sharma NK, Taieb J, Heinemann V, Ricke J, et al. First-line selective internal radiotherapy plus chemotherapy versus chemotherapy alone in patients with liver metastases from colorectal cancer (FOXFIRE, SIRFLOX, and FOXFIRE-Global): a combined analysis of three multicentre, randomised, phase 3 trials. Lancet Oncol. 2017;18(9):1159-71.
84. van Hazel GA, Heinemann V, Sharma NK, Findlay MP, Ricke J, Peeters M, et al. SIRFLOX: Randomized Phase III Trial Comparing First-Line mFOLFOX6 (Plus or Minus Bevacizumab) Versus mFOLFOX6 (Plus or Minus Bevacizumab) Plus Selective Internal Radiation Therapy in Patients With Metastatic Colorectal Cancer. J Clin Oncol. 2016;34(15):1723-31.
85. Garlipp B, Gibbs P, Van Hazel GA, Jeyarajah R, Martin RCG, Bruns CJ, et al. Secondary technical resectability of colorectal cancer liver metastases after chemotherapy with or without selective internal radiotherapy in the randomized SIRFLOX trial. Br J Surg. 2019;106(13):1837-46.
86. Mulcahy MF, Mahvash A, Pracht M, Montazeri AH, Bandula S, Martin RCG, 2nd, et al. Radioembolization With Chemotherapy for Colorectal Liver Metastases: A Randomized, Open-Label, International, Multicenter, Phase III Trial. J Clin Oncol. 2021:JCO2101839.
87. Kennedy AS, Ball D, Cohen SJ, Cohn M, Coldwell DM, Drooz A, et al. Multicenter evaluation of the safety and efficacy of radioembolization in patients

with unresectable colorectal liver metastases selected as candidates for (90)Y resin microspheres. J Gastrointest Oncol. 2015;6(2):134-42.
88. Hickey R, Lewandowski RJ, Prudhomme T, Ehrenwald E, Baigorri B, Critchfield J, et al. 90Y Radioembolization of Colorectal Hepatic Metastases Using Glass Microspheres: Safety and Survival Outcomes from a 531-Patient Multicenter Study. J Nucl Med. 2016;57(5):665-71.
89. Prince JF, van den Bosch M, Nijsen JFW, Smits MLJ, van den Hoven AF, Nikolakopoulos S, et al. Efficacy of Radioembolization with (166)Ho-Microspheres in Salvage Patients with Liver Metastases: A Phase 2 Study. J Nucl Med. 2018;59(4):582-8.
90. Rosenbaum CE, Verkooijen HM, Lam MG, Smits ML, Koopman M, van Seeters T, et al. Radioembolization for treatment of salvage patients with colorectal cancer liver metastases: a systematic review. J Nucl Med. 2013;54(11):1890-5.
91. Frilling A, Modlin IM, Kidd M, Russell C, Breitenstein S, Salem R, et al. Recommendations for management of patients with neuroendocrine liver metastases. Lancet Oncol. 2014;15(1):e8-21.
92. Braat A, Bruijnen RCG, van Rooij R, Braat M, Wessels FJ, van Leeuwaarde RS, et al. Additional holmium-166 radioembolisation after lutetium-177-dotatate in patients with neuroendocrine tumour liver metastases (HEPAR PLuS): a single-centre, single-arm, open-label, phase 2 study. Lancet Oncol. 2020;21(4):561-70.
93. Feretis M, Solodkyy A. Yttrium-90 radioembolization for unresectable hepatic metastases of breast cancer: A systematic review. World J Gastrointest Oncol. 2020;12(2):228-36.
94. Cardoso F, Paluch-Shimon S, Senkus E, Curigliano G, Aapro MS, Andre F, et al. 5th ESO-ESMO international consensus guidelines for advanced breast cancer (ABC 5). Ann Oncol. 2020;31(12):1623-49.
95. Braat AJ, Smits ML, Braat MN, van den Hoven AF, Prince JF, de Jong HW, et al. (9)(0)Y Hepatic Radioembolization: An Update on Current Practice and Recent Developments. J Nucl Med. 2015;56(7):1079-87.
96. Koay EJ, Owen D, Das P. Radiation-Induced Liver Disease and Modern Radiotherapy. Semin Radiat Oncol. 2018;28(4):321-31.
97. Cremonesi M, Ferrari M, Bartolomei M, Orsi F, Bonomo G, Arico D, et al. Radioembolisation with 90Y-microspheres: dosimetric and radiobiological investigation for multi-cycle treatment. Eur J Nucl Med Mol Imaging. 2008;35(11):2088-96.
98. Strigari L, Sciuto R, Rea S, Carpanese L, Pizzi G, Soriani A, et al. Efficacy and toxicity related to treatment of hepatocellular carcinoma with 90Y-SIR spheres: radiobiologic considerations. J Nucl Med. 2010;51(9):1377-85.
99. Chiesa C, Mira M, Bhoori S, Bormolini G, Maccauro M, Spreafico C, et al. Radioembolization of hepatocarcinoma with (90)Y glass microspheres: treatment

optimization using the dose-toxicity relationship. Eur J Nucl Med Mol Imaging. 2020;47(13):3018-32.
100. Smits ML, Nijsen JF, van den Bosch MA, Lam MG, Vente MA, Mali WP, et al. Holmium-166 radioembolisation in patients with unresectable, chemorefractory liver metastases (HEPAR trial): a phase 1, dose-escalation study. Lancet Oncol. 2012;13(10):1025-34.
101. Kallini JR, Gabr A, Thorlund K, Balijepalli C, Ayres D, Kanters S, et al. Comparison of the Adverse Event Profile of TheraSphere((R)) with SIR-Spheres((R)) for the Treatment of Unresectable Hepatocellular Carcinoma: A Systematic Review. Cardiovasc Intervent Radiol. 2017;40(7):1033-43.
102. Lam M, Banerjee S, Louie JD, Abdelmaksoud MHK, Iagaru AH, Ennen RE, et al. Root cause analysis of gastroduodenal ulceration after yttrium-90 radioembolization. Cardiovasc Intervent Radiol. 2013;36(6):1536-47.
103. Reinders MTM, Smits MLJ, van Roekel C, Braat A. Holmium-166 Microsphere Radioembolization of Hepatic Malignancies. Semin Nucl Med. 2019;49(3):237-43.
104. Piana PM, Bar V, Doyle L, Anne R, Sato T, Eschelman DJ, et al. Early arterial stasis during resin-based yttrium-90 radioembolization: incidence and preliminary outcomes. HPB (Oxford). 2014;16(4):336-41.
105. Sato K, Lewandowski RJ, Bui JT, Omary R, Hunter RD, Kulik L, et al. Treatment of unresectable primary and metastatic liver cancer with yttrium-90 microspheres (TheraSphere): assessment of hepatic arterial embolization. Cardiovasc Intervent Radiol. 2006;29(4):522-9.
106. Hermann AL, Dieudonne A, Ronot M, Sanchez M, Pereira H, Chatellier G, et al. Relationship of Tumor Radiation-absorbed Dose to Survival and Response in Hepatocellular Carcinoma Treated with Transarterial Radioembolization with (90)Y in the SARAH Study. Radiology. 2020;296(3):673-84.
107. Dewaraja YK, Devasia T, Kaza RK, Mikell JK, Owen D, Roberson PL, et al. Prediction of Tumor Control in (90)Y Radioembolization by Logit Models with PET/CT-Based Dose Metrics. J Nucl Med. 2020;61(1):104-11.
108. Garin E, Lenoir L, Edeline J, Laffont S, Mesbah H, Poree P, et al. Boosted selective internal radiation therapy with 90Y-loaded glass microspheres (B-SIRT) for hepatocellular carcinoma patients: a new personalized promising concept. Eur J Nucl Med Mol Imaging. 2013;40(7):1057-68.
109. Garin E, Tselikas L, Guiu B, Chalaye J, Edeline J, de Baere T, et al. Personalised versus standard dosimetry approach of selective internal radiation therapy in patients with locally advanced hepatocellular carcinoma (DOSISPHERE-01): a randomised, multicentre, open-label phase 2 trial. Lancet Gastroenterol Hepatol. 2021;6(1):17-29.
110. van den Hoven AF, Rosenbaum CE, Elias SG, de Jong HW, Koopman M, Verkooijen HM, et al. Insights into the Dose-Response Relationship of

Radioembolization with Resin 90Y-Microspheres: A Prospective Cohort Study in Patients with Colorectal Cancer Liver Metastases. J Nucl Med. 2016;57(7):1014-9.
111. Willowson KP, Hayes AR, Chan DLH, Tapner M, Bernard EJ, Maher R, et al. Clinical and imaging-based prognostic factors in radioembolisation of liver metastases from colorectal cancer: a retrospective exploratory analysis. EJNMMI Res. 2017;7(1):46.
112. Alsultan AA, van Roekel C, Barentsz MW, Smits MLJ, Kunnen B, Koopman M, et al. Dose-response and dose-toxicity relationships for yttrium-90 glass radioembolization in patients with colorectal cancer liver metastases. J Nucl Med. 2021.
113. van Roekel C, Bastiaannet R, Smits MLJ, Bruijnen RC, Braat A, de Jong H, et al. Dose-Effect Relationships of (166)Ho Radioembolization in Colorectal Cancer. J Nucl Med. 2021;62(2):272-9.
114. Kao YH, Steinberg JD, Tay YS, Lim GK, Yan J, Townsend DW, et al. Post-radioembolization yttrium-90 PET/CT - part 2: dose-response and tumor predictive dosimetry for resin microspheres. EJNMMI Res. 2013;3(1):57.
115. Chan KT, Alessio AM, Johnson GE, Vaidya S, Kwan SW, Monsky W, et al. Prospective Trial Using Internal Pair-Production Positron Emission Tomography to Establish the Yttrium-90 Radioembolization Dose Required for Response of Hepatocellular Carcinoma. Int J Radiat Oncol Biol Phys. 2018;101(2):358-65.

2. Aims of the thesis

The objective of the thesis is to focus on dosimetry performed in liver radioembolization. Dosimetry refers to the calculation of absorbed doses and its optimization in dose delivery in patients treated by radiation therapy.

In this field, many avenues remain to be explored in RE from the dose planning to the post-treatment evaluation. Optimized dosimetry could result in more effective and safe therapy.

For post-therapy dosimetry, ^{90}Y PET/CT is able to precisely evaluate the liver and individual tumor activity deposition, hence absorbed doses. Our large clinical database accumulated over more than 10 years with a systematic post-therapy PET/CT can be used for dosimetry studies. With this imaging, the dose parameters can be accurately calculated and correlated with the radiological response and the patient outcome. Moreover, the tumor dose deposition at a voxel level can be evaluated to better characterize the effects of radiation in tumors and better understand the factors inducing response to radiation. Besides, glass and resin microspheres have different physical and radioactive characteristics, which can be analyzed and compared using PET/CT.

For the workup, the manufacturers' recommended methods to calculate the activity are semi-empirical, not personalized and can be responsible for underdosing and be ineffective in some patients. MAA imaging is nowadays the only way to perform personalized dosimetry before RE with ^{90}Y microspheres; its

accuracy has to be investigated further in the way of optimizing this activity planning.

Moreover, different types of microcatheters may be used to deliver the radioactive microspheres. One of them, i.e. antireflux catheter is expected to induce changes in the downstream arterial flux and modify the tumor targeting. The effects of this type of catheter was investigated to identify its influence on the tumor dose deposition.

This thesis will evaluate different ways to use dosimetry in RE for the purpose of treatment optimization.

3- Post therapy imaging using Yttrium-90 PET-CT: prediction of tumor response and patient outcome[2]

Abstract

^{90}Y-radioembolization (RE) using glass or resin microspheres is increasingly used for the treatment of hepatocellular carcinoma (HCC). The aim of this retrospective study is to determine the prognostic relevance of dosimetric parameters defined with ^{90}Y-PET-CT obtained immediately following RE.

Methods: Forty-five HCC patients, mostly with multiple lesions were treated by RE between 2011 and 2017. After treatment, all underwent a ^{90}Y PET-CT with time of flight reconstruction (^{90}Y-TOF-PET-CT). Tumor absorbed doses and tumor dose volume histograms (DVH) were calculated using a dose point Kernel convolution algorithm. The radiological tumor response was assessed using modified (m)-RECIST criteria. Threshold absorbed doses for radiological response were determined using ROC curves. Progression-free-survival (PFS) and overall survival (OS) were analyzed using the Kaplan Meier method and Cox regression analysis.

Results: Twenty-six patients were treated with glass microspheres (73 lesions) and nineteen with resin microspheres (60 lesions). Thresholds of 118 Gy and 61 Gy for glass and resin microspheres respectively correlate well with radiological response (PPV: 98% and 80%) and discriminate patient outcome with regard to PFS (P= 0.03

[2] Adapted from d'Abadie et al. Nucl Med Commun. 2021; 42: 747-754

and 0.005) and OS (P= 0.003 and 0.007). Using DVH, a minimal absorbed dose of 40 Gy in 66% of the tumor volume (defined as D_{66}) was highly predictive of radiological response (PPV: 94%), PFS (P<0.001) and OS (P=0.008), for either device.

Conclusion: Dosimetric parameters obtained using ^{90}Y-PET-CT are predictive of tumor response, PFS and OS. In clinical practice, a systematic dosimetric evaluation using ^{90}Y PET should be implemented to help predicting patient outcome.

3.1 Introduction

Early convincing tumor absorbed dose-response correlations were obtained from pre-therapy ^{99m}Tc-MAA (^{99m}Tc-macro-aggregated albumin) SPECT (1-3) and from post-therapy ^{90}Y bremsstrahlung SPECT (4, 5). During the last decade, following the introduction of the more accurate ^{90}Y-PET imaging modality (6, 7) better correlations were found with the absorbed doses (8). Taking into account the dose distribution heterogeneity as observed with the ^{90}Y-PET based D_{70} still improved this correlation (9, 10).

The aim of this study is to assess whether the ^{90}Y-TOF-PET/CT based dose distribution can predict the impact of the radioembolization step within a whole therapy course, i.e.. including the impact of the selection biases between glass

and resin spheres radioembolization, and without censoring the patient of the follow up when performing a further conventional therapy, conventional meaning other than radioembolization.

3.2 Materials and Methods

Patient characteristics and treatments

Data from 48 HCC patients referred to our institution for RE between July 2011 and July 2017 (table 1) were retrospectively analyzed after approval by the local ethics committee (2017/27JUI/334). Three patients were excluded, because of the lack of ^{90}Y-PET-CT imaging (n=2) or uncorrectable motion artifacts (n=1).

Most had intermediate or advanced stage HCC (78%). 26 patients were treated with glass and 19 with resin microspheres. 59 liver RE were performed according to standard guidelines (11). 14 patients received two treatments within an interval ranging from 16h to 16mo. Glass and resin microspheres were used in 34 and 25 treatments, respectively, with a median activity of 2.6 and 1.5 GBq at the injection time. Treatments with glass microspheres were performed one week after ^{90}Y calibration.

Vascular invasion was more frequent in patients treated with glass microspheres (38% *vs* 10%; P<0.05) and especially segmental portal thrombosis. Conversely,

more patients (73% *vs* 35%; P<0.05) treated with resin microspheres had large tumors (size≥ 5 cm).

Table 1: Patients' characteristics

	Glass microspheres	Resin microspheres
Number of patients	26	19
Age (mean ± S.D.)	69 ± 12	71 ± 10
Male / Female (%)	85/15	79/21
Cirrhosis (%)	77	63
Child A/B (%)	77/23	95/5
BCLC A/B/C (%)	23/39/38	21/68/11
Multifocal ≥ 5 (%)	31	47
Vascular invasion (%)* Segmental portal vein (%) Branch portal vein (%) Main portal vein (partial ; %)	**38** 19 8 11	**10** 0 5 5
Tumor size ≥ 5cm (%)*	35	73
Bilobar tumor involvement (%)	42	47
Extra hepatic metastases[+] (%)	4 (lung and bone)	5 (lung)

Therapies before last radioembolization (%)	**65**	**42**
Radiofrequency- alcoholization(%)	8	16
Chemoembolization (%)	31	26
Radioembolization (%)	35	21
Tyrosine-kinase inhibitor (%)	0	11
Liver surgery (%)	4	5
Liver transplantation (%)	0	5
Therapies after last radioembolization (%)	**38**	**37**
External beam radiotherapy (%)	4	0
Chemoembolization (%)	8	16
Tyrosine-kinase inhibitor (%)	15	10
Liver surgery (%)	8	0
Liver transplantation (%)	0	5

* Differences between groups are statistically significant ($P < 0.05$)
+ Detected after radioembolization and not related to death

Dose distribution assessment

Within 20h following RE, a 45-min-^{90}Y-TOF-PET/CT (Gemini TF 16, Philips Medical Systems, Cleveland, OH) was acquired. ^{90}Y activity distribution was transformed into a 3D map of absorbed doses using a previously detailed method (7). In short, reconstruction was performed with the 3-D line of response (LOR)-TOF blob-based Philips algorithm (2 iterations, 33 subsets; reconstructed voxels of $[4mm]^3$). Voxel counts were converted in activity using the PET calibration factor and ^{90}Y positron yield. Absorbed dose distributions of individual tumors were calculated by convolving the ^{90}Y activity distribution with a dose point kernel algorithm, jointly with a spatial resolution recovery (7) .

Lesions were delineated manually on pretherapy imaging using T1-weighted contrast-enhanced MRI (n=50) or arterial contrast enhanced CT-scan (n=8, when there was a contraindication for MRI), using PMOD 3.7 (PMOD Technologies LLC, Zürich, Switzerland). Tumor volumes of interest (VOIs) were fused with the 3D-map of tumor voxel doses on ^{90}Y-PET-CT images using a rigid transformation (PMOD 3.7). For all lesions, a dose-volume histogram (DHV) was computed and also the D_{66} defined as the minimum absorbed dose deposited in 66% of the tumor volume (e.g. Figure 3). A reduction of 66% in viable tumor volume corresponds to a reduction of 30% of the diameter, criterium for radiological response with mRECIST.

A total of 73 and 60 lesions were analyzed after glass and resin microspheres RE, respectively. For lesions treated in the previous 6 months, the absorbed dose was the cumulative dose of both treatments (n=12).

Dosimetric parameters were analyzed retrospectively and did not influence the patient management.

Tumor response evaluation

Only lesions with a transverse axis >10 mm were analyzed. Tumor response was assessed using recommended modified RECIST criteria (mRECIST) at last time point available. Contrast-enhanced MRI or CT scan were obtained every 2 months until progression or death. Targeted lesions were assessed by a senior radiologist

expert in liver tumors, blinded to tumor uptake and dosimetry data. At any time, response was defined as 30% decrease and progression as 20% increase of viable tumor (enhancing during the arterial phase) compared to baseline imaging. Moreover, a stable lesion 6 mo after therapy is categorized as a non-responding lesion. The number (s.d.) of tumors per patient was 2.5 (1.8) and 2 (1.6) in the resin and glass microspheres groups (P= 0.06).

Patient outcome evaluation

Overall survival (OS) was defined as the time between RE (first one if appropriate) and death from any cause. Progression free survival (PFS) was defined as the time from RE to objective progression in the liver or death.

Censoring was applied for patients still alive (OS analysis) or without objective progression, at last radiological time point available (PFS analysis).

Only the largest lesion was analyzed for the OS and PFS in order to avoid excessive partial volume effect on the dose distribution assessment. All lesion sizes were above 20 mm except in one patient (15mm). For univariate and multivariate analyses, all patients were combined using an effective tumor dose D_{eff}. For this purpose, the cutoff for resin microspheres absorbed dose was converted into an "equivalent glass microspheres absorbed dose (Equ. Glass TD)" using a multiplication factor of 1.9, as explained in the discussion section. For univariate analysis, the following variables were evaluated: Equ. Glass TD, D_{66}, portal

thrombosis, bilobar tumor involvement, total bilirubinemia ≥2 mg/dl, Child B score, tumor size ≥5cm, stages BCLC B and C, anemia (Hb ≤ 10 g/dl), age ≥75 years. For multivariate analysis, variables with significant results in the univariate analysis were included.

Statistical analysis

Wilcoxon distribution free comparison test or Student's t test were used to compare groups receiving different devices. Sensitivity (Se) was defined as the ability of the absorbed dose to predict radiological response whereas specificity (Sp) was defined as the ability of the absorbed dose in predicting no radiological response. Absorbed dose thresholds for response were determined using receiver-operating characteristics (ROC) curves, analyzed with a freeware calculator from Johns Hopkins University (12). Kaplan-Meier method with a log-rank test was used for univariate analysis. Cox proportional hazard model was used for uni- and multivariate analyses. Analyses were conducted using Prism (version 7.0, GraphPad Software, La Jolla, Ca) and IBM SPSS statistics software (version 25.0, Armonk, NY). A P value <0.05 was considered significant.

3.3 Results

Tumor response

For glass microspheres, median (range) absorbed doses were 194 Gy (70-1426 Gy) and 95 Gy (51-142 Gy) in responding and progressive lesions, respectively (P<0.001). For resin microspheres, median absorbed doses were 102 Gy (55-568 Gy) and 46 Gy (0.4-314 Gy) in responding and progressive lesions, respectively (P <0.001). An example is given in Figure 1.

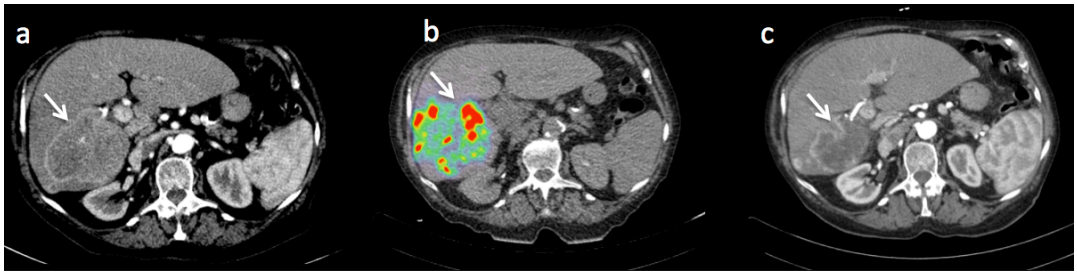

Figure 1: Example of large HCC lesion (white arrow) developed in the right liver on the arterial phase of the contrast enhanced CT scan (a). ^{90}Y PET/CT (b) obtained just after glass microsphere therapy demonstrated an excellent tumor uptake (TD=134 Gy, D_{66}=81 Gy). Four months later, the CT scan confirmed an excellent radiological response with a large tumor necrosis (c).

In responding lesions, the absorbed doses were statistically higher with glass microspheres ($p < 0.001$) with a glass/resin tumor dose ratio of 1.9. ROC curves (Fig. 2-A) demonstrated that the threshold of 118 Gy resulted in the best prediction of tumor response using glass microspheres (Se: 93%; Sp: 75% ; PPV :98%, NPV :50%, AUC: 0.91±0.08); the threshold was 61 Gy using resin microspheres (Se :87%, Sp :64%, PPV :98%, NPV :80%, AUC: 0.88±0.07).

Examples of dose volume histogram (DVH) demonstrating radiological response or progression are seen in Figure 3.

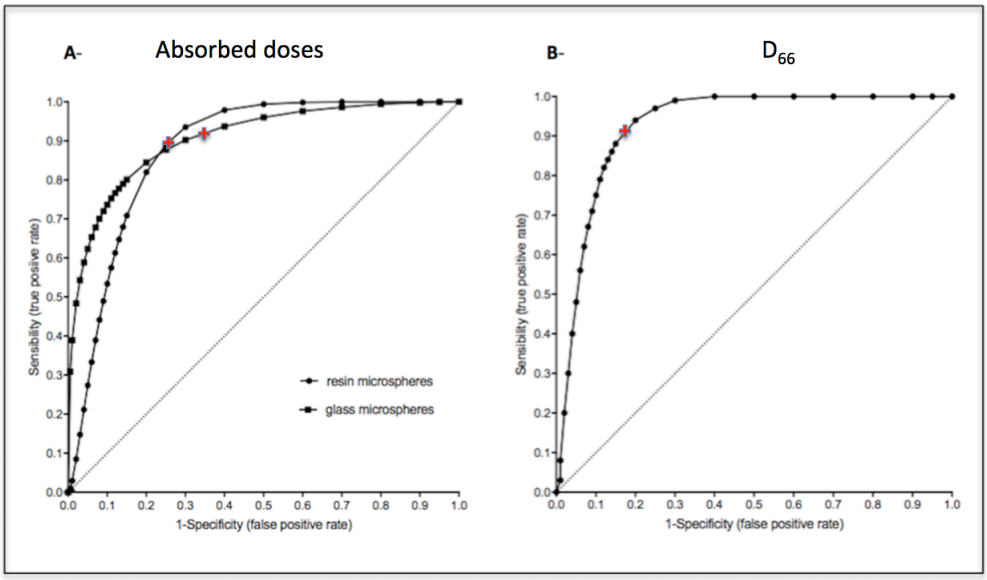

Figure 2: ROC curves for tumor response prediction using the tumor absorbed doses (A) and D_{66} (B). Points of the curves were fitted using specific software (giving slight discordance with thresholds (red crosses) (12). ROC curves analysis for resin and glass sphere radioembolizations together (Fig. 2-B) showed a best

threshold of 40 Gy using D_{66} (Se: 91%, Sp: 78%, PPV: 94%, NPV: 70% and AUC: 0.93±0.05).

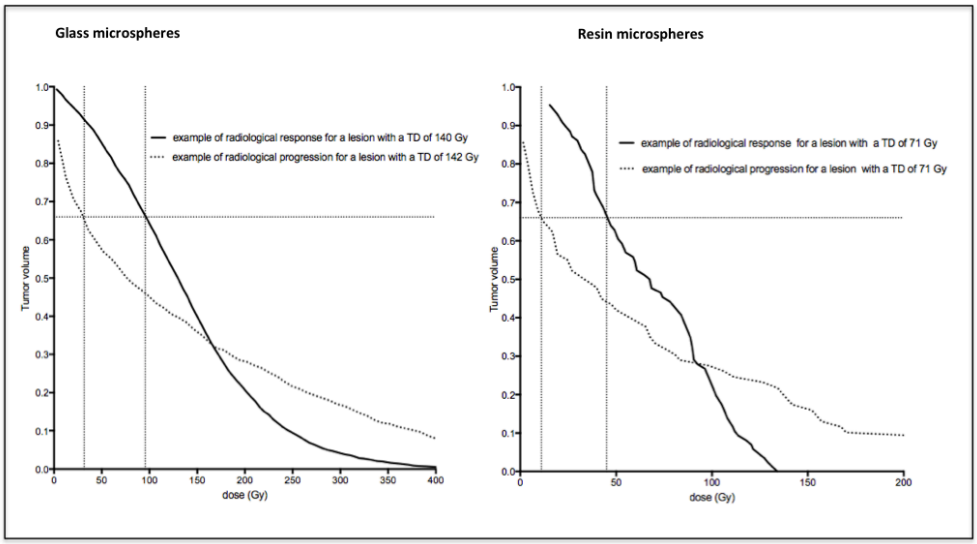

Figure 3: Examples of DVH using glass (left panel) and resin microspheres (right panel). The DVH are shown for examples of tumors with similar absorbed doses but different radiological responses. Using glass microspheres and two lesions with similar absorbed doses (140-142 Gy), the responding lesion has a DVH characterized by D_{66}=96 Gy (continuous line) and the progressive lesion has a DVH characterized by D_{66}=31 Gy (grid lines). A similar behavior is found using resin microspheres for which the absorbed dose is lower ie. 71 Gy.

Survival Analysis

Table 2 summarizes median OS and PFS for glass and resin microspheres treatments. Tumor control and patient survival were strongly correlated to the tumor absorbed doses, with a clear discrimination using threshold doses of 118 Gy and 61 Gy with glass and resin microspheres respectively.

Table 2: Overall survival and progression-free survival.

	Glass			Resin			D_{66} (resin & glass)		
	< 118 Gy	≥ 118 Gy	all	< 61 Gy	≥ 61 Gy	all	< 40 Gy	≥ 40 Gy	all
Number of patients	7	19	26	5	14	19	13	32	45
Median OS (mo)	5.6	14.6^{+}	12.3	5.3	16^{+}	13.4	6.5	16^{+}	12.4
Median PFS (mo)	1.8	5.5*	3	1.6	4.6^{+}	2.9	1.8	5.4°	2.9

P< 0.05* P< 0.01^{+} P< 0.001°

Kaplan-Meier curves of OS and PFS (Figure 4) demonstrated also the significant discrimination between groups.

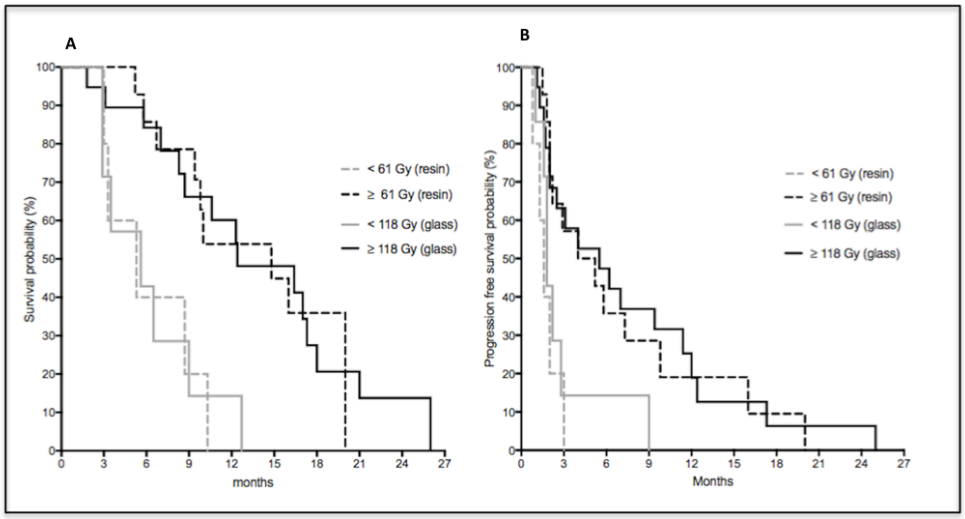

Figure 4: Kaplan-Meier analyses for OS (A) and PFS (B) using tumor absorbed doses. See table 2 for P values.

Using the same cutoff of 40 Gy for either type of microspheres, a similar discrimination was found with D_{66} (table 2 and figure 5). Accordingly, D_{66}<40 Gy was analysed for all patients using the Kaplan- Meier method (table 2) and uni/multivariate Cox analyses (table 3).

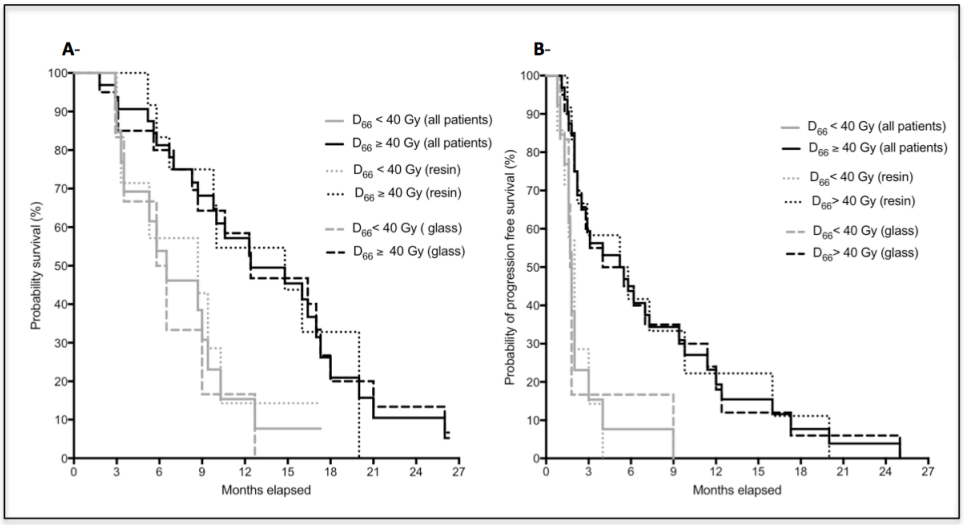

Figure 5: Kaplan-Meier analyses for OS (A) and PFS (B) using D_{66}.

As shown in Table 3, univariate analysis of OS demonstrated that Equ. glass TD <118 Gy, D_{66}<40 Gy and portal thrombosis correlated with worse prognosis using the Cox regression. Only Equ. glass TD <118 Gy and D_{66}<40 Gy correlated with worse PFS using univariate analysis.

Only Equ. glass TD <118 Gy and portal thrombosis were statistically associated with a worse OS in the multivariate analysis. D_{66} and Equ. Glass TD are both dosimetric parameters and matched similarly with the patient outcome, explaining why only one of them is statistically significant at the multivariate analysis. Thus, D_{66} was secondarily analyzed in a second multivariate analysis excluding equ. glass TD (table 4). Then, this parameter became significant for the OS analysis.

Table 3: Overall survival and progression-free survival Cox analyses

&	Factors	Univariate analysis		Multivariate analysis	
		HR* (95% CI)	P value	HR* (95% CI)	P value
OS	Equ. glass TD^+ < 118 Gy	5.9 2.6-13.7)	< 0.001	17.9 (3.2-100)	< 0.001
	D_{66} < 40 Gy	2.9 (1.4-6.1)	0.006	0.3 (0.1- 1.7)	0.18
	Portal thrombosis	2.9 (1.3-6.4)	0.07	3.5 (1.4- 9.1)	0.01
PFS	Equ. Glass TD^+ < 118 Gy	3.3 (1.6-6.8)	0.001	1.8 (0.6- 5.5)	0.28
	D_{66} < 40 Gy	3.4 (1.7-7)	0.001	2.3 (0.7-7.0)	0.15

HR* : Hazard Ratio. Equ. glass TD^+ : Equivalent glass microsphere tumor absorbed mean dose

Table 4: Overall survival Cox analyses after exclusion of Equ. Glass TD

	Factors	Univariate analysis		Multivariate analysis	
		HR* (95% CI)	P value	HR* (95% CI)	P value
OS	D_{66} < 40 Gy	2.9 (1.4-6.1)	0.006	2.8 (1.3-6.0)	0.008

	Portal thrombosis	2.9 (1.3-6.4)	0.07	2.8 (1.3-6.2)	0.01

3.4 Discussion

The three main findings of this study can be summarized as follows. First, a relationship between ^{90}Y-PET based tumor absorbed doses and patient outcome is established. Second, the difference in efficiency per absorbed dose between glass- and resin-microspheres is confirmed. Third, the DVH analysis, using $D_{66,}$ clearly highlights that the heterogeneity of tumor deposition is an essential parameter of clinical outcome.

Based on ROC curves analysis (Fig. 2-A), the best absorbed dose cutoffs for responses according to mRECIST criteria were 61 Gy and 118 Gy for resin and glass microspheres, respectively. This represents a 1.9 ratio between glass and resin microspheres. By multiplying the absorbed dose of each individual tumor treated with resin microspheres by this 1.9 factor, while keeping the absorbed dose value for glass sphere, we generated an effective dose which was further input in the uni- and multivariate analyses. This 118 Gy effective dose cutoff applied to patients treated with either device, results in the best prediction factor in the multivariate analysis for OS, but not for PFS. This 1.9 factor is in agreement with previous data comparing glass and resin microspheres regarding toxicity,

efficiency and clinical outcome. For liver toxicity, the tolerable whole liver absorbed dose has been reported to be 40 Gy with resin and 70 Gy for glass microspheres (factor: 1.8) (8). Monte-Carlo simulations of the microspheres transport from the catheter tip provide a theoretical explanation of this feature (12) nicely confirmed in an animal model (13).

A strong correlation between HCC absorbed doses and efficiency was demonstrated with MAA imaging using a tumor absorbed dose of 205 Gy with glass microspheres and 100 Gy with resin microspheres (factor: 2.05) (14, 15).

The 118 Gy-threshold for glass radioembolization is remarkably lower than MAA-SPECT based 205 Gy-threshold found by Garin et al. (14). Beside the numerous differences in the absorbed doses assessment, a careful analysis of this study shows that this 205 Gy value was especially highly discriminating in patients with portal vein thrombosis (2-8 months survival for TD<205Gy versus 9.5-27 months survival for TD > 205Gy). For the overall patient population the large overlap in survival (3-24 months for TD<205Gy versus 15-27 months for TD > 205Gy) indicates that this threshold value is likely too high. Moreover, Garin et al. used a different method to estimate the tumor volume, an isocontour method based only on MAA SPECT/CT, which exclude the hypoperfused parts of the tumor receiving less absorbed doses(16). In our study, the tumor volume was defined with conventional imaging (CT scan or MRI) and could take into account some necrotic area, which decrease the calculation of the absorbed dose.

The same cutoff of mean absorbed dose (61 Gy) using resin microspheres was correlated with tumor control in the study of Alimant et al., performed with a similar dosimetric method (17, 18).

It is well known that absorbed doses needed for efficient radioembolization are higher than those needed with external beam radiotherapy, either conventional or stereotactic. The main cause is the heterogeneous dose distribution, depending of the arterial tumor microvasculature for RE. Analysis of ^{90}Y-TOF-PET based DVH can explain why some tumors progress despite high average absorbed dose (heterogeneous distribution) and why some tumors respond despite lower average absorbed doses (homogeneous distribution) (see Fig. 3). Owing to its excellent spatial resolution, ^{90}Y-TOF-PET has the ability to assess the tumor dose deposition at the voxel level (19, 20). Monte Carlo simulations of microspheres in the hepatic arterial tree also confirmed a good matching between the spheres distribution texture and ^{90}Y-TOF-PET imaging (21, 22).

In our study, prediction was improved, regarding OS and PFS, using a D_{66} cutoff of 40 Gy for both types of microspheres (Fig. 2B). This D_{66} cutoff reconciles dose levels between external beam radiotherapy (EBRT) and RE (23). D_{70} has already been used in order to predict patient outcome. In a series of 8 patients, Kao et al (9) reported a D_{70} threshold of 100Gy in order to obtain a complete response. However, in line with our study, Flower et al. (10) reported an optimal D_{70} threshold of 42Gy for predicting response in 24 patients treated by resin or glass

microspheres. It could look weird that observing only 66% of the tumor volume above 40Gy is the best cutoff to differentiate good or worse patient outcome while it is commonly observed in EBRT that 100% of the tumor volume has to be above 40Gy in order to get a satisfactory response. Three factors could explain this apparent discrepancy. First, the tumor VOI used to compute the based voxel dose can include small necrotic regions not tapping microspheres, which does not impact the outcome. Second, measured voxel dose at the boundary of the tumor are artificially reduced as a result of the limited spatial resolution of human PET imaging. Last, inside the tumor, some measured voxel doses can also be artificially reduced by statistical fluctuations inherent to acquisition of nuclear decays. All those effects together could explain, in the patient group with more favorable outcome, that although 34% of the tumor volume appears to have received less than the 40Gy threshold with PET imaging, in reality almost all the viable tumor volume received at least 40Gy. This assumption could be evaluated by high resolution PET/CT imaging of excised radioembolized tumors in an animal model.

Recent randomized controlled trials failed to demonstrate a superiority of RE compared to sorafenib in advanced hepatocellular carcinoma (24, 25). No significant differences in OS and PFS were demonstrated in RE and sorafenib arms. However, RE was significantly better tolerated compared to sorafenib with a reduction of the frequency and the severity of side effects (26). Regarding the dosimetric methodology of these trials, the planned activity was based on an

empirical method, the body surface area, without any goal in tumor absorbed dose targeting. This activity planification is known to be responsible of underdosing tumors in many cases (27, 28). A recent secondary analysis of the SARAH trial demonstrated that higher tumor absorbed dose, using MAA SPECT-CT, was associated with better OS in HCC (15). Also, as previously demonstrated with a dosimetry based on MAA SPECT (14, 15), ^{90}Y SPECT(5) or recent data using ^{90}Y-PET (29), we found a strong relationship between measured tumor absorbed doses and clinical response. In future prospective trials, tumor absorbed dose evaluation should clearly be taken into account to allow anticipate better outcome as compared to other therapies available in HCC.

Study limitations

This study suffers from some limitations related to its retrospective nature. First, the choice of the device was not randomized and was clinically driven. Glass microspheres were mostly used in more aggressive HCC lesions (with vascular invasion). Second, patients were allowed later on to any therapy following RE, which happened in more than one out of three patients. It should be noted however that similar therapies were offered after glass and resin microspheres.

Conclusion

These results demonstrate the importance of tumor dose analysis after RE in HCC using ^{90}Y-PET. A systematic evaluation of dose parameters could predict radiological response and patient outcome directly after treatment. In case of low estimated absorbed doses, patient management could be reevaluated and adapted quickly even before radiological response assessment.

References

1. Flamen P, Vanderlinden B, Delatte P, Ghanem G, Ameye L, Van Den Eynde M, et al. Multimodality imaging can predict the metabolic response of unresectable colorectal liver metastases to radioembolization therapy with Yttrium-90 labeled resin microspheres. Phys Med Biol. 2008;53(22):6591-603.
2. Garin E, Lenoir L, Rolland Y, Edeline J, Mesbah H, Laffont S, et al. Dosimetry based on 99mTc-macroaggregated albumin SPECT/CT accurately predicts tumor response and survival in hepatocellular carcinoma patients treated with 90Y-loaded glass microspheres: preliminary results. J Nucl Med. 2012;53(2):255-63.
3. Chiesa C, Maccauro M, Romito R, Spreafico C, Pellizzari S, Negri A, et al. Need, feasibility and convenience of dosimetric treatment planning in liver selective internal radiation therapy with (90)Y microspheres: the experience of the National Tumor Institute of Milan. Q J Nucl Med Mol Imaging. 2011;55(2):168-97.
4. Strigari L, Sciuto R, Rea S, Carpanese L, Pizzi G, Soriani A, et al. Efficacy and toxicity related to treatment of hepatocellular carcinoma with 90Y-SIR spheres: radiobiologic considerations. J Nucl Med. 2010;51(9):1377-85.
5. Kappadath SC, Mikell J, Balagopal A, Baladandayuthapani V, Kaseb A, Mahvash A. Hepatocellular Carcinoma Tumor Dose Response After (90)Y-radioembolization With Glass Microspheres Using (90)Y-SPECT/CT-Based Voxel Dosimetry. Int J Radiat Oncol Biol Phys. 2018;102(2):451-61.
6. Lhommel R, Goffette P, Van den Eynde M, Jamar F, Pauwels S, Bilbao JI, et al. Yttrium-90 TOF PET scan demonstrates high-resolution biodistribution after liver SIRT. Eur J Nucl Med Mol Imaging. 2009;36(10):1696.

7. Lhommel R, van Elmbt L, Goffette P, Van den Eynde M, Jamar F, Pauwels S, et al. Feasibility of 90Y TOF PET-based dosimetry in liver metastasis therapy using SIR-Spheres. Eur J Nucl Med Mol Imaging. 2010;37(9):1654-62.
8. Cremonesi M, Chiesa C, Strigari L, Ferrari M, Botta F, Guerriero F, et al. Radioembolization of hepatic lesions from a radiobiology and dosimetric perspective. Front Oncol. 2014;4:210.
9. Kao YH, Steinberg JD, Tay YS, Lim GK, Yan J, Townsend DW, et al. Post-radioembolization yttrium-90 PET/CT - part 2: dose-response and tumor predictive dosimetry for resin microspheres. EJNMMI Res. 2013;3(1):57.
10. Fowler KJ, Maughan NM, Laforest R, Saad NE, Sharma A, Olsen J, et al. PET/MRI of Hepatic 90Y Microsphere Deposition Determines Individual Tumor Response. Cardiovasc Intervent Radiol. 2016;39(6):855-64.
11. Padia SA, Lewandowski RJ, Johnson GE, Sze DY, Ward TJ, Gaba RC, et al. Radioembolization of Hepatic Malignancies: Background, Quality Improvement Guidelines, and Future Directions. J Vasc Interv Radiol. 2017;28(1):1-15.
12. Walrand S, Hesse M, Jamar F, Lhommel R. A hepatic dose-toxicity model opening the way toward individualized radioembolization planning. J Nucl Med. 2014;55(8):1317-22.
13. Pasciak AS, Abiola G, Liddell RP, Crookston N, Besharati S, Donahue D, et al. The number of microspheres in Y90 radioembolization directly affects normal tissue radiation exposure. Eur J Nucl Med Mol Imaging. 2019.
14. Garin E, Rolland Y, Pracht M, Le Sourd S, Laffont S, Mesbah H, et al. High impact of macroaggregated albumin-based tumour dose on response and overall survival in hepatocellular carcinoma patients treated with (90) Y-loaded glass microsphere radioembolization. Liver Int. 2017;37(1):101-10.
15. Hermann AL, Dieudonne A, Ronot M, Sanchez M, Pereira H, Chatellier G, et al. Relationship of Tumor Radiation-absorbed Dose to Survival and Response in Hepatocellular Carcinoma Treated with Transarterial Radioembolization with (90)Y in the SARAH Study. Radiology. 2020;296(3):673-84.
16. Garin E, Lenoir L, Rolland Y, Laffont S, Pracht M, Mesbah H, et al. Effectiveness of quantitative MAA SPECT/CT for the definition of vascularized hepatic volume and dosimetric approach: phantom validation and clinical preliminary results in patients with complex hepatic vascularization treated with yttrium-90-labeled microspheres. Nucl Med Commun. 2011;32(12):1245-55.
17. Allimant C, Kafrouni M, Delicque J, Ilonca D, Cassinotto C, Assenat E, et al. Tumor Targeting and Three-Dimensional Voxel-Based Dosimetry to Predict Tumor Response, Toxicity, and Survival after Yttrium-90 Resin Microsphere Radioembolization in Hepatocellular Carcinoma. J Vasc Interv Radiol. 2018;29(12):1662-70 e4.
18. Walrand S, Chiesa C, Gabina PM, Chouin N, Gear J, Stokke C, et al. Re: Tumor Targeting and Three-Dimensional Voxel-Based Dosimetry to Predict Tumor

Response, Toxicity, and Survival after Yttrium-90 Resin Microsphere Radioembolization in Hepatocellular Carcinoma. J Vasc Interv Radiol. 2019;30(12):2047-8.
19. Walrand S HM. PET/CT Specificities in 90Y Imaging Post Radioembolization. PET clinics. 2019;14(4):469-76.
20. Hesse M, Walrand S. Significant artefactual noise in (90)Y TOF-PET imaging of low specific activity phantoms arises despite increased acquisition time. EJNMMI Phys. 2019;6(1):20.
21. Walrand S, Hesse M, Chiesa C, Lhommel R, Jamar F. The low hepatic toxicity per Gray of 90Y glass microspheres is linked to their transport in the arterial tree favoring a nonuniform trapping as observed in posttherapy PET imaging. J Nucl Med. 2014;55(1):135-40.
22. Crookston N. FG, Frey E. Development of a customizable hepatic arterial tree and particle transport model for use in treatment planning. IEEE TRANSACTIONS ON RADIATION AND PLASMA MEDICAL SCIENCES. 2019;3(1).
23. Sanuki N, Takeda A, Kunieda E. Role of stereotactic body radiation therapy for hepatocellular carcinoma. World J Gastroenterol. 2014;20(12):3100-11.
24. Vilgrain V, Pereira H, Assenat E, Guiu B, Ilonca AD, Pageaux GP, et al. Efficacy and safety of selective internal radiotherapy with yttrium-90 resin microspheres compared with sorafenib in locally advanced and inoperable hepatocellular carcinoma (SARAH): an open-label randomised controlled phase 3 trial. Lancet Oncol. 2017;18(12):1624-36.
25. Chow PKH, Gandhi M, Tan SB, Khin MW, Khasbazar A, Ong J, et al. SIRveNIB: Selective Internal Radiation Therapy Versus Sorafenib in Asia-Pacific Patients With Hepatocellular Carcinoma. J Clin Oncol. 2018;36(19):1913-21.
26. Sposito C, Mazzaferro V. The SIRveNIB and SARAH trials, radioembolization vs. sorafenib in advanced HCC patients: reasons for a failure, and perspectives for the future. Hepatobiliary Surg Nutr. 2018;7(6):487-9.
27. Bastiaannet R, Kappadath SC, Kunnen B, Braat A, Lam M, de Jong H. The physics of radioembolization. EJNMMI Phys. 2018;5(1):22.
28. Garin E, Palard X, Rolland Y. Personalised Dosimetry in Radioembolisation for HCC: Impact on Clinical Outcome and on Trial Design. Cancers (Basel). 2020;12(6).
29. Dewaraja YK, Devasia T, Kaza RK, Mikell JK, Owen D, Roberson PL, et al. Prediction of Tumor Control in (90)Y Radioembolization by Logit Models with PET/CT-Based Dose Metrics. J Nucl Med. 2020;61(1):104-11.

4- Post-therapy imaging using Yttrium-90 PET-CT: assessment of the microsphere distribution at voxel level[3]

Abstract

Clinical studies reported a twofold ratio between the efficacy per Gy of resin versus glass spheres. Our aim is to investigate whether this difference could result from the different degrees of heterogeneity in sphere distribution between the two medical devices. The ^{90}Y TOF-PET based equivalent uniform doses (EUD) was used for this purpose.

Method: 58 consecutive HCC radioembolizations were retrospectively analyzed. Absorbed doses D and Jones-Hoban EUD in lesions were computed. Radioembolization efficacy was assessed using Kaplan-Meier survival curves.

Results: In order to match together the glass and resin spheres survival curves using a 40Gy-threshold, an efficacy factor of 0.73 and 0.36 had to be applied to the absorbed doses, respectively. Using EUD, a nice matching between glass and resin survival curves was obtained with a better separation of the responding and not responding survival curves.

Conclusion: The results clearly support the fact that the activity heterogeneity observed in ^{90}Y TOF-PET post radioembolization does not only result from

[3] Adapted from d'Abadie et al. Phys. Med. Biol. 2018; 63:245010 and Hesse et al. Front Oncol. 2021;11:592529

statistical noise, but also reflects the actual heterogeneity of the spheres distribution. Use of EUD reunifies the efficacy of the two medical devices.

4.1 Introduction

Review of clinical studies reported a twofold ratio between the toxicities per Gy of resin and of glass spheres (1), i.e. a whole liver tolerable dose of 70Gy for glass spheres(2) and of 40 Gy for resin spheres (3-6). Monte Carlo (MC) simulations of spheres transport in hepatic arterial tree (7-9) evidenced that glass spheres give a more heterogeneous dose distribution that quantitatively explains the difference in liver toxicity (7). The sphere distribution measured in liver biopsies post radioembolization (10) was in agreement with the MC simulations (11).

A twofold absorbed dose efficacy ratio has also been reported (12) when comparing the results of glass and of resin sphere radioembolization studies in HCC (3, 13). The aim of this study is to investigate whether this difference is also linked to the sphere distribution heterogeneity in the tumor's. This distribution cannot be modelled in a meaningful way regarding the anarchic tumor vasculature. Thus, the patient survival probability was predicted by the uniform equivalent dose (EUD) computed from the tumor activity distribution assessed by ^{90}Y TOF-PET imaging.

4.2 Material and methods

Radioembolizations

A total of 58 consecutive liver radioembolizations (see supplemental material) in 45 patients with HCC imaged by ^{90}Y TOF-PET were retrospectively analyzed under approval of the local ethics committee. Patient CHILD scores were A5 (n=30), A6 (n=8), B7 (n=2), B8 (n=4) and B9 (n=1). The radioembolizations were performed according to the standard liver radioembolization guidelines(14). Glass and resin spheres were used in 33 and 25 radioembolizations with a mean activity of 2.6 and 1.5 GBq, respectively. No decaying was applied on the sphere vials before radioembolization, i.e. specific activity at the treatment day of resin and glass sphere was about 50 and 2500 Bq, respectively.

A 45-min ^{90}Y TOF-PET scan (Gemini TF, Philips Medical Systems, Cleveland, OH, USA) was performed within 4 h (n=55) or within 16h (n=3) following the radioembolization.

Dose assessment

Voxel absorbed dose distribution was assessed using a validated scheme (15). In summary: ^{90}Y activity distribution was reconstructed using the vendor 3D line of response (LOR)–TOF blob-based reconstruction algorithm with 2 iterations and 33 subsets and a 4×4 mm^3 voxel size. Afterwards, an expectation maximization (EM) based spatial resolution recovery was applied. This spatial resolution correction post reconstruction was shown to provide similar recovery coefficients than that

observed from other PET systems including a PSF modelling in the reconstruction (16). Last, the activity distribution was convolved with the ^{90}Y dose kernel distribution in water taking into account the continuous beta energy spectrum (17).

Volume of interest (VOI) was drawn on up to the 9 biggest lesions, if any, using the MRI (n=50) or injected CT scan (n=8) and further fused on the ^{90}Y TOF-PET image. Two dosimetry quantities in the tumor VOIs were evaluated:

The effective absorbed dose D_{eff} obtained by multiplying the conventional mean absorbed dose D with an efficacy factor (a_{dev}) depending on the medical device, i.e.:

$$D_{eff} = a_{dev}\, D \qquad \text{(Equation 1)}$$

The Jones and Hoban EUD (18), which is the uniform dose that would give the same survival fraction than that resulting from the actual dose distribution, i.e:

$$EUD = -\frac{1}{\alpha}\, ln\left(\frac{\sum_i e^{-\alpha D_i}}{N}\right) \qquad \text{(Equation 2)}$$

where D_i is the absorbed dose in the voxel i inside the tumor VOI, α is the HCC cell radiosensitivity and N the number of voxels contained in the tumor VOI. Regarding equation 2, EUD takes into account the dose in each voxel of the tumor

(D_i) with a reverse exponential correlation. EUD drops exponentially when D_i is small. In other words, the more the tumor dose deposition is heterogeneous (low doses in voxels) and the more EUD strongly decreases.

The α parameter derives from the linear quadratic radiobiological model and defines the sensibility of tumor cells to radiation. The surviving fraction (SF) of clonogenic cells depends on the radiation dose D and the cell radiosensibility defined by the α parameter as follows:

$$SF = e^{-\alpha D} \quad \text{(Equation 3)}$$

The α parameter can be measured in tumor cell lines (in vitro) or estimated in vivo based the clinical efficacy to radiation. However, a large variability of α values was measured, depending on the study design and on the tumor properties (tumor histology, hypoxia…)(19). Besides, the α parameter was estimated in this study, defining the best correlation between the dose and the probability survival of patients.

Efficacy assessment

Efficacy of each medical device was assessed by analyzing the patient survival probability. In this analyze a total of 26 radioembolizations were censored due to an additional treatment performed in the patient (see supplemental material), i.e. were withdrawn at that time from the curve and from the overall number of

patients. These additional treatments were: additional radioembolization performed in order to target a novel lesion (n=13); sorafenib (n=4); chemotherapy (n=3); additional external beam radiotherapy (EBRT) (n=1); additional chemo-embolization (n=2); transplantation (n=1); hepatectomy (n=2). Three radioembolizations were censored, the patient being still alive.

A set of Kaplan-Meyer survival curves for the D_{eff} and *EUD* of the largest lesion being below and above a 40Gy-threshold were computed from a wide range of discrete radiobiological α_{dev} and α values, respectively. The use of this 40Gy-threshold derived from EBRT is justified by the fact that the efficacy reduction resulting from the sphere distribution heterogeneity has to be taken into account by equations (equ. 1 & 2). The mean tumor diameter was 5.2 ± 3.2 cm (see supplemental material).

Choice of the optimal radiobiological values

The optimal radiobiological values were chosen as the α_{dev} and α values corresponding to the Kaplan-Meyer probability survival curves showing the best agreement between the two medical devices, while preserving a clear separation between the overall survival fraction (OSF) curves corresponding to D_{eff} and *EUD* lower and higher than a 40Gy-threshold, respectively, i.e. by maximizing the objective function (O):

$$O = \frac{\sum_t \left|OSF_{res}^{<}(t) - OSF_{res}^{\geq}(t)\right|^2 + \sum_t \left|OSF_{glass}^{<}(t) - OSF_{glass}^{\geq}(t)\right|^2}{\sum_t \left|OSF_{res}^{<}(t) - OSF_{glass}^{<}(t)\right|^2 + \sum_t \left|OSF_{res}^{\geq}(t) - OSF_{glass}^{\geq}(t)\right|^2}$$

(equation 3)

Where *t* is the delay post radioembolization.

The justification of computing a set of Kaplan-Meyer probability survival curves for a wide range of discrete radiobiological α_{dev} and α values is linked to the fact that the objective function O is not a continuous function. Conventional fitting algorithms estimating the objective function derivative are not adapted to this feature. Dose parameters were compared using a Wilcoxon

4.3 Results

Figure 1 shows the probability survival curves for the two medical devices and using the two dosimetry quantities (equ. 1 & 2). The fitted efficacy factors were a_{res} = 0.73 and a_{glass} = 0.36, while the objective function O held on a maximal plateau for α ranging from 0.034 to 0.038 Gy^{-1}. Figure 1A shows that it is required to assume different medical device efficacies in order to get similar survival curves. Figure 1B shows that the agreement between resin and glass survival curves is further improved when using the EUD (equ. 2) with a single fitted parameter rather than using the two empirical efficacy factors (1).

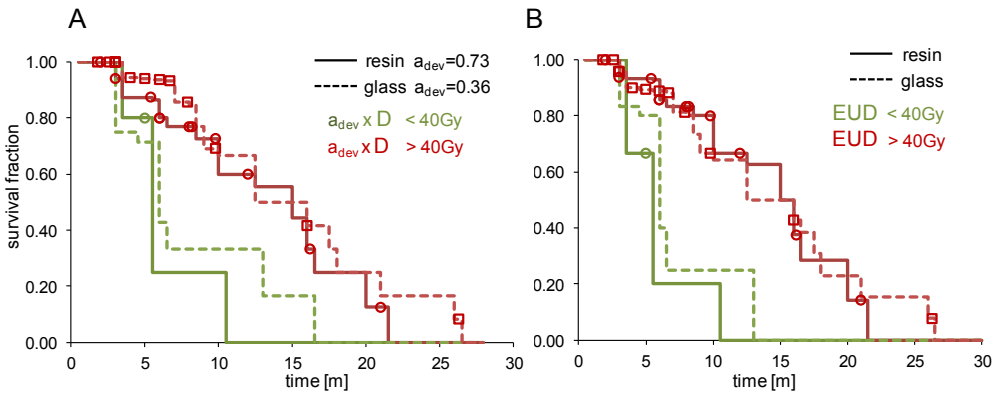

Figure 1: A and B: Kaplan-Meyer survival fraction curves using D_{eff} (equ.1) and EUD (equ.2) of the biggest lesion below (green) and upper (red) the 40Gy-threshold. Solid and dashed lines correspond to resin and glass sphere, respectively. Open symbols correspond to censored radioembolizations. Figure 1B was constructed using α values with a range from 0.034 to 0.038 Gy^{-1}.

Taking into account the fitted efficacies (Figure 1A), the optimal efficacies factors (a_{dev}) in order to get a good match between resin and glass sphere probability survival curves, while preserving a clear separation between not responding and responding patients, are 0.73 for resin microspheres (corresponding to an absorbed dose of 55 Gy) and 0.36 for glass microspheres (corresponding to an absorbed dose of 111 Gy).

Table 1 summarizes the tumor absorbed dose D and EUD in the 45 patients of the study.

Table 1: Comparison of the dose parameters

	Median	Confidence Interval 95%
D (Gy)	139	97-198
EUD (Gy)	59	48-76

Figure 2 shows the correspondence between the absorbed dose D and the EUD for the tumors having an absorbed dose lower than 120 Gy, i.e. in the region surrounding the 40Gy-threshold when taking into account the dose efficacy.

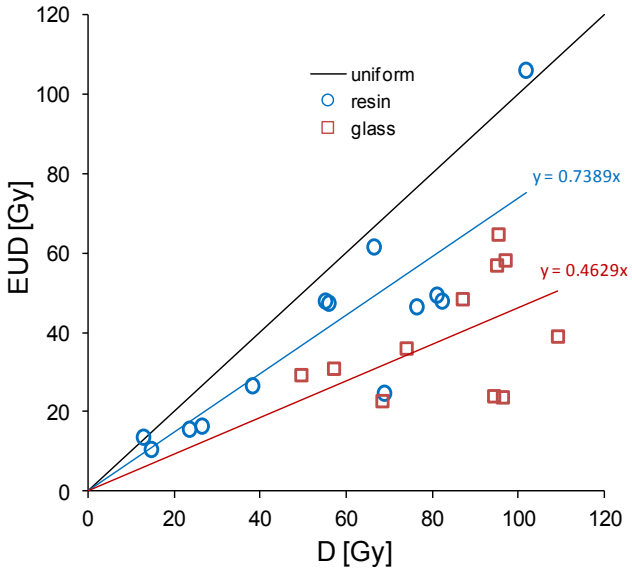

Figure 2: EUD as a function of the absorbed dose D in the range 0-120 Gy. In order to get a similar EUD, glass spheres (red squares) require an absorbed dose D about twofold higher than that of resin spheres (blue circles). A uniform absorbed dose would be the identity line.

4.4 Discussion

This study demonstrates a two-fold efficacy factor between resin and glass microspheres (demonstrated by the efficacy factors; Figure 1A), in line with that reported in previous studies (3, 12, 13).

Assessing the optimal predictive clinical dose threshold between responding and no responding patients was not the purpose of this study. Clinicians are mainly interested in evaluating the impact of a specific medical device radioembolization within a whole treatment frame. Thus, this assessment is usually performed without aiming to get similar survival curves for the two medical devices, and without censoring the radioembolization follow up when the patient get an additional therapy. However, despite these two additional constraints, overall survival duration of responding patients in this study are about twofold that of not responding.

Similar probability survival curves, jointly with a better agreement between the two medical devices, are directly obtained using the EUD for a radiosensitivity of HCC cells ranging from 0.034 to 0.038 Gy^{-1} (corresponding to the α values used to calculate EUD in Figure 1B). The fact that a maximal plateau was found rather than a maximal peak is explained by the fact that Kaplan-Meier curves and the objective function O remain constant until a small variation of the radiosensitivity α shifts one patient from one curve to another.

The 40 Gy dose threshold is commonly used for many cancer types in EBRT where the dose distribution is homogeneous. A retrospective study in 155 patients treated by EBRT for HCC also showed that 40 Gy was the minimal threshold in order to observe some patients with a survival longer than 3 years (20). A recent review confirm also the efficacy of this cumulative dose in HCC (21). The successful utilization of this threshold in this study further supports the correct handling by the TOF-PET based EUD of the dose distribution heterogeneities arising in radioembolization. The relation between EUD and absorbed dose D (Figure 2) clearly evidenced that glass spheres distribution in tumour is more heterogeneous than that of resin spheres, explaining the twofold efficacy ratio. The linear fit of EUD versus D gave slopes in line with the medical device efficacies.

We also investigated the impact of using the voxel BED instead of the voxel D (equ.2) as originally proposed by Jones and Hoban (18). In agreement with Chiesa et al. (22), using α/β = 10Gy and a repair half-life of 1.5h (3), only a slight difference between EUD and EUDBED was found (see supplemental material). This results from the fact that for a heterogeneous dose distribution, the cell survival fraction is mainly given by the voxels receiving the small doses for which BED≈D.

The 40 Gy given in EBRT per 2 Gy fractions corresponds to a BED of 48 Gy. However, using the EUD-BED with this 48 Gy BED threshold, the same optimal

Kaplan-Meier curves than those of Figure 1B were found but for a radiosensitivity ranging from 0.026 to 0.031 Gy. This observation means that due to the step behavior of the Kaplan-Meier curves resulting in a finite number of different survival curves, the patient series is too limited in order to probe the quadratic dependence of the radiobiological effects.

Table 1 summarizes the different assessments of the radiosensitivity α reported in the literature.

Table 1: Values of radiosensitivity α parameter reported in the literature for HCC

Studies	derived from	α [Gy^{-1}]	input distribution:	spatial resolution
Strigari et al. 2010 (3)	human in vivo	0.001	tumour mean dose	tumour diameter
Chiesa et al. 2015 (22)	human in vivo	0.003	^{99m}TcMAA-SPECT/CT	≈1.5 cm
this study EUDBED	human in vivo	0.026-0.031	^{90}Y TOF-PET/CT	≈0.7 cm
this study EUD	human in vivo	0.034-0.038	^{90}Y TOF-PET/CT	≈0.7 cm
Wigg et al. 2010 (23)	cell assay	0.1-0.43	uniform irradiation	cell level

Tai et al. 2008 (24)	Human in vivo	0.01-0.04	uniform irradiation (EBRT)	Tumor diameter

The α value measured by Strigari et al. (3) in human HCC radioembolization is 2 orders of magnitude lower than those measured in cell assay (23) and 1 order lower than those measured in patients treated by external radiotherapy (24) (Table 1). Indeed Strigari et al. neglected the tumor dose heterogeneity and computed the tumor control probability (TCP) by directly multiplying the mean tumor dose by α. Thus, this α value does not only take into account the intrinsic cell radiosensitivity, but also the reduction of the dose efficacy resulting from the heterogeneous distribution. Besides, the lower α value of Chiesa et al. (22) was found using ^{99m}TcMAA-SPECT/CT for the tumor dose distribution. SPECT and PET imaging takes into account the intra-tumor voxel dose distribution up to a certain point depending on their effective spatial resolution. Interestingly, our HCC cell radiosensitivity coefficient obtained with 90Y TOF-PET/CT based EUD is within the ranges reported in EBRT, i.e. 0.01-0.04 Gy^{-1} (table 1).

These results support that the activity heterogeneities observed in ^{90}Y TOF-PET post radioembolization do not only arise from statistical noise, but mainly represent the actual spheres distribution. This was already evidenced in liver tissue by MC simulations of spheres transport in the hepatic arterial tree (7, 9) in which simulated sphere distribution texture matched that observed in ^{90}Y TOF-

PET imaging. This was still more expected in tumor tissue that takes up about fourfold more spheres per g than the liver tissue, which results in lower statistical noise. Moreover, our group confirm very recently this prediction in a work performed with phantom acquisitions(25). For rods with a diameter above 9mm, a good agreement was found between the EUD estimated with ^{90}Y-TOF-PET and the true EUD defined in a phantom study.

To our knowledge, it is the first time that the use of EUD was shown to provide a better separation between responding and not responding patients. More valuably, the ^{90}Y TOF-PET based EUD directly allows taking into account the actual sphere distribution and also the actual activity per sphere that can be tuned by decaying the spheres vial before radioembolization.

When an additional radioembolization was performed in a patient to target a novel threatening lesion, the follow up of the previous radioembolization was censored. The new radioembolization was then followed with regards to the dosimetry quantities of this novel lesion which, by becoming the major threat to the patient life at that time, has triggered the additional radioembolization. This justifies the use of the biggest lesion alone to build the survival curves, regarding that a smaller lesion will trigger an additional treatment if it progresses. A literature review of 72 studies including a total of 23968 patients showed that the size of the largest region had a major impact on the patient survival (26). This

impact was also observed in the previously cited local EBRT treatments of HCC (20).

The present study suffers from the limitation that the radioembolization medical device was not randomly chosen, but was chosen in function of the HCC pattern requiring or not a highly selective radioembolization. However, it should be very unlikely that this could have induced a bias leading to the success in using the EUD.

Conclusion

The results clearly support the fact that the heterogeneity observed in ^{90}Y TOF-PET post radioembolization does not only result from low statistics, but also reflects the actual heterogeneity of the spheres distribution. Using realistic HCC radiosensitivity, ^{90}Y TOF-PET based EUD reunifies the efficacy of both ^{90}Y medical devices.

References

1. Spreafico C, Maccauro M, Mazzaferro V, Chiesa C. The dosimetric importance of the number of 90Y microspheres in liver transarterial radioembolization (TARE). Eur J Nucl Med Mol Imaging. 2014;41(4):634-8.
2. Chiesa C, Mira M, Maccauro M, Romito R, Spreafico C, Sposito C, et al. A dosimetric treatment planning strategy in radioembolization of hepatocarcinoma with 90Y glass microspheres. Q J Nucl Med Mol Imaging. 2012;56(6):503-8.

3. Strigari L, Sciuto R, Rea S, Carpanese L, Pizzi G, Soriani A, et al. Efficacy and toxicity related to treatment of hepatocellular carcinoma with 90Y-SIR spheres: radiobiologic considerations. J Nucl Med. 2010;51(9):1377-85.
4. Cremonesi M, Ferrari M, Bartolomei M, Orsi F, Bonomo G, Arico D, et al. Radioembolisation with 90Y-microspheres: dosimetric and radiobiological investigation for multi-cycle treatment. Eur J Nucl Med Mol Imaging. 2008;35(11):2088-96.
5. Sangro B, Gil-Alzugaray B, Rodriguez J, Sola I, Martinez-Cuesta A, Viudez A, et al. Liver disease induced by radioembolization of liver tumors: description and possible risk factors. Cancer. 2008;112(7):1538-46.
6. Lau WY, Kennedy AS, Kim YH, Lai HK, Lee RC, Leung TW, et al. Patient selection and activity planning guide for selective internal radiotherapy with yttrium-90 resin microspheres. Int J Radiat Oncol Biol Phys. 2012;82(1):401-7.
7. Walrand S, Hesse M, Chiesa C, Lhommel R, Jamar F. The low hepatic toxicity per Gray of 90Y glass microspheres is linked to their transport in the arterial tree favoring a nonuniform trapping as observed in posttherapy PET imaging. J Nucl Med. 2014;55(1):135-40.
8. Walrand S, Hesse M, Jamar F, Lhommel R. A hepatic dose-toxicity model opening the way toward individualized radioembolization planning. J Nucl Med. 2014;55(8):1317-22.
9. Crookston NR, Fung GSK, Frey EC. Development of a Customizable Hepatic Arterial Tree and Particle Transport Model for Use in Treatment Planning. IEEE Trans Radiat Plasma Med Sci. 2019;3(1):31-7.
10. Hogberg J, Rizell M, Hultborn R, Svensson J, Henrikson O, Molne J, et al. Heterogeneity of microsphere distribution in resected liver and tumour tissue following selective intrahepatic radiotherapy. EJNMMI Res. 2014;4(1):48.
11. Pasciak AS, Bourgeois AC, Bradley YC. A Microdosimetric Analysis of Absorbed Dose to Tumor as a Function of Number of Microspheres per Unit Volume in 90Y Radioembolization. J Nucl Med. 2016;57(7):1020-6.
12. Chiesa C, Maccauro M, Romito R, Spreafico C, Pellizzari S, Negri A, et al. Need, feasibility and convenience of dosimetric treatment planning in liver selective internal radiation therapy with (90)Y microspheres: the experience of the National Tumor Institute of Milan. Q J Nucl Med Mol Imaging. 2011;55(2):168-97.
13. Mazzaferro V, Sposito C, Bhoori S, Romito R, Chiesa C, Morosi C, et al. Yttrium-90 radioembolization for intermediate-advanced hepatocellular carcinoma: a phase 2 study. Hepatology. 2013;57(5):1826-37.
14. Kennedy A, Nag S, Salem R, Murthy R, McEwan AJ, Nutting C, et al. Recommendations for radioembolization of hepatic malignancies using yttrium-90 microsphere brachytherapy: a consensus panel report from the radioembolization

brachytherapy oncology consortium. Int J Radiat Oncol Biol Phys. 2007;68(1):13-23.
15. Lhommel R, van Elmbt L, Goffette P, Van den Eynde M, Jamar F, Pauwels S, et al. Feasibility of 90Y TOF PET-based dosimetry in liver metastasis therapy using SIR-Spheres. Eur J Nucl Med Mol Imaging. 2010;37(9):1654-62.
16. Willowson KP, Tapner M, Team QI, Bailey DL. A multicentre comparison of quantitative (90)Y PET/CT for dosimetric purposes after radioembolization with resin microspheres : The QUEST Phantom Study. Eur J Nucl Med Mol Imaging. 2015;42(8):1202-22.
17. Cross WG FN, Wong PY. Tables of beta-ray dose distributions in water. Atomic Energy of Canada. 1992;Ltd, Report No AECL-10421:Ontario, Canada.
18. Jones LC, Hoban PW. Treatment plan comparison using equivalent uniform biologically effective dose (EUBED). Phys Med Biol. 2000;45(1):159-70.
19. van Leeuwen CM, Oei AL, Crezee J, Bel A, Franken NAP, Stalpers LJA, et al. The alfa and beta of tumours: a review of parameters of the linear-quadratic model, derived from clinical radiotherapy studies. Radiat Oncol. 2018;13(1):96.
20. Seong J, Park HC, Han KH, Chon CY, Chu SS, Kim GE, et al. Clinical results of 3-dimensional conformal radiotherapy combined with transarterial chemoembolization for hepatocellular carcinoma in the cirrhotic patients. Hepatol Res. 2003;27(1):30-5.
21. Perez-Romasanta LA, Gonzalez-Del Portillo E, Rodriguez-Gutierrez A, Matias-Perez A. Stereotactic Radiotherapy for Hepatocellular Carcinoma, Radiosensitization Strategies and Radiation-Immunotherapy Combination. Cancers (Basel). 2021;13(2).
22. Chiesa C, Mira M, Maccauro M, Spreafico C, Romito R, Morosi C, et al. Radioembolization of hepatocarcinoma with (90)Y glass microspheres: development of an individualized treatment planning strategy based on dosimetry and radiobiology. Eur J Nucl Med Mol Imaging. 2015;42(11):1718-38.
23. Wigg AJ, Palumbo K, Wigg DR. Radiotherapy for hepatocellular carcinoma: systematic review of radiobiology and modeling projections indicate reconsideration of its use. J Gastroenterol Hepatol. 2010;25(4):664-71.
24. Tai A, Erickson B, Khater KA, Li XA. Estimate of radiobiologic parameters from clinical data for biologically based treatment planning for liver irradiation. Int J Radiat Oncol Biol Phys. 2008;70(3):900-7.
25. Hesse M, d'Abadie P, Lhommel R, Jamar F, Walrand S. Yttrium-90 TOF-PET-Based EUD Predicts Response Post Liver Radioembolizations Using Recommended Manufacturer FDG Reconstruction Parameters. Front Oncol. 2021;11:592529.
26. Tandon P, Garcia-Tsao G. Prognostic indicators in hepatocellular carcinoma: a systematic review of 72 studies. Liver Int. 2009;29(4):502-10.

Supplemental material

pat.	treat.	CHILD	OS	censoring reason	device	diam.	D	EUD	EUDBED	EUD/D
			[m]			[cm]	[Gy]	[Gy]	[Gy]	
1	1	A5	5.3		resin	5.1	38	26	28	0.69
2	1	A5	3.3		resin	13.6	24	16	16	0.66
3	1	A6	> 2.5	additional RE	glass	5.1	121	36	37	0.30
3	2	A6	5.8		glass	2.7	58	25	26	0.44
4	1	A5	7.0		glass	3.8	254	70	72	0.27
5	1	B8	> 6	additional sorafenib	glass	6.8	96	24	24	0.24
6	1	A5	> 2.6	additional sorafenib	glass	4.0	95	57	61	0.60
7	1	A5	> 16	additional RE	glass	3.3	87	48	51	0.55
7	2	A5	17.3		glass	2.9	320	199	246	0.62
8	1	A5	> 6	additional RE	glass	5.7	414	65	67	0.16
8	2	A6	16.0		glass	2.3	227	80	83	0.35
9	1	A6	5.6		glass	12.0	109	39	40	0.36
10	1	A6	12.7		glass	4.0	94	24	24	0.25
11	1	A6	21.0		glass	5.5	148	53	55	0.36
12	1	B7	> 1.8	additional sorafenib	glass	10.6	68	23	23	0.33
13	1	A5	> 3	additional RE	glass	8.3	140	72	76	0.52
13	2	A5	> 3		glass	6.2	169	93	100	0.55
14	1	A5	12.3		glass	9.8	135	49	49	0.36

15	1	A5	10.3		resin	9.2	15	10	11	0.71
16	1	B8	> 1.8		glass	3.6	307	136	146	0.44
17	1	B8	18.0		glass	3.7	251	90	93	0.36
18	1	A6	12.4		glass	2.0	450	144	155	0.32
19	1	A5	> 6	additional RE	glass	7.3	253	47	49	0.19
19	2	A5	> 6	additional RE	resin	1.1	66	61	69	0.92
19	3	A5	3.4		resin	4.7	69	25	25	0.36
20	1	A5	> 12	additional RE	glass	4.5	210	103	108	0.49
20	2	A5	9.8		resin	1.3	397	43	43	0.11
21	1	B7	2.9		glass	7.7	97	58	62	0.60
22	2	A5	20.0		resin	3.3	334	96	100	0.29
23	1	A5	> 3	additional RE	glass	3.3	402	94	98	0.24
23	2	A5	26.0		resin	3.2	174	96	107	0.55
24	1	A5	3.0		resin	2.0	56	47	47	0.85
25	1	A6	8.3		glass	6.6	137	110	110	0.80
26	1	B9	5.2		resin	2.6	13	14	14	1.05
27	1	A5	> 6.7	additional RE	resin	7.0	227	93	98	0.41
27	2	A5	> 26.3	additional EBRT	glass	6.2	785	107	111	0.14
28	1	A5	> 21	additional RE	resin	3.3	81	49	52	0.61
28	2	A5	> 8.2	still alive	resin	4.0	204	62	65	0.31
29	1	A5	14.8		resin	6.7	82	48	48	0.58

30	1	A6	> 4	additional RE	resin	1.8	50	29	30	0.59
30	2	A6	> 3	additional CE	glass	1.7	198	50	50	0.25
31	1	A5	16.0		resin	2.5	314	115	115	0.37
32	1	A5	> 3	additional chemo	resin	10.6	76	46	49	0.61
33	1	A5	> 2	additional chemo	resin	2.9	102	106	106	1.04
34	1	B8	3.1		glass	5.1	451	82	85	0.18
35	1	A5	2.9		glass	12.0	74	36	38	0.48
36	1	A5	> 5	additional sorafenib	resin	6.9	26	16	17	0.62
37	1	A5	> 16.2	still alive	resin	2.8	158	76	81	0.48
38	1	A5	5.8		resin	8.2	137	51	51	0.37
39	1	A6	> 8	transplantation	resin	1.4	143	114	134	0.80
40	1	A5	> 2	additional RE	resin	9.8	57	31	32	0.54
40	2	A5	> 9.8	hepatectomy	glass	2.0	271	89	93	0.33
41	1	A5	8.7		glass	8.4	134	66	69	0.49
42	1	A5	> 4	additional RE	glass	7.3	225	94	100	0.42
42	2	A5	> 7.9	additional CE	glass	5.0	592	182	195	0.31
43	1	A5	> 5	hepatectomy	glass	4.3	1426	106	108	0.07
44	1	A5	> 5.4	additional chemo	resin	2.7	55	48	52	0.87
45	1	A5	> 9.8	still alive	resin	3.0	143	60	63	0.42

RE: radioembolization, CE: chemo-embolization, chemo: chemotherapy, OS: overall survival duration, censoring time is indicated by the symbol >.

5- EUD based ^{90}Y-TOF-PET post selective internal radionuclide therapy provides a similar TCP in HCC than observed in EBRT[4]

Abstract: Background: Tumor equivalent uniform dose (EUD) is a predictor of patient outcome after selective internal radionuclide therapy (SIRT) of hepatocellular carcinoma (HCC) and can be evaluated with ^{90}Y-TOF-PET. The aim is to evaluate the correlation between PET based tumors EUD and the clinical response evaluated with dual molecular tracer (^{11}C-acetate and ^{18}F-FDG) PET/CT post SIRT. Methods: 34 HCC tumors in 22 patients were prospectively evaluated. The metabolic response was characterized by the Total Lesion Metabolism variation (ΔTLM) between baseline and follow up. This response allowed to compute a Tumor Control Probability (TCP) as a function of the tumor EUD. Results: The dose response correlation was exponential-asymptotic shaped and highly significant ($R=0.72$, $P < 0.001$). With a cutoff of 40Gy, the metabolic response was strongly different in both groups (median response 35% versus 100%, $P< 0.001$). Moreover, the TCP (EUD) was very similar to that observed in External Beam Radiation Therapy (EBRT). Conclusions: EUD based ^{90}Y TOF-PET/CT predicts the metabolic response after SIRT of HCC assessed using dual molecular

[4] **Submitted, in peer review.** authors' list: Philippe d'Abadie, Stephan Walrand, Michel Hesse, Ivan Borbath, Renaud Lhommel and François Jamar.

PET tracers and provides a similar TCP curve to that observed in EBRT. Both TCPs show that a EUD of 100 Gy is needed and sufficient to control a HCC.

5.1 Introduction

Liver selective internal radionuclide therapy (SIRT) is part of the treatment strategy of hepatocellular carcinoma (HCC) (1) and aims to deliver high efficient doses to tumors (2). The tumor-absorbed dose is a predictive factor of the treatment's effectiveness (3). Comparing the different types of radiation therapies, the absorbed dose efficacy cutoff for glass microspheres is twice that for resin microspheres and up to five times more than with external beam radiation therapy (EBRT) (4-7). The heterogeneous dose distribution in SIRT explains these differences and can be accurately revealed with Time of Flight (TOF)-PET ^{90}Y imaging (8, 9) when taking into account the Equivalent Uniform dose (EUD) (10). EUD reunifies the efficacy threshold doses in SIRT (performed with resin or glass microspheres) but also in EBRT (11). Previous radiobiological models developed in SIRT for HCC demonstrated an exponential correlation between the tumor-absorbed dose and the clinical response assessed with conventional imaging (5, 12-13). In colorectal liver metastases, a similar correlation was demonstrated using the metabolic response assessed with ^{18}F-FDG PET/CT (14, 15).

Functional imaging (PET/CT) is currently not recommended for the management of HCC, especially because ^{18}F-FDG PET/CT has a low sensitivity, with a definite uptake in less than 50-65% of the cases (16). ^{11}C-Acetate PET/CT is more sensitive for HCC detection, with an uptake reaching 85% (17).

^{11}C acetate enters the Krebs cycle as a substrate for β-oxidation in fatty acid and cholesterol synthesis which is likely the explanation of its uptake by differentiated HCC (17). On the other hand, the high level of glucose-6-phosphatase in differentiated HCC leads to the release of ^{18}FDG while poorly differentiated HCC, which has a low abundance of this enzyme, tends accumulate ^{18}F-FDG (16, 17). As a result, performing a dual molecular tracer PET/CT acquisition (^{11}C- acetate and ^{18}F- FDG) was able to improve this sensibility up to 98% (18).

This study aims to demonstrate a radiobiological model in HCC built on ^{90}Y TOF-PET/CT based EUD and the metabolic response assessed with dual molecular PET tracer.

5.2 Materials and Methods

Patients

23 HCC patients, referred to our department for SIRT, were prospectively enrolled in this study after their informed consent and approval by the local ethics committee (2015/01OCT/522).

Each patient was evaluated with dual isotope (^{11}C-acetate and ^{18}F-FDG) PET/CT at baseline and at follow-up (FU) 2 and 4 months after SIRT. 4 patients received a second treatment after an interval of 5 months and were evaluated again. 4 patients had multifocal tumors (2 to 6) while the majority had only one tumor.

A total of 34 tumors demonstrated a metabolic uptake, 80% were positive with acetate PET/CT, 52% with FDG PET/CT and 40% with both imaging. In one patient, the tumor uptake was not significant with either PET tracers and the metabolic evaluation was not possible, resulting in 22 studied patients. No other exclusion factor was applied.

The patients' characteristics are summarized in table 1.

Table 1: Patients characteristics

Characteristics	**Data**
Age (Years)	73 (68-79)
Sex	Male: 14 (64%)
	Female: 8 (34%)
BCLC staging	A: 8 (36%)
	B: 8 (36%)
	C: 6 (28%)
Tumor volume (ml)	36 (11-97)

Continuous variables described with median and 95% confidence interval between parentheses. BCLC: Barcelona Clinic Liver Cancer

Treatment

SIRT was performed according to standard recommendations (19). Resin microspheres (Sir-Spheres®, Sirtex Medical Ltd., Sydney, Australia) and glass microspheres (Therasphere®, Boston Scientific, Boston, MA) were used in 17 and 9 treatments, respectively.

A 40-min 2-bed positions ^{90}Y TOF-PET scan (Gemini TF64 Philips Medical Systems, Cleveland, OH) was acquired within 4 h following the SIRT. Reconstruction was performed with the 3D line of response (LOR)–TOF blob-based OSEM algorithm from Philips with 2 iterations times 33 subsets and a 4x4 mm^3 voxel size. ^{90}Y activity distribution was transformed into a 3D-map of absorbed doses using a previously validated method (20). In summary, voxel counts were converted to absorbed dose distribution by convolving the ^{90}Y activity distribution with a dose point kernel, after spatial resolution recovery.

Tumor response assessment

Whole body TOF-PET/CT acquisition (Gemini TF 64, Philips Medical Systems, Cleveland, OH) was acquired 20 minutes after intravenous injection of ^{11}C-acetate (370-540 MBq, half-life: 20 minutes). 30 minutes after this first acquisition, ^{18}F-FDG was injected (280-310 MBq) and images were acquired after an incorporation of 60 minutes. Acquisitions were performed at baseline and during FU at 2 and 4 months after treatment.

Tumor contours were automatically defined with acetate or FDG PET/CT using an isocontour method (41% SUVmax threshold) performed with the MIM software (V7.1, MIM Software Inc., Cleveland, OH).

For each patient, the tracer, i.e., ^{11}C-acetate or ^{18}F-FDG, giving the highest normal liver to tumor tissue ratio on the baseline PET imaging was selected to assess the tumor response metabolism.

For each tumor and each time point, the total lesion metabolism (TLM) was defined as:

$$\mathrm{TLM} = \mathrm{SUV}_{\mathrm{mean}} \times \mathrm{Volume} \quad (1)$$

The ΔTLM between baseline (B) and FU defined the metabolic response:

$$\Delta\ \mathrm{TLM}\ (\%) = \frac{\mathrm{TLM_B} - \mathrm{TLM_{FU}}}{\mathrm{TLM_B}}.\ 100 \quad (2)$$

The best metabolic response between the baseline and either 2- or 4-month was considered (corresponding to the maximal effects of radiation).

No TLM cutoffs are established to classify the metabolic response of tumors. However, regarding EUD, a threshold of 40 Gy was previously defined as an efficacy cutoff in HCC (11) and corresponded also to the efficacy cutoff in EBRT (7). Therefore, this cutoff was applied for comparing the metabolic responses.

Tumor dosimetry

Tumor contours were matched with the 3D map of absorbed doses, as previously defined, using a rigid co-registration with the MIM software.

Equivalent uniform dose (EUD) was calculated according to the Jones and Hoban formalism (21):

$$\mathrm{EUD} = -\frac{1}{\alpha}\ln\left(\frac{\sum_i e^{-\alpha D_i}}{N}\right) \quad (3)$$

where α is the apparent HCC radiosensitivity, N the number of voxels in the tumor and Di the absorbed dose in tumor voxel i. The terminology apparent radiosensitivity was introduced by Chiesa et al. (13) to take into account that this value depends on the spatial resolution of the imaging system as shown in (22). In a previous ^{90}Y TOF-PET based EUD analyses, the apparent α coefficient was estimated to be 0.038 Gy^{-1} (11), i.e., about tenfold lower than the intrinsic in vitro HCC 0.40 Gy^{-1} radiosensitivity (23).

The Tumor Control Probability (TCP) was determined in consecutive EUD bins of 20 Gy. Tumor control was defined as a metabolic response with ΔTLM ≥0.80, the value giving the best sigmoid shaped curve.

Statistical analysis

Wilcoxon signed rank test was used to compare groups. The correlation was analyzed using a Spearman coefficient (R).

Analyses were conducted with Prism software (version 7.0, GraphPad Software, La Jolla, Ca).

5.3 Results

The metabolic response correlated well with EUD (Figure 1): the larger the EUD the higher the metabolic response. This dose response correlation was linear-exponential and highly significant according to the Spearman coefficient ($R=0.72$, $P < 0.001$). Moreover, the metabolic response to radiation was very similar for tumors positive with FDG PET/CT and with acetate PET/CT (Figure 1). The metabolic response was significantly higher in tumors receiving more than 40 Gy (median ΔTLM: 1.0) compared to tumors receiving a lower dose (median ΔTLM: 0.35, $P< 0.001$).

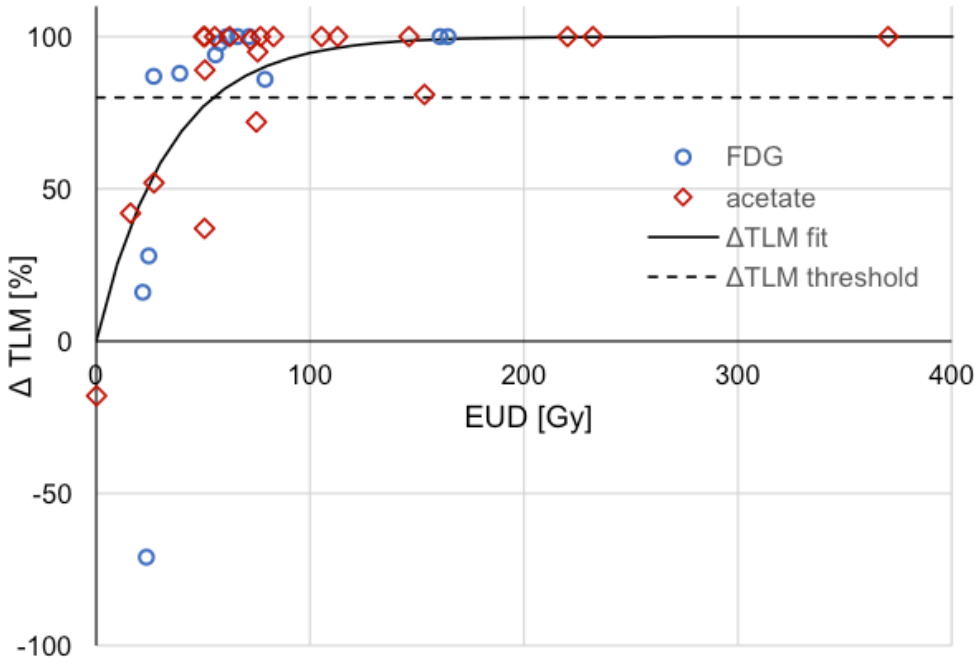

Figure 1: ΔTLM as a function of the EUD obtained from post-SIRT ^{90}Y TOF-PET. Blue circles: measured on ^{11}C-acetate PET. Red diamonds: measured on ^{18}F-FDG PET. Dashed line: ΔTLM threshold used to discriminate responding and not responding tumor in the TCP computation.

Moreover, the TCP- EUD correlation in this study was in very good agreement with previous data reported in EBRT (Figure 2) (24).

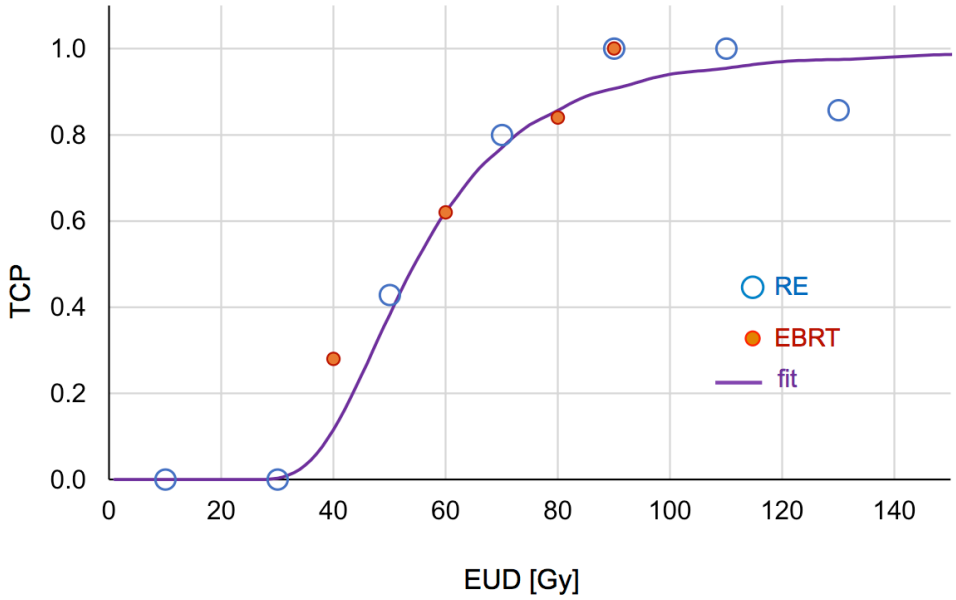

Figure 2: TCP as a function of the EUD. Blues circles: this SIRT study. Red bullets: External Beam Radiation Therapy (EBRT) derived from Lausch et al.(24). Red solid line: EBRT TCP fitted with a logistic function.

5.4 Discussion

This study confirms the strong correlation already observed between reduction of tumor metabolism and EUD (13, 14), as well as between the TCP and the tumor EUD (12, 13). A novelty of the present observation is that this correlation holds true when mixing acetate and FDG data for the tumor metabolism assessment. This makes sense considering the fact that reduction of acetate or FDG uptake mainly results from the reduction of tumor living cells number. Indeed, proteins

which constitute the metabolic engines are hugely radioresistant. For instance, a dose of 100 Gy damages less than 5% of albumin (25) whereas 40 Gy, assuming a radiosensitivity α = 0.4 Gy^{-1} (23), kills $1-e^{-0.4\times40}$ ≈ 99.99999% of HCC cells (23). Finally, the use of ^{90}Y TOF-PET to compute the dose, rather than ^{99m}Tc-macroaggregated albumin (MAA) or bremsstrahlung ^{90}Y-SPECT used in previous studies (12-14), improved the correlation.

Beyond this dose-response confirmation, the main finding of the study is that the observed TCP as a function of the EUD in SIRT is very similar to that of EBRT. We already demonstrated that ^{90}Y TOF-PET based EUD provided the same threshold to discriminate “responding” and “non- responding” patients in glass SIRT, resin SIRT and EBRT, i.e., 40 Gy (26). These results proved that ^{90}Y TOF-PET based EUD rightly takes into account the impact of the heterogeneity of the dose distribution. In addition, the similarity of the SIRT and EBRT TCPs consolidates that to surely control a tumor, i.e., TCP ≈ 1, the needed and sufficient EUD is 100 Gy. The sigmoid shape of the TCP curve enlightens the importance to reach at least a EUD of 100 Gy in each tumor and emphasize the necessity to optimize the treatment planning liver to reach this goal (3, 27, 28). Note that the absorbed dose D needed to achieve this EUD can vary from 190 to 1800 Gy depending on the dose distribution heterogeneity (see table in supplementary material).

The observed SIRT TCP also explains why the EUD = 40 Gy threshold well split the patient survival curves into 2 clear different groups (26). Indeed, this threshold

correspond to the EUD50, as a result one group contains a majority of responding patients and the other one a majority of non-responding patients.

The optimal ΔTLM 80% threshold, and not 100%, used to obtain a well-shaped TCP sigmoid curve results from different effects: errors in the TLM assessment, FU delay too short to allow all the tumor cells to die or in contrary FU delay sufficiently long enough to allow a repopulation of the tumor site by healthy liver tissue which also takes up ^{11}C-acetate or ^{18}F-FDG.

This study has some limitations. First, analyses were performed in a limited number of patients and tumors compared to previous reported studies (12-14). However, the better accuracy of ^{90}Y TOF-PET in dose distribution assessment, versus MAA or bremsstrahlung ^{90}Y-SPECT, reduces the statistical blurring, allowing to get a good correlation with a reduced number of patients. Only few tumors received low absorbed doses and demonstrated a poor metabolic response, limiting the accuracy of our radiobiological model for low doses. Second, the follow up was 4 months at maximum but some tumors could respond later to radiation and hence the effects of radiation could be sometimes underestimated, justifying the choice of the threshold ΔTLM= 80% rather than 100% in the TCP derivation (2). EUD is based on a single alpha value and it is likely that the radiosensitivity may vary between HCC occurring within different clinical entities. Accordingly, this delayed response may explain why some tumors did not disclose complete metabolic response 4 months after therapy despite a very efficient EUD.

Conclusions

^{90}Y-TOF-PET based EUD is strongly correlated with the metabolic response in HCC assessed by dual molecular tracer PET imaging and is associated with a TCP close to that in EBRT. ^{90}Y-TOF-PET based EUD reconciles dose levels in SIRT and EBRT. The use of this parameter must be encouraged in future dosimetry studies for a better understanding of the toxicity and efficacy threshold doses in SIRT.

Appendix A

pat.	tum.	device	PET	D [Gy]	EUD [Gy]	diff TLM [%]
1	1	glass	FDG	306	165	100
2	2	resin	acetate	531	370	100
3	3	glass	FDG	126	72	100
4	4	resin	acetate	191	113	100
4	5	resin	acetate	380	232	100
5	6	resin	acetate	229	76	95
5	7	glass	acetate	970	83	100
6	8	resin	FDG	86	56	94
7	9	resin	acetate	84	51	37
8	10	resin	acetate	95	50	100
9	11	resin	FDG	51	27	87
10	12	glass	FDG	186	66	100
11	13	glass	FDG	146	79	86
12	14	glass	acetate	1811	146	100
12	15	glass	acetate	308	154	81
13	16	glass	acetate	692	220	100
14	17	glass	acetate	128	72	99
15	18	resin	FDG	74	22	16
15	19	resin	FDG	93	23	-71
15	20	resin	FDG	317	161	100
16	21	glass	acetate	87	51	89
17	22	resin	FDG	100	39	88
17	23	resin	FDG	179	58	98
18	24	resin	acetate	701	105	100
19	25	resin	acetate	102	55	100
19	26	resin	acetate	111	75	72
20	27	resin	acetate	121	62	100
21	28	resin	FDG	107	61	100
22	29	resin	acetate	28	16	42
22	30	resin	acetate	45	27	52
22	31	resin	acetate	91	51	100
22	32	resin	acetate	100	77	100
22	33	resin	acetate	0	0	-18
22	34	resin	FDG	43	25	28

References

1. Marrero, J. A., L. M. Kulik, C. B. Sirlin, A. X. Zhu, R. S. Finn, M. M. Abecassis, L. R. Roberts and J. K. Heimbach. "Diagnosis, staging, and management of hepatocellular carcinoma: 2018 practice guidance by the american association for the study of liver diseases." Hepatology 68 (2018): 723-50. 10.1002/hep.29913.
2. Sangro, B., M. Inarrairaegui and J. I. Bilbao. "Radioembolization for hepatocellular carcinoma." J Hepatol 56 (2012): 464-73. 10.1016/j.jhep.2011.07.012.
3. Garin, E., L. Tselikas, B. Guiu, J. Chalaye, J. Edeline, T. de Baere, E. Assenat, V. Tacher, C. Robert, M. Terroir-Cassou-Mounat, et al. "Personalised versus standard dosimetry approach of selective internal radiation therapy in patients with locally advanced hepatocellular carcinoma (dosisphere-01): A randomised, multicentre, open-label phase 2 trial." Lancet Gastroenterol Hepatol 6 (2021): 17-29. 10.1016/S2468-1253(20)30290-9.
4. Garin, E., L. Lenoir, J. Edeline, S. Laffont, H. Mesbah, P. Poree, L. Sulpice, K. Boudjema, M. Mesbah, A. Guillygomarc'h, et al. "Boosted selective internal radiation therapy with 90y-loaded glass microspheres (b-sirt) for hepatocellular carcinoma patients: A new personalized promising concept." Eur J Nucl Med Mol Imaging 40 (2013): 1057-68. 10.1007/s00259-013-2395-x.
5. Hermann, A. L., A. Dieudonne, M. Ronot, M. Sanchez, H. Pereira, G. Chatellier, E. Garin, L. Castera, R. Lebtahi, V. Vilgrain, et al. "Relationship of tumor radiation-absorbed dose to survival and response in hepatocellular carcinoma treated with transarterial radioembolization with (90)y in the sarah study." Radiology 296 (2020): 673-84. 10.1148/radiol.2020191606.
6. d'Abadie, P., S. Walrand, M. Hesse, L. Annet, I. Borbath, M. Van den Eynde, R. Lhommel and F. Jamar. "Prediction of tumor response and patient outcome after radioembolization of hepatocellular carcinoma using 90y-pet-computed tomography dosimetry." Nucl Med Commun (2021): 10.1097/MNM.0000000000001395.
7. Seong, J., H. C. Park, K. H. Han, C. Y. Chon, S. S. Chu, G. E. Kim and C. O. Suh. "Clinical results of 3-dimensional conformal radiotherapy combined with transarterial chemoembolization for hepatocellular carcinoma in the

cirrhotic patients." Hepatol Res 27 (2003): 30-35. 10.1016/s1386-6346(03)00162-1.

8. Pasciak, A. S., A. C. Bourgeois, J. M. McKinney, T. T. Chang, D. R. Osborne, S. N. Acuff and Y. C. Bradley. "Radioembolization and the dynamic role of (90)y pet/ct." Front Oncol 4 (2014): 38. 10.3389/fonc.2014.00038.
9. Walrand, S., M. Hesse, C. Chiesa, R. Lhommel and F. Jamar. "The low hepatic toxicity per gray of 90y glass microspheres is linked to their transport in the arterial tree favoring a nonuniform trapping as observed in posttherapy pet imaging." J Nucl Med 55 (2014): 135-40. 10.2967/jnumed.113.126839.
10. Hesse, M., P. d'Abadie, R. Lhommel, F. Jamar and S. Walrand. "Yttrium-90 tof-pet-based eud predicts response post liver radioembolizations using recommended manufacturer fdg reconstruction parameters." Front Oncol 11 (2021): 592529. 10.3389/fonc.2021.592529. https://www.ncbi.nlm.nih.gov/pubmed/34676157.
11. d'Abadie, P., M. Hesse, F. Jamar, R. Lhommel and S. Walrand. "(90)y tof-pet based eud reunifies patient survival prediction in resin and glass microspheres radioembolization of hcc tumours." Phys Med Biol 63 (2018): 245010. 10.1088/1361-6560/aaf205.
12. Strigari, L., R. Sciuto, S. Rea, L. Carpanese, G. Pizzi, A. Soriani, G. Iaccarino, M. Benassi, G. M. Ettorre and C. L. Maini. "Efficacy and toxicity related to treatment of hepatocellular carcinoma with 90y-sir spheres: Radiobiologic considerations." J Nucl Med 51 (2010): 1377-85. 10.2967/jnumed.110.075861.
13. Chiesa, C., M. Mira, M. Maccauro, C. Spreafico, R. Romito, C. Morosi, T. Camerini, M. Carrara, S. Pellizzari, A. Negri, et al. "Radioembolization of hepatocarcinoma with (90)y glass microspheres: Development of an individualized treatment planning strategy based on dosimetry and radiobiology." Eur J Nucl Med Mol Imaging 42 (2015): 1718-38. 10.1007/s00259-015-3068-8.
14. Flamen, P., B. Vanderlinden, P. Delatte, G. Ghanem, L. Ameye, M. Van Den Eynde and A. Hendlisz. "Multimodality imaging can predict the metabolic response of unresectable colorectal liver metastases to radioembolization therapy with yttrium-90 labeled resin microspheres." Phys Med Biol 53 (2008): 6591-603. 10.1088/0031-9155/53/22/019.
15. Levillain, H., I. Duran Derijckere, G. Marin, T. Guiot, M. Vouche, N. Reynaert, A. Hendlisz, B. Vanderlinden and P. Flamen. "(90)y-pet/ct-based dosimetry after selective internal radiation therapy predicts outcome in patients with liver metastases from colorectal cancer." EJNMMI Res 8 (2018): 60. 10.1186/s13550-018-0419-z.

16. Sacks, A., P. J. Peller, D. S. Surasi, L. Chatburn, G. Mercier and R. M. Subramaniam. "Value of pet/ct in the management of primary hepatobiliary tumors, part 2." AJR Am J Roentgenol 197 (2011): W260-5. 10.2214/AJR.11.6995.
17. Park, J. W., J. H. Kim, S. K. Kim, K. W. Kang, K. W. Park, J. I. Choi, W. J. Lee, C. M. Kim and B. H. Nam. "A prospective evaluation of 18f-fdg and 11c-acetate pet/ct for detection of primary and metastatic hepatocellular carcinoma." J Nucl Med 49 (2008): 1912-21. 10.2967/jnumed.108.055087.
18. Ho, C. L., S. Chen, D. W. Yeung and T. K. Cheng. "Dual-tracer pet/ct imaging in evaluation of metastatic hepatocellular carcinoma." J Nucl Med 48 (2007): 902-9. 10.2967/jnumed.106.036673.
19. Padia, S. A., R. J. Lewandowski, G. E. Johnson, D. Y. Sze, T. J. Ward, R. C. Gaba, M. O. Baerlocher, V. L. Gates, A. Riaz, D. B. Brown, et al. "Radioembolization of hepatic malignancies: Background, quality improvement guidelines, and future directions." J Vasc Interv Radiol 28 (2017): 1-15. 10.1016/j.jvir.2016.09.024.
20. Lhommel, R., L. van Elmbt, P. Goffette, M. Van den Eynde, F. Jamar, S. Pauwels and S. Walrand. "Feasibility of 90y tof pet-based dosimetry in liver metastasis therapy using sir-spheres." Eur J Nucl Med Mol Imaging 37 (2010): 1654-62. 10.1007/s00259-010-1470-9.
21. Jones, L. C. and P. W. Hoban. "Treatment plan comparison using equivalent uniform biologically effective dose (eubed)." Phys Med Biol 45 (2000): 159-70. 10.1088/0031-9155/45/1/311.
22. Hesse, M., P. d'Abadie, R. Lhommel, F. Jamar and S. Walrand. "Yttrium-90 tof-pet-based eud predicts response post liver radioembolizations using recommended manufacturer fdg reconstruction parameters." Frontiers in Oncology (2021): 3876.
23. Wigg, A. J., K. Palumbo and D. R. Wigg. "Radiotherapy for hepatocellular carcinoma: Systematic review of radiobiology and modeling projections indicate reconsideration of its use." J Gastroenterol Hepatol 25 (2010): 664-71. 10.1111/j.1440-1746.2009.06126.x.
24. Lausch, A., K. Sinclair, M. Lock, B. Fisher, N. Jensen, S. Gaede, J. Chen and E. Wong. "Determination and comparison of radiotherapy dose responses for hepatocellular carcinoma and metastatic colorectal liver tumours." Br J Radiol 86 (2013): 20130147. 10.1259/bjr.20130147.
25. Mishra, K., H. Ojha, S. Kallepalli, A. Alok and N. K. Chaudhury. "Protective effect of ferulic acid on ionizing radiation induced damage in bovine serum albumin." International Journal of Radiation Research 12 (2014): 113.
26. d'Abadie, P., M. Hesse, F. Jamar, R. Lhommel and S. Walrand. "90y tof-pet based eud reunifies patient survival prediction in resin and glass

microspheres radioembolization of hcc tumours." Physics in Medicine & Biology 63 (2018): 245010.
27. Chiesa, C., M. Mira, S. Bhoori, G. Bormolini, M. Maccauro, C. Spreafico, T. Cascella, A. Cavallo, M. C. De Nile, S. Mazzaglia, et al. "Radioembolization of hepatocarcinoma with (90)y glass microspheres: Treatment optimization using the dose-toxicity relationship." Eur J Nucl Med Mol Imaging 47 (2020): 3018-32. 10.1007/s00259-020-04845-4.
28. d'Abadie, P., S. Walrand, M. Hesse, N. Amini, R. Lhommel, K. Sawadogo and F. Jamar. "Accurate non-tumoral ^{99m}Tc-MAA absorbed dose prediction to plan optimized activities in liver radioembolization using resin microspheres." Phys Med 89 (2021): 250-57.10.1016/j.ejmp.2021.07.032.

6- ^{99m}Tc-MAA imaging to optimize the dose planning in radioembolization[5]

Abstract

Aim: The methods recommended by the manufacturers to calculate delivered activities in liver radioembolization are simplistic and only slightly personalized. Activity planning can also be based on a ^{99m}Tc-macroaggregated albumin SPECT/CT (MAA) using the partition model but its accuracy is controversial. This study evaluates the dose parameters in the normal liver and in the tumor compartments using MAA SPECT/CT (pre-therapeutic imaging) and ^{90}Y TOF-PET/CT (post-therapy imaging). Finally, we propose a prescription of the activity as a function of the MAA distribution in the normal liver.

Method: 66 procedures of RE (with resin microspheres) corresponding to 171 lesions were analyzed. Tumor to normal targeted liver uptake (T/NTL), tumor absorbed dose (TD) and whole normal liver absorbed (WNLD) were assessed with MAA and ^{90}Y imaging. Secondly, activities were recalculated using the MAA distribution in the normal liver compartment to reach the maximal tolerable liver dose. These activities were compared to activities defined with the BSA method.

Results: Compared to ^{90}Y imaging, our study demonstrated an accurate estimation of the WNLD using MAA imaging (Pearson's R=0.97, P < 0.001). Contrarily,

[5] d'Abadie et al. Phys. Med. 2021 ; 89: 250-257

significant variations were found for TD (R=0.65, P < 0.001). The MAA T/NTL ratio has an 85% positive predictive value in identifying patients who will get a ^{90}Y T/NTL ratio above 1.5. Moreover, activities calculated using the MAA distribution in the normal liver compartment were significantly higher than activities defined with the BSA method.

Conclusion: Whole normal liver absorbed doses are accurately predicted with MAA imaging and could be used to optimize the activity planning.

6.1 Introduction

The manufacturers' recommended methods to calculate the activities in liver radioembolization are simplistic and only slightly personalized. The body surface area (BSA) method is the most commonly used for ^{90}Y resin spheres (Sir-Spheres®, Sirtex Medical Ltd., Sydney, Australia) and does not provide accurate dosimetry that separately takes into account the dose deposition in tumors and in the normal liver parenchyma for a dose optimization as requested by the article 56 of the EEC Directive 2013/59 (1).

Some centers have adopted a more personalized dosimetric method based on the 99mTc-macroaggregated albumin (MAA) distribution in the tumor and the normal liver compartments known as the partition model (2). This dosimetric method is considered to be more accurate and enables to plan a safe absorbed dose to the normal liver and an effective absorbed dose to tumors (3). However, this model assumes a perfect correlation between MAA particles and the actual distribution

of the radioactive ^{90}Y microspheres; this consideration is questionable and subject to debate. Indeed, previous studies demonstrated heterogeneous results in the ability of MAA imaging to precisely determine the tumor doses (4-6).

The aim of this study is to provide a more optimized dosimetric method for activity planning in liver radioembolization with resin microspheres. For this purpose, we firstly evaluated the accuracy of a dosimetric model based on MAA imaging. We compared tumor absorbed dose (TD) and whole normal liver absorbed dose (WNLD) calculated with MAA and ^{90}Y datasets in procedures performed in similar arteriographic conditions. As a second endpoint, we aim to propose a more accurate dosimetric model based on the MAA absorbed dose in the normal liver compartment. In this model, the injected radioactivity is calculated to reach the maximal absorbed dose tolerated by the normal liver without the risk of severe toxicity.

6.2 Material and methods

Patients and procedures

Patients treated by RE with resin microspheres between 2011 and 2019 were retrospectively analyzed after approval of the local ethics committee

(2017/27JUI/334). Each treatment was performed according to the standards of clinical practice (2).

Characteristics of each arteriography were firstly reviewed by a senior interventional radiologist with a systematic analysis of the catheter tip position using the 2D angiography. Only patients with angiograms with similar catheter positions (difference < 1 cm) and comparable catheter positions (range 1 to 2 cm) between the preliminary and the therapeutic angiographies were included in this study. Small tumors (< 2 cm diameter) were excluded from the analysis (underestimation of the tumor activity due to partial volume effect). No other exclusion criteria were applied.

Imaging protocols

^{99m}Tc-MAA imaging was performed after injection of 150 to 170 MBq ^{99m}Tc-MAA (Technescan LyoMAA, Mallinckrodt Medical BV, Petten, The Netherlands), using a BrightView XCT scanner (Philips Healthcare, Cleveland, OH). Abdominal SPECT/CT images were obtained with a 128x128 matrix with a low-energy, high-resolution collimator (64 angles per head, 25 sec /angle). Image reconstruction was achieved using an OSEM algorithm (8 iterations and 16 subsets) with attenuation and scatter corrections.

^{90}Y imaging was performed with a 650 ps TOF-PET/CT (Gemini-TF PET/CT, Philips Medical Systems, Cleveland, OH) with an abdominal acquisition of 40 minutes (2

bed positions). Reconstruction was performed with the 3-D line of response (LOR)-TOF blob-based algorithm (2 iterations, 33 subsets) and with a voxel reconstruction of 4x4x4 mm^3.

Tumor uptake and grading

For each lesion, the tumor to normal targeted liver uptake ratio (T/NTL) was defined as:

$$T/_{NTL} = \frac{C_T/_{V_T}}{C_{NTL}/_{V_{NTL}}}$$

where C_T and V_T represent the counts and volume of each individual tumor, respectively. C_{NTL} and V_{NTL} represent the counts and volume of the normal targeted liver, respectively. NTL is the non-tumoral liver receiving radioactive microspheres (example in figure 1). C_T and C_{NTL} were measured with ^{99m}Tc-MAA SPECT and ^{90}Y PET datasets.

T/NTL was arbitrarily classified as low grade uptake for values less than 1.5 and as high grade for values higher or equal than 1.5.

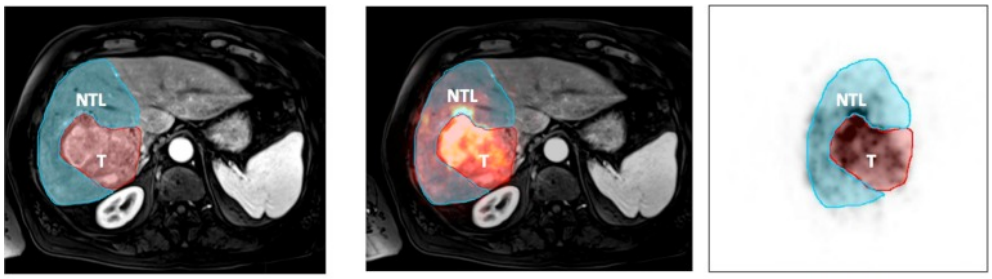

Figure 1: Example of a patient with a large hepatocellular carcinoma shown on MRI (left panel). T represents the tumor and NTL, the normal targeted liver. The liver distribution of ^{90}Y-microspheres is assessed by ^{90}Y PET (right panel), fused with MRI (middle panel).

Absorbed dose

Absorbed doses (D_{VOI}) have been determined using the MIRD equation(7), i.e.:

$$D_{VOI}(Gy) = \frac{A_{VOI}\ (GBq)}{M_{VOI}\ (kg)} . 50\ (J/GBq)$$

where A and M are the activity and the mass within the VOI (volume x 1.03), respectively.

VOIs were first delineated using the baseline contrast enhanced MRI or CT scan using MIM 6.7 (MIM Software Inc., Cleveland, OH). Afterwards, MRI/CT scans and VOIs were fused with ^{99m}Tc-MAA SPECT and ^{90}Y PET using a rigid co-registration in order to measure the activity in the VOI.

Tumor absorbed dose (TD) and whole normal liver absorbed dose (WNLD) were calculated with ^{99m}Tc-MAA SPECT and ^{90}Y PET.

Calculations of activities using different dosimetric methods

In our cohort, we recalculated the activities needed for treatments of our 66 patients using the VOIs as defined above.

First, we calculated activities based on the BSA method (A_{BSA}) following the standard formula(8):

for a whole liver treatment,

$$A\ (Gbq) = BSA\ (m^2) - 0.2 + \frac{V_{tumor}}{V_{total\ liver}}$$

for a treatment considering a part of the liver (target),

$$A\ (GBq) = \left((BSA\ (m^2) - 0.2) + \frac{V_{target\ tumor}}{V_{target\ liver}} \right) x\ \frac{V_{target\ liver}}{V_{total\ liver}}$$

where A is the activity, V, the volume and BSA, the body surface area defined as:

$$0.20247\ x\ height^{0.725}\ (m)\ x\ weight^{0.425}(kg)$$

Secondly, activities were calculated from MAA imaging (A_{MAA}) using a two-compartment dosimetry model (9). The injected radioactivity was calculated to reach the maximal absorbed dose tolerated by the normal targeted liver (NTLD) without expecting severe toxicity. The absorbed dose applied to the NTL was 50 Gy. A more aggressive target absorbed dose of 70 Gy was given for treatments

only in patients with a functional liver reserve above 30% (percentage of non irradiated liver) and without risks of impaired liver function (underlying liver disease, previous hepatotoxic treatments). The formula was derived from the MIRD equation (7):

$$A_{MAA}[GBq] = \frac{\left({}^{C_{WL}}/_{C_{NTL}}\right).NTLD[Gy].M_{NTL}[kg].(1+LSF)}{50}$$

with C_{WL} and C_{NTL}, the counts defined with ^{99m}Tc-MAA SPECT in the whole liver and in the normal targeted liver (NTL) respectively; with NTLD the Maximal absorbed Dose tolerated by the NTL (50 or 70 Gy) and with M_{NTL}, the mass of the NTL. *LSF is* the lung shunt fraction estimated from planar images of the ^{99m}Tc-MAA scintigraphy.

Thirdly, we recalculated activities reaching the maximal tolerable whole normal liver absorbed dose (WNLD) of 40 Gy. The formula was also derived from the MIRD equation:

$$A_{MAA}[GBq] = \frac{\left({}^{C_{WL}}/_{C_{NTL}}\right).WNLD[Gy].M_{WL}[kg].(1+LSF)}{50}$$

Statistics

Analyses were conducted by a senior statistician using SAS V9.4 software (SAS Institute Inc., Cary, NC, USA). Descriptive statistics were used to summarize the results considering absolute and relative frequencies, medians and absolute median deviations. Log base 10 was used for plotting lognormal distributions. Differences between ^{90}Y and MAA absorbed doses were analyzed using a Bland-Altman plot. Variances of the differences between the tumor doses and between the whole normal liver absorbed doses were compared with a Brown and Forsythe's test. The correlation between parameters was also evaluated by a Pearson coefficient.

Wilcoxon rank sum test for paired data was used to analyze the differences in T/NTL and absorbed doses between ^{90}Y and MAA and to analyze the difference in planned activities between the classic BSA method and the two-compartment dosimetry method.

A linear mixed-effect model was used to account for correlation of tumors within patients.

The performance of MAA imaging to predict T/NTL, was assessed using the ^{90}Y imaging as gold standard. Sensitivity, specificity, accuracy, negative and positive predictive values were calculated as usual.

A P-value with a confidence level of 95% was defined as statistically significant.

6.3 Results

66 patients corresponding to 66 procedures of planning (with MAA imaging) and treatment (with ^{90}Y imaging) are reported in this study. Angiograms were classified similar (delta <1cm) and comparable (delta: 1-2cm) in 48 and 18 procedures, respectively.

Main characteristics of patients and procedures are reported in table 1. In summary, patients were treated mostly for hepatocellular carcinoma (HCC, 33%), colorectal metastases (32%) and for neuroendocrine tumors metastases (24%). 171 lesions were analyzed corresponding to an average of 3 lesions per patient. Lobar radioembolization was performed in 53%, whole liver treatment in 44% (mostly by bilobar injection) and selective in only 3%. At the time of treatment, the activity that was actually injected was defined using the BSA method in 54 procedures (82%) and the partition dosimetric method in 12 (18%).

Table 1: Patient characteristics

Characteristics		
Gender (n, %)	Female	22 (33%)
	Male	44 (67%)
Age (median- range; years)		67 (34-83)
Tumor type by patient (n, %)	HCC	22 (33%)
	Colorectal mets	21 (32%)
	Neuroendocrine mets	16 (24%)
	Cholangiocarcinoma	3 (5%)
	Melanoma mets	3 (5%)
	Oesophagus mets	1 (1%)
Liver target for planning or treatment (n; %)	Whole liver	29 (44%)
	lobar	35 (53%)
	Selective	2 (3%)
Number of lesions		171
Number of lesions per patient (median; range)		3 (1-11)
Tumor volume (median; ml)		23.5 (4.2-1312)

mets: metastases; HCC: hepatocellular carcinoma

The estimates of the whole normal liver dose using MAA imaging (Figures 2 and 3 and table 2) were highly accurate. The correlation between MAA and ^{90}Y whole normal liver doses was very strong (R=0.97, P < 0.001) with a median absolute deviation of only 1.9 Gy. The maximum relative deviation from the linear fit was

29.6%. This variation was less than 5% for 39 patients (59%), less than 15% for 56 patients (85%) and less than 25% for 63 patients (95%).

Table 2: Variability of the differences between ^{90}Y and ^{99m}Tc-MAA absorbed doses in tumors and whole normal liver according to the catheter position.

Factor			Tumor	Whole normal liver	P value[$]
Difference between ^{90}Y and ^{99m}Tc-MAA absorbed doses (^{90}Y - ^{99m}Tc-MAA doses)	similar and comparable catheter positions	n	171	66	
		Mean (Gy)	10.9	- 0.6	
		Standard deviation (Gy)	89.34	2.69	
		Median (Gy)	3.7	- 0.5	0.153
		Median absolute deviation (Gy)	49.4	1.9	<0.001[*]
	Similar catheter positions	n	127	48	
		Mean (Gy)	9.6	- 0.6	
		Standard deviation (Gy)	82.72	2.53	
		Median (Gy)	4.7	-0.7	0.081
		Median absolute deviation (Gy)	47.8	1.8	<0.001[*]
	Comparable catheter positions	n	44	18	
		Mean (Gy)	14.6	- 0.3	
		Standard deviation (Gy)	107.18	3.13	
		Median (Gy)	-1.1	0	0.883
		Median absolute deviation (Gy)	55.1	2.2	< 0.058

[$]: Wilcoxon signed rank test for comparing medians and Brown and Forsythe's test for homogeneity of variance. [*]: Indicates a significant P value at the 5% threshold

Bland-Altman plot (Figure 3) demonstrated also that in 95% of cases, whole normal liver doses calculated with ^{90}Y imaging were 21.2% below and 20.6%

above whole normal liver doses calculated with MAA imaging (0.788-1.206; 95% limits of agreement). For example, for a WNLD of 50 Gy calculated with MAA imaging, the real WNLD evaluated with ^{90}Y imaging could be between 39 Gy and 60 Gy with 95% confidence.

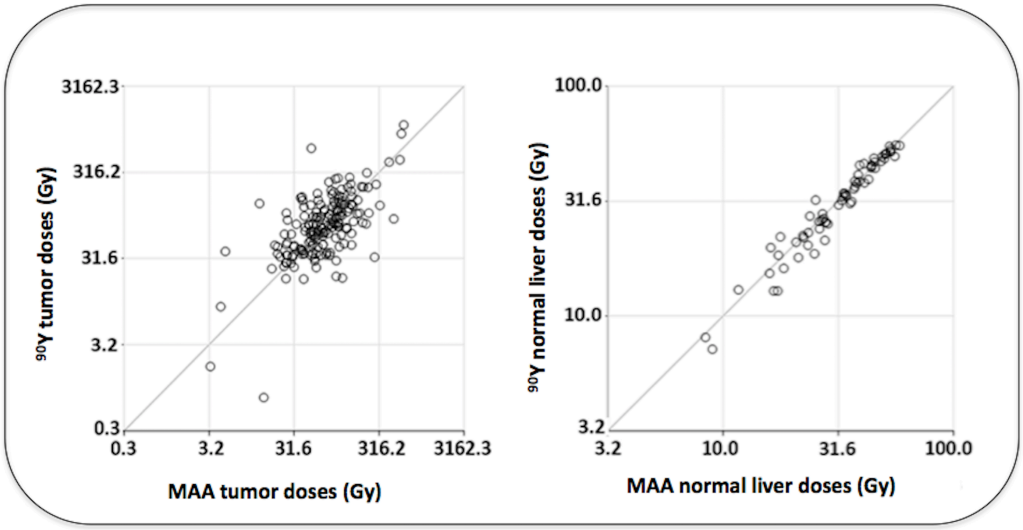

Figure 2: Relation between ^{99m}Tc-MAA and ^{90}Y absorbed doses (Log 10), determined in tumors (n=171; left panel) and in whole normal livers (n=66; right panel).

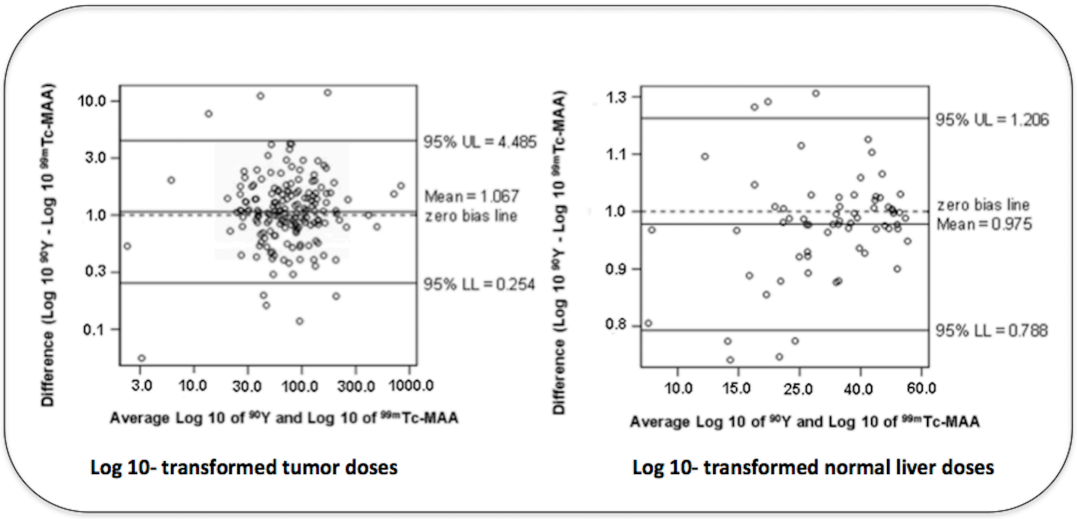

Figure 3: Bland-Altman plots of log 10-transformed tumor absorbed doses (left panel) and log 10-transformed whole normal liver absorbed doses (right panel).

For tumor absorbed doses, the correlation was less precise (R=0.65, P <0.001) with quite significant differences between ^{90}Y and MAA doses (median absolute deviation 49.4 Gy; Figures 2 and 3 & table 2). Bland-Altman analyses (Figure 3) demonstrated that in 95% of cases, tumor absorbed doses calculated with ^{90}Y imaging were 0.75 below and up to 4.5 times above tumor absorbed doses evaluated with MAA imaging (0.254-4.485; 95% limits of agreement). For example, for a TD of 100 Gy calculated with MAA imaging, the real (^{90}Y) TD could be between 25 and 450 Gy with 95% confidence. The linear mixed-effects regression model showed an intraclass correlation coefficient of 0.37 meaning that measurements within patients were no more similar than measurements from different patients.

No significant differences were found for procedures realized in similar or comparable catheter positions (median absolute deviation: 47.8 Gy vs 55.1 Gy; table 2). The differences between ^{90}Y and MAA tumor absorbed doses were substantial for each tumor type (table 3).

The T/NTL grade was well predicted with MAA imaging using ^{90}Y imaging as gold standard (table 4). The low or high grades were predicted with a sensitivity of 77.6%, a specificity of 70.9%, a positive predictive value of 84.9% and a negative predictive value of 60%. In other words, MAA imaging was able to predict a high T/NTL uptake in 85%.

Moreover, T/NTL calculated with ^{90}Y imaging was statistically higher to T/NTL calculated from MAA imaging (table 5).

Table 3: Variability of the differences between ^{90}Y and ^{99m}Tc-MAA absorbed doses in tumors and whole normal liver according to the type of tumor

Type			Tumor	Whole normal liver	P value$^{\$}$
Difference between ^{90}Y and ^{99m}Tc-MAA absorbed doses (^{90}Y - ^{99m}Tc-MAA doses)	Hepatocellular carcinoma	N	36	22	
		Mean (Gy)	- 3.6	0.6	
		Standard deviation (Gy)	98.4	2.98	
		Median (Gy)	4.4	0.0	0.706
		Median absolute deviation (Gy)	63.1	2.4	0.001 *
	Colorectal metastases	N	71	21	
		Mean (Gy)	3.6	- 1.1	
		Standard deviation (Gy)	75.76	2.69	
		Median (Gy)	2.2	- 0.8	0.392
		Median absolute deviation (Gy)	33.5	1.9	0.080
	Neuroendocrine metastases	N	48	16	
		Mean (Gy)	37.3	-1.6	
		Standard deviation (Gy)	107.06	2.12	
		Median (Gy)	23.1	- 0.8	0.093
		Median absolute deviation (Gy)	66.4	1.6	0.019*

$: Wilcoxon signed rank test for comparing medians and Brown and Forsythe's test for homogeneity of variance· *: Indicates a significant P value at the 5% threshold.

Table 4: Tumor to normal targeted liver (T/NTL) grades defined with ^{99m}Tc-MAA SPECT/CT and ^{90}Y PET/CT. Tumor grades were defined as low and high using a threshold of 1.5.

T/NTL	High grade $_{90Y}$ (≥ 1.5)	Low grade $_{90Y}$ (<1.5)
High grade $_{MAA}$ (≥ 1.5)	90	16
Low grade $_{MAA}$ (<1.5)	26	39

Table 5: Differences between ^{90}Y and ^{99m}Tc-MAA tumor to normal targeted liver uptake (T/NTL).

Factor	T/NTL MAA	T/NTL ^{90}Y	P value$^{\$}$
n	171	171	0.015*
Mean	2.59	3.09	
Standard deviation	2.840	4.320	
Median	1.80	1.84	
Minimum	0.09	0.02	
Maximum	20.94	41.69	

$: P-value from Wilcoxon rank sum test for paired data
*: Indicates a significant p-value at the 5% threshold

The comparison between the BSA method and the two-compartment dosimetry method demonstrated significant differences in planned activities. Activities determined with the two-compartment dosimetry method were significantly higher than activities calculated with the BSA method using the different thresholds of whole or targeted normal liver absorbed doses (table 6 and Figure 4). Using a threshold of 50 or 70 Gy in the normal targeted liver, the injected activity would have been increased by more than 30% in 22 procedures (33%) and decreased by more than 30% in 2 procedures (3%), by comparison with the BSA method.

Table 6: Differences in activities retrospectively planned with the BSA method and with the two-compartment dosimetry method reaching different absorbed doses to the normal liver compartment.

		Activity BSA method (GBq)	Activity two-compartment dosimetry method (GBq)	P value[$]
Normal targeted liver absorbed dose = 70 Gy	n	17	17	0.042[*]
	Mean	1.00	1.84	
	Standard deviation	0.390	1.400	
	Median	1.01	1.26	
	Minimum	0.48	0.62	
	Maximum	1.80	5.31	
Normal targeted liver absorbed dose = 50 Gy	n	49	49	0.047[*]
	Mean	1.56	1.95	
	Standard deviation	0.430	0.910	
	Median	1.61	1.75	
	Minimum	0.29	0.35	
	Maximum	2.63	5.02	
Normal targeted liver absorbed dose = 50 Gy or 70 Gy (all patients)	n	66	66	0.009[*]
	Mean	1.41	1.92	
	Standard deviation	0.490	1.050	
	Median	1.51	1.69	
	Minimum	0.29	0.35	
	Maximum	2.63	5.31	
Whole normal liver absorbed dose = 40 Gy (all patients)	n	66	66	<0.0001[*]
	Mean	1.41	1.86	

	Standard deviation	0.490	1.120	
	Median	1.51	1.59	
	Minimum	0.29	0.82	
	Maximum	2.63	8.18	

*: Indicates a significant P value at the 5% threshold. $: P value from Wilcoxon signed rank test for paired data.

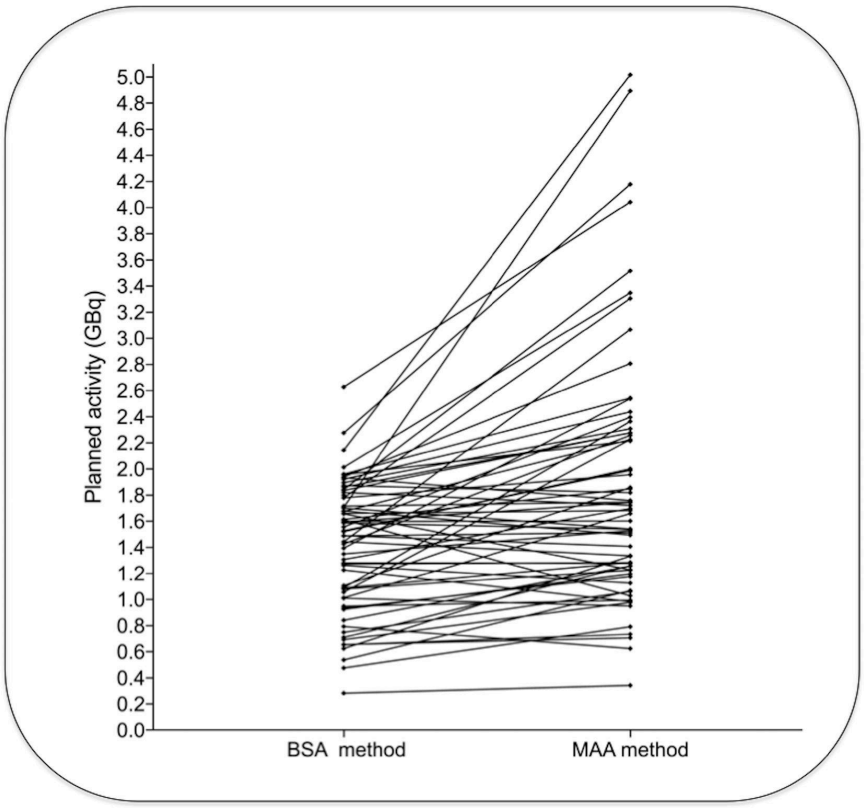

Figure 4: Comparison of the planned activity defined with the BSA method and the two- compartment dosimetry method reaching the maximum tolerable absorbed dose to the normal targeted liver.

Using a simulation in the normal targeted liver compartment (50 or 70 Gy), tumor absorbed doses were significantly higher with the two-compartment dosimetry method than tumor absorbed doses estimated with the BSA method (median ^{90}Y TD: 93 Gy vs 76 Gy, P< 0.001). In HCC patients, a tumor absorbed dose greater or equal to 100 Gy was achieved in 31 of the 47 tumors (66%) with the two-compartment dosimetry method and in only 24 tumors (51%) using the BSA method.

6.4 Discussion

In external beam radiation therapy (EBRT), dose planning is a essential step before treatment, and includes performing a segmentation of the tumor and surrounding healthy tissues, and evaluating their dose distribution (4). This planning aims to deliver an efficient absorbed dose to the tumor while minimizing the absorbed dose to the adjacent organs, avoiding radiation induced morbidity(10). Compared to EBRT, dosimetry in ^{90}Y-RE is not fully developed yet and only MAA SPECT/CT is currently available for dose simulations.

In this study, MAA imaging predicted with accuracy the whole normal liver absorbed dose, in agreement with recent studies (5, 6, 11). Based on this knowledge, the activity could be planned accurately and safely, reaching the maximal tolerated absorbed dose of the normal liver. In this study, the maximal variation of the $WNLD_{MAA}$ compared to the linear fit was 29.6% but for a large majority of patients, this variation was below 15% (56 patients, 85%).

Threshold doses for liver toxicity and especially for radioembolization induced liver disease (REILD) were analyzed in previous studies. With resin microspheres, the parenchyma exposure should be kept below 50 Gy for whole liver treatment and 70 Gy for lobar radioembolization, with low and acceptable risks of toxicity under these thresholds (12). The tolerable absorbed dose to the healthy liver could be higher for lobar treatment (e.g. 70 Gy), especially when the liver reserve was superior to 30%. With glass microspheres, Garin et al. found that a high healthy liver absorbed dose associated with a liver reserve lower than 30% was a strong factor for severe liver toxicity (13). Using a computational model, Walrand et al. demonstrated also a dose-toxicity relationship dependent on the targeted liver volume. The predicted normal tissue complication probability (NTCP) was reduced when two thirds of the liver were targeted compared to a whole liver treatment (14). However, the maximum tolerable whole normal liver dose in patients treated with resin microspheres is not precisely identified by a radiobiological model demonstrating the risk of liver decompensation as a function of the whole liver non tumoral absorbed dose. Sangro et al. observed a REILD in 9 patients out of 33, who received a whole normal liver absorbed dose of 37 ± 12 Gy (15). In 20 patients treated by a whole liver approach for metastatic lesions and receiving 40 Gy to the whole non-tumoral liver, Cremonesi et al. did not observe toxicity(16). Strigari et al. demonstrated also a 50% probability of liver toxicity (≥ Grade 2) with a whole normal liver absorbed dose of 52 Gy (95%

CI, 44-61 Gy) with a dosimetry based on bremsstrahlung SPECT (17). However, in this cohort of HCC patients, 15 of the 73 patients (20%) had advanced cirrhosis (Child B or more) and then a lower tolerability to radiation. Accordingly, recent international recommendations determined that the mean absorbed dose to the non-tumoral whole liver ≤ 40 Gy is considered safe (18). Moreover, the liver tolerance to radiation also differs as a function of the individual patient status. The liver tolerance is reduced in HCC patients as compared to metastatic liver patients (19). Most of the HCC patients have an underlying liver disease (cirrhosis of any causes, chronic HBV, …) with an impaired hepatic function, hence a lower tolerance to radiation. The stage of the liver disease is an important parameter and especially, an abnormal baseline bilirubin ≥ 1.1 mg/dl or a Child-Pugh score B or C are strongly correlated with the occurrence of toxicity (20, 21). Previous hepatotoxic chemotherapies can also reduce the liver function reserve and the tolerance to radiation (22).

In comparison to the classic BSA method, the two-compartment dosimetry method developed here demonstrated the possibility to significantly increase the planned activity in many cases, expecting an increase in tumor absorbed dose and hence in tumor control probability (17). Tumor absorbed doses were significantly higher with the two-compartment dosimetry method than tumor absorbed doses estimated with the BSA method (median ^{90}Y TD: 93 Gy vs 76 Gy, P< 0.001). In HCC patients, a tumor absorbed dose greater or equal to 100 Gy was associated with

higher tumor control and longer survival in a secondary analysis of the prospective SARAH study (23). In our data, the absorbed dose threshold of 100 Gy was achieved in 66% of tumors with the two-compartment dosimetry method and in only 51% using the BSA method. The activity planned with the BSA method could result in low tumor absorbed doses. This might explain the negative results of previous prospective trials (24-26). Moreover, in a few patients of our study, activity planned with the two-compartment dosimetry was lower by comparison with the activity delivered by the BSA method. Previous studies have confirmed the risks of overdosing using the BSA model, especially for patients with small livers or with limited tumor involvement (15, 27, 28). As suggested by some previous data (29, 30), our results support to abandon the BSA method for activity planning with resin microspheres for a more optimized method based on the two-compartment dosimetry model.

In this study, we defined two models of activity planning based on the MAA non-tumoral distribution. A first model targeted the maximum non-ablative absorbed to the normal targeted liver and the second model targeted the maximum tolerable absorbed dose to the whole non-tumoral liver. This second approach was recently suggested by Chiesa et al., in order to improve the treatment planning (21). In this study, the absorbed dose averaged over the whole non-tumoral liver was a strong risk factor for liver decompensation. In this large cohort of HCC patients treated with glass microspheres, a 15% liver decompensation risk

(NTCP analysis) was associated with a non-tumoral whole liver absorbed dose of 90 Gy, or 50 Gy for patients with increased bilirubinemia (bilirubin > 1.1 mg/dl). Previously, Strigari et al. came to similar conclusions with resin microspheres (17). In EBRT, the absorbed dose averaged over the whole normal liver is also the strong predictor of radiotherapy induced liver disease (31). Moreover, Dawson et al. analysed the correlation between the liver tolerance to radiation and the proportion of the irradiated liver volume (19). Using the Lyman NTCP model, they demonstrated that the liver tolerance was inversely proportional to the irradiated liver fraction. In other words, the absorbed dose to the irradiated normal liver could be increased when the irradiated volume proportion decreases, without higher risks of liver decompensation. Therefore, the activity planning based on the WNLD is the most optimized method permitting to deliver the maximal tolerable activity. With regards to this radiobiological approach, a dose limitation on the normal targeted liver is unnecessary to avoid a REILD. However, the two-compartment dosimetry method using a WNLD approach could result in significant effects in the normal targeted liver especially when the targeted volume is relatively small as compared to the whole liver volume (high normal targeted liver absorbed dose). Besides, a lobar normal liver absorbed above 70 Gy with resin microspheres could be ablative (radiation lobectomy) (18). Local toxicity can be expected such as cholangitis, biloma and fibrosis (32-34). Moreover, due to the high number of microspheres per GBq, a high activity of

resin microspheres injected in a small volume increases the risk of vascular saturation, flow stasis and reflux in non-targeted tissues(35). Therefore, this method is not the preferable approach when a small proportion of the liver volume is irradiated (i.e. < 40%), to avoid local toxicity (other than liver decompensation).

With regards to the tumor absorbed doses, significant variations between the planned dose (MAA imaging) and the real dose (^{90}Y imaging) were demonstrated in our study. This variability was sometimes very substantial despite a similar catheter placement between the preliminary and therapeutic arteriographies. However, many other angiographic parameters could influence the particles' delivery by the catheter and generate local differences in the liver distribution(36). This tumor absorbed dose approximation demonstrates the lack of accuracy of MAA imaging for dose planning in the tumor compartment. Recent recommendations purposed a personalised approach reaching an efficacy tumor absorbed dose cut-off of 100-120 Gy for HCC using ^{99m}Tc-MAA SPECT/CT (18). Indeed, using the partition model, the activity prescription consists in delivering a target tumor absorbed dose while preserving the liver parenchyma by a safety absorbed dose to the normal liver compartment. However, previous radiobiological analyses demonstrated a continuous relationship (sigmoid shape) between the tumor absorbed dose and the tumor control probability (17, 23). In our MAA model, we would reach the maximum tolerable activity and then the

maximum absorbed dose to tumor to expect the maximal probability of tumor control.

Regarding our analysis of the tumor absorbed dose, MAA imaging was not very accurate with a risk of underestimation or overestimation (table 2, Figure 2 and 3). Moreover, the grade of tumor to normal liver targeted uptake (T/NTL) could be misestimated. Nevertheless, a T/NTL at least 1.5-fold higher than the normal targeted liver was well predicted in 85% (table 5). Therefore, a high tumor absorbed dose (i.e. a high T/NTL) was well predicted with MAA in most cases which could explain the good clinical results of previous studies using a tumor dosimetry performed with MAA imaging and using a threshold tumor absorbed dose (23, 37). Using the two-compartment dosimetry method reaching the maximal tolerable absorbed dose to the targeted normal liver (50 Gy or 70 Gy), the simulated MAA tumor absorbed doses and the ^{90}Y tumor absorbed doses could be recalculated in our 47 HCC tumors. Then, 28 out of 47 tumors had a MAA tumor absorbed dose ≥ 100 Gy (60%) and 31 tumors (66%) reached this threshold dose in reality (^{90}Y imaging). The MAA threshold absorbed dose of 100 Gy defined by Hermann et al. was well predicted in 90% in this population of tumors (23). Nevertheless, in this data, a low tumor absorbed dose (i.e. low T/NTL) could be underestimated with MAA imaging in a significant number of tumors (table 4). Therefore, RE should not be withheld in all cases when the efficacy absorbed dose cut-off is not reached with the partition model.

Previously, in a large cohort of patients, Ilhan et al. found more discordance between ^{99m}Tc-MAA SPECT and ^{90}Y-bremsstrahlung SPECT tumor uptakes using a visual scale (38). This difference could be explained by the lower image quality of ^{90}Y-bremsstrahlung SPECT compared to ^{90}Y-TOF-PET systems (39). In accordance with this study, some previous data showed also a trend of MAA imaging to underestimate the actual absorbed dose(5, 40, 41). However, Gnesin et al. demonstrated the opposite in a series of HCC patients and Kafrouni et al. identified only minimal differences especially when the catheter position was deemed identical between procedures (6, 42).

Our results have to deal with several limitations. Firstly, a threshold of 2 cm between the catheter tip positions was used for patient inclusion in this study. However, unnoticeable differences in catheter tip positions (e.g. 5mm) could be responsible for important variations in particle distributions in segment-to-segment distribution and explain some differences in tumor absorbed doses (43). Secondly, this dosimetry was realized with a rigid co-registration of SPECT and PET images with the baseline enhanced CT scan or MRI. Due to physiological liver deformations and differences in spatial resolution between imaging techniques, some misalignments could occur and lead to variations in absorbed dose calculations(44). Future developments in deformable/ elastic registration and its implementation in the workflow of commercially available dosimetry softwares may improve the accuracy of the dose planning(45). Thirdly, the activities based

on MAA imaging were calculated with a correction for the lung shunt, using planar scintigraphic images. However, this lung shunt is significantly overestimated with planar images and can be more accurately predicted using SPECT/CT (46). In most cases, the lung shunt is low and the effect of the correction is limited.

Fourthly, this study is retrospective: the activity choice through the two-compartment dosimetry model, reaching the maximum tolerable liver absorbed dose, needs to be validated in future studies. The lack of data that precisely determine the correlation between the whole normal liver absorbed dose and the risk of liver decompensation is a limitation for an application in clinical practice. Similarly to the previous works of Strigari et al. and Chiesa et al., only a NTCP analysis in a large cohort of patients would allow to clarify this risk using resin microspheres (17, 21). Moreover, additional dose-toxicity studies focusing on local radiation damage are necessary to estimate the maximal absorbed doses tolerated by the targeted normal liver volume.

Finally, some patients were simulated using a classic end-hole catheter and treated with an antireflux catheter (ARC). ARC can modify the hemodynamic flux in the downstream compartment and improve the tumor targeting and tumor absorbed doses in neuroendocrine and HCC tumors (47). Using this catheter in some patients can explain why T/TNL and tumor doses were higher in this subgroup for neuroendocrine tumors (mean differences between 90Y and MAA tumor absorbed dose: 37.3 Gy).

Conclusion

^{99m}Tc-MAA SPECT dosimetry offers an excellent prediction of the whole normal liver absorbed dose. ^{99m}Tc-MAA SPECT/CT could be used in practice to plan the injected activity reaching the maximal tolerable absorbed dose to the whole normal liver. With this approach, the radioembolization treatment planning would be better personalized and optimized, expecting more efficiency, while keeping the risk of toxicity under control.

References

1. euratom Ecd. Basic safety standards for protection against the dangers arising from exposure to ionising radiation and repealing Directives 89/618/Euratom, 90/641/Euratom, 96/29/Euratom, 97/43/Euratom and 2003/122/Euratom. OJ of the EU 2014;L53;57:1-73.
2. Padia SA, Lewandowski RJ, Johnson GE, Sze DY, Ward TJ, Gaba RC, et al. Radioembolization of Hepatic Malignancies: Background, Quality Improvement Guidelines, and Future Directions. J Vasc Interv Radiol. 2017;28(1):1-15.
3. Kao YH, Tan EH, Ng CE, Goh SW. Clinical implications of the body surface area method versus partition model dosimetry for yttrium-90 radioembolization using resin microspheres: a technical review. Ann Nucl Med. 2011;25(7):455-61.
4. Justin K. Mikell YKD, Dawn Owen. Transarterial radiombolization for hepatocellular carcinoma and hepatic metastases: Clinical aspects and dosimetry models. Seminars in radiation oncology. 2019;30:68-76.
5. Jadoul A, Bernard C, Lovinfosse P, Gerard L, Lilet H, Cornet O, et al. Comparative dosimetry between (99m)Tc-MAA SPECT/CT and (90)Y PET/CT in primary and metastatic liver tumors. Eur J Nucl Med Mol Imaging. 2020;47(4):828-37.
6. Kafrouni M, Allimant C, Fourcade M, Vauclin S, Guiu B, Mariano-Goulart D, et al. Analysis of differences between (99m)Tc-MAA SPECT- and (90)Y-microsphere PET-based dosimetry for hepatocellular carcinoma selective internal radiation therapy. EJNMMI Res. 2019;9(1):62.

7. Giammarile F, Bodei L, Chiesa C, Flux G, Forrer F, Kraeber-Bodere F, et al. EANM procedure guideline for the treatment of liver cancer and liver metastases with intra-arterial radioactive compounds. Eur J Nucl Med Mol Imaging. 2011;38(7):1393-406.
8. Kennedy A, Coldwell D, Sangro B, Wasan H, Salem R. Radioembolization for the treatment of liver tumors general principles. Am J Clin Oncol. 2012;35(1):91-9.
9. Ho S, Lau WY, Leung TW, Chan M, Ngar YK, Johnson PJ, et al. Partition model for estimating radiation doses from yttrium-90 microspheres in treating hepatic tumours. Eur J Nucl Med. 1996;23(8):947-52.
10. Amjad Hussain WM. Treatment planning in radiation therapy. In: Springer, editor. An introduction to medical physics2018. p. 63-127.
11. Thomas MA, Mahvash A, Abdelsalam M, Kaseb AO, Kappadath SC. Planning dosimetry for (90) Y radioembolization with glass microspheres: Evaluating the fidelity of (99m) Tc-MAA and partition model predictions. Med Phys. 2020;47(10):5333-42.
12. Lau WY, Kennedy AS, Kim YH, Lai HK, Lee RC, Leung TW, et al. Patient selection and activity planning guide for selective internal radiotherapy with yttrium-90 resin microspheres. Int J Radiat Oncol Biol Phys. 2012;82(1):401-7.
13. Garin E, Lenoir L, Edeline J, Laffont S, Mesbah H, Poree P, et al. Boosted selective internal radiation therapy with 90Y-loaded glass microspheres (B-SIRT) for hepatocellular carcinoma patients: a new personalized promising concept. Eur J Nucl Med Mol Imaging. 2013;40(7):1057-68.
14. Walrand S, Hesse M, Jamar F, Lhommel R. A hepatic dose-toxicity model opening the way toward individualized radioembolization planning. J Nucl Med. 2014;55(8):1317-22.
15. Sangro B, Gil-Alzugaray B, Rodriguez J, Sola I, Martinez-Cuesta A, Viudez A, et al. Liver disease induced by radioembolization of liver tumors: description and possible risk factors. Cancer. 2008;112(7):1538-46.
16. Cremonesi M, Ferrari M, Bartolomei M, Orsi F, Bonomo G, Arico D, et al. Radioembolisation with 90Y-microspheres: dosimetric and radiobiological investigation for multi-cycle treatment. Eur J Nucl Med Mol Imaging. 2008;35(11):2088-96.
17. Strigari L, Sciuto R, Rea S, Carpanese L, Pizzi G, Soriani A, et al. Efficacy and toxicity related to treatment of hepatocellular carcinoma with 90Y-SIR spheres: radiobiologic considerations. J Nucl Med. 2010;51(9):1377-85.
18. Levillain H, Bagni O, Deroose CM, Dieudonne A, Gnesin S, Grosser OS, et al. International recommendations for personalised selective internal radiation therapy of primary and metastatic liver diseases with yttrium-90 resin microspheres. Eur J Nucl Med Mol Imaging. 2021.

19. Dawson LA, Ten Haken RK. Partial volume tolerance of the liver to radiation. Semin Radiat Oncol. 2005;15(4):279-83.
20. Chiesa C, Maccauro M, Romito R, Spreafico C, Pellizzari S, Negri A, et al. Need, feasibility and convenience of dosimetric treatment planning in liver selective internal radiation therapy with (90)Y microspheres: the experience of the National Tumor Institute of Milan. Q J Nucl Med Mol Imaging. 2011;55(2):168-97.
21. Chiesa C, Mira M, Bhoori S, Bormolini G, Maccauro M, Spreafico C, et al. Radioembolization of hepatocarcinoma with (90)Y glass microspheres: treatment optimization using the dose-toxicity relationship. Eur J Nucl Med Mol Imaging. 2020;47(13):3018-32.
22. Koay EJ, Owen D, Das P. Radiation-Induced Liver Disease and Modern Radiotherapy. Semin Radiat Oncol. 2018;28(4):321-31.
23. Hermann AL, Dieudonne A, Ronot M, Sanchez M, Pereira H, Chatellier G, et al. Relationship of Tumor Radiation-absorbed Dose to Survival and Response in Hepatocellular Carcinoma Treated with Transarterial Radioembolization with (90)Y in the SARAH Study. Radiology. 2020;296(3):673-84.
24. Vilgrain V, Pereira H, Assenat E, Guiu B, Ilonca AD, Pageaux GP, et al. Efficacy and safety of selective internal radiotherapy with yttrium-90 resin microspheres compared with sorafenib in locally advanced and inoperable hepatocellular carcinoma (SARAH): an open-label randomised controlled phase 3 trial. Lancet Oncol. 2017;18(12):1624-36.
25. Chow PKH, Gandhi M, Tan SB, Khin MW, Khasbazar A, Ong J, et al. SIRveNIB: Selective Internal Radiation Therapy Versus Sorafenib in Asia-Pacific Patients With Hepatocellular Carcinoma. J Clin Oncol. 2018;36(19):1913-21.
26. Garin E, Palard X, Rolland Y. Personalised Dosimetry in Radioembolisation for HCC: Impact on Clinical Outcome and on Trial Design. Cancers (Basel). 2020;12(6).
27. Lam MG, Louie JD, Abdelmaksoud MH, Fisher GA, Cho-Phan CD, Sze DY. Limitations of body surface area-based activity calculation for radioembolization of hepatic metastases in colorectal cancer. J Vasc Interv Radiol. 2014;25(7):1085-93.
28. Gil-Alzugaray B, Chopitea A, Inarrairaegui M, Bilbao JI, Rodriguez-Fraile M, Rodriguez J, et al. Prognostic factors and prevention of radioembolization-induced liver disease. Hepatology. 2013;57(3):1078-87.
29. Cremonesi M, Chiesa C, Strigari L, Ferrari M, Botta F, Guerriero F, et al. Radioembolization of hepatic lesions from a radiobiology and dosimetric perspective. Front Oncol. 2014;4:210.
30. Kafrouni M, Allimant C, Fourcade M, Vauclin S, Delicque J, Ilonca AD, et al. Retrospective Voxel-Based Dosimetry for Assessing the Ability of the Body-

Surface-Area Model to Predict Delivered Dose and Radioembolization Outcome. J Nucl Med. 2018;59(8):1289-95.
31. Pan CC, Kavanagh BD, Dawson LA, Li XA, Das SK, Miften M, et al. Radiation-associated liver injury. Int J Radiat Oncol Biol Phys. 2010;76(3 Suppl):S94-100.
32. Singh P, Anil G. Yttrium-90 radioembolization of liver tumors: what do the images tell us? Cancer Imaging. 2014;13(4):645-57.
33. Golfieri R. SIR-Spheres yttrium-90 radioembolization for the treatment of unresectable liver cancers. Hepat Oncol. 2014;1(3):265-83.
34. Minocha J, Lewandowski RJ. Radioembolization for hepatocellular carcinoma complicated by biliary stricture. Semin Intervent Radiol. 2011;28(2):226-9.
35. Lam M, Banerjee S, Louie JD, Abdelmaksoud MHK, Iagaru AH, Ennen RE, et al. Root cause analysis of gastroduodenal ulceration after yttrium-90 radioembolization. Cardiovasc Intervent Radiol. 2013;36(6):1536-47.
36. Aramburu J, Anton R, Rivas A, Ramos JC, Sangro B, Bilbao JI. Liver Radioembolization: An Analysis of Parameters that Influence the Catheter-Based Particle-Delivery via CFD. Curr Med Chem. 2020;27(10):1600-15.
37. Garin E, Tselikas L, Guiu B, Chalaye J, Edeline J, de Baere T, et al. Personalised versus standard dosimetry approach of selective internal radiation therapy in patients with locally advanced hepatocellular carcinoma (DOSISPHERE-01): a randomised, multicentre, open-label phase 2 trial. Lancet Gastroenterol Hepatol. 2021;6(1):17-29.
38. Ilhan H, Goritschan A, Paprottka P, Jakobs TF, Fendler WP, Todica A, et al. Predictive Value of 99mTc-MAA SPECT for 90Y-Labeled Resin Microsphere Distribution in Radioembolization of Primary and Secondary Hepatic Tumors. J Nucl Med. 2015;56(11):1654-60.
39. Elschot M, Vermolen BJ, Lam MG, de Keizer B, van den Bosch MA, de Jong HW. Quantitative comparison of PET and Bremsstrahlung SPECT for imaging the in vivo yttrium-90 microsphere distribution after liver radioembolization. PLoS One. 2013;8(2):e55742.
40. Rhee S, Kim S, Cho J, Park J, Eo JS, Park S, et al. Semi-Quantitative Analysis of Post-Transarterial Radioembolization (90)Y Microsphere Positron Emission Tomography Combined with Computed Tomography (PET/CT) Images in Advanced Liver Malignancy: Comparison With (99m)Tc Macroaggregated Albumin (MAA) Single Photon Emission Computed Tomography (SPECT). Nucl Med Mol Imaging. 2016;50(1):63-9.
41. Richetta E, Pasquino M, Poli M, Cutaia C, Valero C, Tabone M, et al. PET-CT post therapy dosimetry in radioembolization with resin (90)Y microspheres: Comparison with pre-treatment SPECT-CT (99m)Tc-MAA results. Phys Med. 2019;64:16-23.

42. Gnesin S, Canetti L, Adib S, Cherbuin N, Silva Monteiro M, Bize P, et al. Partition Model-Based 99mTc-MAA SPECT/CT Predictive Dosimetry Compared with 90Y TOF PET/CT Posttreatment Dosimetry in Radioembolization of Hepatocellular Carcinoma: A Quantitative Agreement Comparison. J Nucl Med. 2016;57(11):1672-8.
43. Aramburu J, Anton R, Rivas A, Ramos JC, Sangro B, Bilbao JI. Computational particle-haemodynamics analysis of liver radioembolization pretreatment as an actual treatment surrogate. Int J Numer Method Biomed Eng. 2017;33(2).
44. Bastiaannet R, Kappadath SC, Kunnen B, Braat A, Lam M, de Jong H. The physics of radioembolization. EJNMMI Phys. 2018;5(1):22.
45. Rigaud B, Simon A, Castelli J, Lafond C, Acosta O, Haigron P, et al. Deformable image registration for radiation therapy: principle, methods, applications and evaluation. Acta Oncol. 2019;58(9):1225-37.
46. Allred JD, Niedbala J, Mikell JK, Owen D, Frey KA, Dewaraja YK. The value of (99m)Tc-MAA SPECT/CT for lung shunt estimation in (90)Y radioembolization: a phantom and patient study. EJNMMI Res. 2018;8(1):50.
47. d'Abadie P, Walrand S, Goffette P, Amini N, Maanen AV, Lhommel R, et al. Antireflux catheter improves tumor targeting in liver radioembolization with resin microspheres. Diagn Interv Radiol. 2021;27(6):768-73.

7- Liver arteriography using an antireflux catheter: which impact on microsphere distribution? [6]

Abstract:

Purpose: To determine whether antireflux catheter (ARC) may result in better tumor targeting in liver radioembolization using ^{90}Y-resin microspheres.

Materials and Methods: Patients treated with resin microspheres for hepatocellular carcinoma (HCC) and secondary liver malignancies were retrospectively analyzed. All patients underwent a ^{99m}Tc-macroaggregated albumin (^{99m}Tc-MAA) SPECT/CT following the planning arteriography with a conventional end-hole catheter. For ^{90}Y-microspheres injection, two groups were defined depending on the type of catheter used : an ARC group (n=38) and a conventional (conv.) group treated with a conventional end-hole catheter (n=23). ^{90}Y-PET/CT was performed after the therapeutic arteriography. The choice of the catheter was not randomized but left to the choice of the interventional radiologist. ^{99m}Tc-MAA SPECT and ^{90}Y PET were co-registered with the baseline imaging to determine a tumor to normal liver ratio ($T/NL_{[MAA \text{ or } 90Y]}$) and tumor dose ($TD_{[MAA \text{ or } 90Y]}$) for the planning and therapy.

[6] Adapted from d'Abadie et al. Diagn Interv Radiol 2021 ; 27 : 768-773

Results: 38 patients (115 lesions) and 23 patients (75 lesions) were analyzed in the ARC and conv. groups, respectively. In the ARC group, T/NL_{90Y} and TD_{90Y} were significantly higher than T/NL_{MAA} and $TD_{MAA.}$ Median (IQR) T/NL_{90y} was 2.16 (2.15) versus 1.74 (1.43) for T/NL_{MAA} ($P < 0.001$). Median (IQR) TD_{90y} was 90.96 Gy (98.31 Gy) versus 73.72 Gy (63.82 Gy) for TD_{MAA} ($P< 0.001$). In this group, the differences were highly significant for neuroendocrine metastases (NEM) and HCC and less significant for colorectal metastases (CRM). In the conv. group, no significant differences were demonstrated.

Conclusion: The use of an ARC significantly improves tumor deposition of microspheres in liver radioembolization.

7.1 Introduction

Better tumor targeting is a real challenge to improve clinical results of radioembolization. An increase in the tumor dose leads to an increase in the tumor control probability and improved patient outcome (1). The technique has evolved recently, especially in the field of interventional radiology, for instance with the use of cone beam CT for accurate planning or by using special microcatheters, such as antireflux catheters (ARC) i.e. Surefire Infusion System® (Surefire Medical Inc., Westminster, CO, USA). ARC has a funnel shaped expanding tip (Figure 1) designed to minimize reflux of radioactive microspheres and the risk of extrahepatic deposition (2, 3). Changes in the downstream hepatic arterial

blood pressure were reported using this catheter (4). When the ARC is deployed, the arterial blood pressure decreases in the antegrade distribution and may reduce the resistance in the tumor vasculature. This hemodynamic effect seems responsible for an increase in tumor targeting in few previous reports (5, 6).

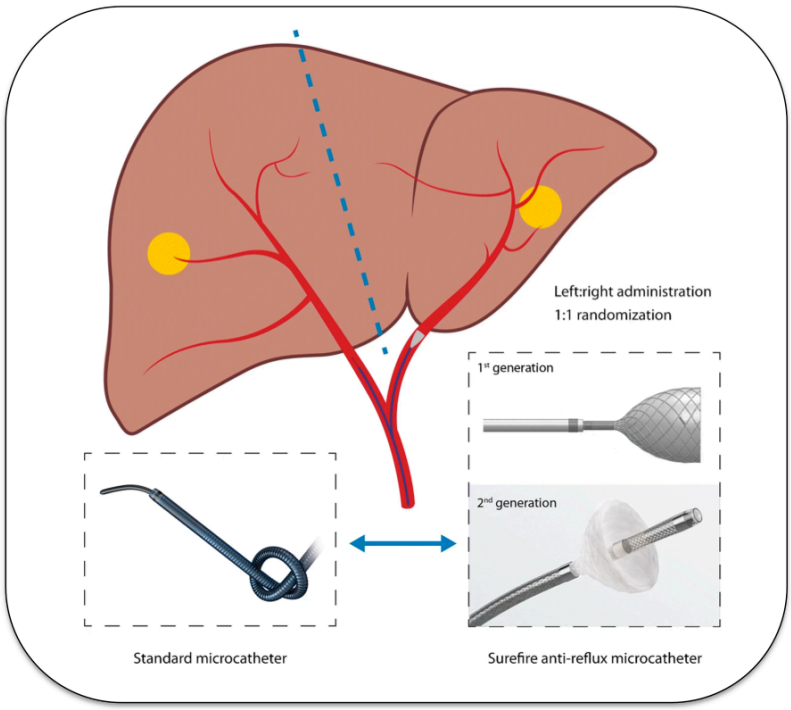

Figure 1: Schematic representation of a standard end-hole catheter in the right hepatic artery and an antireflux catheter in the left hepatic artery (adapted from van Roekel et al. (7)).

Our study aims to compare tumor to normal liver ratio (T/NL) and tumor absorbed doses (TD) when a conventional end-hole catheter (EHC) and an ARC are used in the same patient at two different time points. As a second endpoint, we investigated this effect as a function of the tumor type.

7.2 Methods

Procedures

Patients treated by radioembolization with resin microspheres were retrospectively analyzed from 2010 to 2019 after approval by the local ethics committee (2017/27JUI/334). Informed consent was waived because the entire study was retrospective. Each procedure was performed according to standards of clinical practice (8). A planning angiography was performed to identify the vascular supply of the tumor, to embolize some extrahepatic branches and finally radioembolization was simulated with ^{99m}Tc-MAA injection (TechneScan LyoMAA, Mallinckrodt Medical BV/Curium, Petten, The Netherlands). Then, ^{99m}Tc-MAA SPECT/CT imaging was obtained to confirm the absence of extrahepatic uptake and allowed to quantify a potential hepatopulmonary shunt. Within 1-3 weeks following the planning angiography, ^{90}Y-resin microspheres were injected (activity determined according to the BSA method), and the treatment was followed by a ^{90}Y PET-CT to assess the ^{90}Y microspheres deposition.

Characteristics of each arteriography were reviewed by a senior interventional radiologist and only procedures (planning and therapy) performed with similar catheter tip placement are reported in this study. Angiograms with differences in excess of 2cm in catheter tip positions were excluded from the analysis. ARC was used for patients with high-risk liver anatomy, particularly for microsphere injection in the close vicinity of a non-embolizable hepato-enteric arterial branch, to avoid extra-hepatic deposition. This decision though was left to the senior interventional radiologist, without randomization. All arteriographies were performed without the use of cone-beam CT.

The preliminary arteriography, performed was always executed with a conventional EHC.

Patients simulated with a classic EHC and treated with use of ARC were classified as the ARC group. The conv. group was defined as patients in whom EHC was used in both planning and therapeutic arteriographies.

Patients and tumors

Patients and tumor characteristics are summarized in tables 1 and 2. Briefly, 38 patients with 115 lesions were identified in the ARC group and 23 patients with 75 lesions in the conv. group. In the ARC group, the types of tumors were colorectal metastases (CRM) with 48 lesions (41.7%), neuroendocrine metastases (NEM) with 30 lesions (26.1%) and HCC with 24 lesions (20.9%), as compared with 22

lesions (29.3%), 34 lesions (45.3%) and 19 lesions (25.3%) in the conv. group, respectively.

Table 1: Patient characteristics

Characteristics		ARC* group (n= 38)	Conv. group (n= 23)	P value
Gender	Female	11 (28.9%)	8 (34.8%)	0.633
	Male	27 (71.1%)	15 (65.2%)	
Age (Years)	Median (IQR)	65.5 (17.7)	68.0 (12)	0.421
Tumor type	Cholangiocarcinoma	2 (5.3%)	0 (0.0%)	0.288
	Colorectal m.	15 (39.5%)	6 (26.1%)	
	HCC	9 (23.7%)	10 (43.5%)	
	Melanoma m.	3 (7.9%)	0 (0.0%)	
	Neuroendocrine m.	8 (21.1%)	7 (30.4%)	
	Esophagus m.	1 (2.6%)	0 (0.0%)	
Number of lesions per patient	Median (IQR)	3.0 (2)	2.0 (4)	0.421

Table 2: Individual lesions characteristics

Characteristics		ARC* group (n= 115)	Conv. group (n= 75)	P value
Volume lesion (ml)	Median (IQR)	25.3 (73.6)	10.8 (20.5)	0.010+
Target	Whole liver (bilobar)	51 (44.3%)	46 (61.3%)	0.052
	Lobar	58 (50.4%)	28 (37.3%)	
	Selective	6 (5.2%)	1 (1.3%)	
Tumor type	Colorectal m.	48 (41.7%)	22 (29.3%)	0.001+
	HCC	24 (20.9%)	19 (25.3%)	
	Neuroendocrine m.	30 (26.1%)	34 (45.3 HCC :	
	Miscellaneous	13 (11.3%)	0 (0.0%)	

QR : interquartile range; * Anti Reflux Catheter; m. metastases

Imaging protocols

^{99}Tc-MAA SPECT/CT was performed within 1 hour after injection of 150 to 170 MBq using a BrightView XCT scanner (Philips Healthcare, Cleveland, OH). Abdominal SPECT/CT images were acquired with a 128x128matrix with a low energy-high resolution collimator (64 angles per head, 25 sec /angle). Image reconstruction was achieved using an OSEM algorithm (8 iterations and 16 subsets) with attenuation and scatter corrections.

^{90}Y post-treatment imaging was performed with a TOF-PET-CT (Gemini TF, Philips Medical Systems, Cleveland, OH) with an abdominal acquisition of 40 minutes (2 bed positions). Reconstruction was performed with the 3-D line of response (LOR)-TOF blob-based algorithm (2 iterations, 33 subsets) and with a voxel reconstruction of 4x4x4 mm^3.

Tumor uptake and tumor absorbed dose

Lesions were firstly delineated using the baseline contrast-enhanced MRI or CT scan with MIM 6.7 (MIM Software Inc., Cleveland, OH) performed before the workup. In 3 patients of the ARC group, tumor delineation was based on FDG PET/CT because no baseline MRI or contrast-enhanced CT scan was available before treatment. Volumes of interest (normal liver and tumors) were fused with ^{99}Tc-MAA SPECT and ^{90}Y PET using a rigid co-registration.

The tumor to normal liver uptake ratio (T/NL) is a concentration ratio defined as:

$$T/_{NL} = \frac{Counts_T/_{Volume_T}}{Counts_{NL}/_{Volume_{NL}}}$$

where $Counts_T$ represents the total counts on the entire tumor volume of each individual tumor (diameter superior to 1 cm) and $Counts_{NL}$ the total counts in the injected normal liver volume. $Counts_T$ and $Counts_{NL}$ were measured from ^{99m}Tc-MAA SPECT or ^{90}Y PET datasets.

The absorbed dose to tumors was determined by the simplified MIRD-based equation (9, 10):

$$TD = \frac{Injected\ Activity\ (GBq)\ .50\ .\ (1 - LSF)\ .\ f_{tumor}}{Tumor\ mass\ (kg)}$$

where *LSF is* the lung shunt fraction and f_{tumor}, the fractional uptake of the tumor defined on ^{99m}Tc-MAA SPECT and on ^{90}Y PET:

$$f_{tumor} = \frac{total\ counts_{tumor}}{total\ counts_{liver}}$$

At the end, for each lesion a set of 4 data was available for analysis: for ^{99m}Tc-MAA SPECT, T/NL_{MAA} and TD_{MAA} and for ^{90}Y PET, T/NL_{90Y} and TD_{90Y}.

Statistics

Analyses were conducted using SAS V9.4 software (SAS Institute Inc., Cary, NC, USA). The main objective was to compare tumor uptake and tumor dose between ^{99m}Tc-MAA SPECT and ^{90}Y PET. T/NL_{MAA} and TD_{MAA} with T/NL_{90Y} and TD_{90Y}, respectively, were compared within each group (ARC and conv. separately) using a Wilcoxon signed rank test. The homogeneity of the patients and lesions characteristics were compared between the two groups using a Mann-Whitney U-test for the continuous variables. For categorical variables, comparisons were made using a Chi-square test or, when expected counts problem occurred, a Fisher-Freeman-Halton test. $P < 0.05$ was accepted as the significance level. Descriptive statistics were showed using frequencies with percentages, CI 95% of the medians and interquartile ranges.

7.3 Results

When pooling all tumors from both groups, where all patients received the ^{99m}Tc-MAA injection using EHC, the median T/NL_{MAA} was 2.19 in HCC (CI 95%: 1.53-2.85), 1.82 in NEM (CI 95%: 1.57-2.43) and 1.35 for CRM (CI 95%: 1.16-1.68). T/NL_{MAA} was significantly lower in CRM compared to NEM ($P = 0.010$) and HCC ($P = 0.002$).

In the ARC group, T/NL_{90Y} and TD_{90Y} were significantly higher than T/NL_{MAA} and TD_{MAA} (Fig. 1- left panel and tables 3 and 4). Detailed data per individual tumor type are found in Table 4. The tumor dose was significantly increased by a median 23% between the planning (measured using ^{99}Tc-MAA SPECT/CT, EHC used) and the treatment (measured using the ^{90}Y-PET/CT, ARC used). The increase of TD was the highest in NEM (increase of 55% between medians; P = 0.009), followed by HCC (increase of 42% between medians; P = 0.034), and lowest for CRC (increase of 13% between medians; P = 0.039), as demonstrated in table 4

(example of a NEM patient in Fig. 2). Similarly, T/NL was also increased by a median of 24% over the entire population of ARC patients (P < 0.001), with an increment of 36% in HCC (P = 0.010), 58% in NEM (P < 0.001) and only 15% in CRC patients (P = 0.162).

In the conv. group, no statistically significant difference was observed for neither the T/NL nor the TD between the planning and the post-treatment study (Fig. 1- right panel and table 3). In addition, no significant difference in tumor uptake (T/NL) was observed for any tumor type (data not shown).

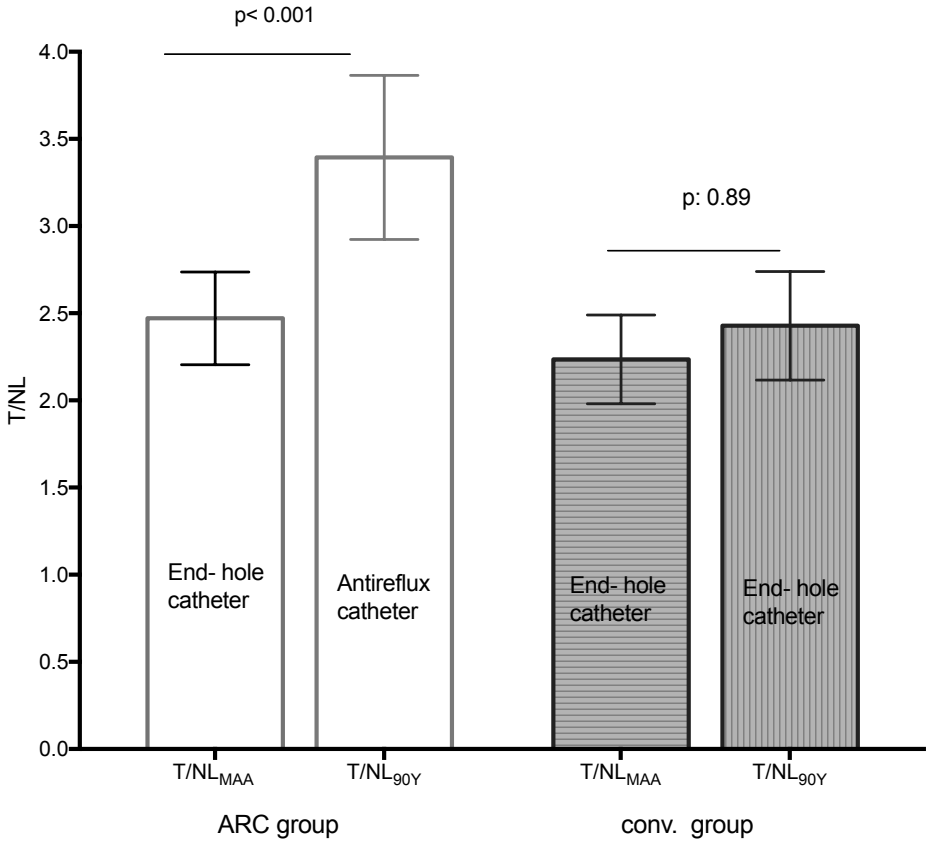

Figure 1: Tumor to normal liver uptake ratio (T/NL) observed with ^{99m}Tc-MAA SPECT/CT (MAA) and ^{90}Y PET/CT (90Y) in the ARC group (left panel) and in the conv. group (right panel).

Table 3: Tumor uptake and dose in groups

Groups	Characteristics		MAA	^{90}Y	P- value
ARC* n= 115	T/NL	Median (IQR)	1.74 (1.43)	2.16 (2.15)	<0.001+
	Dose (Gy)	Median (IQR)	73.72 (62.82)	90.96 (98.31)	<0.001+
Conv. n= 75	T/NL	Median (IQR)	1.60 (2.04)	1.57 (1.38)	0.892
	Dose (Gy)	Median (IQR)	72.92 (80.33)	66.88 (87.71)	0.950

QR:interquartile range. T/NL : tumor to normal liver uptake. *Anti reflux catheter +
Indicates a significant result at a 5% type I error

Table 4: Tumor type analysis in the ARC group

Tumor type	Characteristics		MAA	^{90}Y	P-value
Hepatocellular carcinoma n= 24 (20.9%)	T/NL	Median (IQR)	2.06 (2.10)	2.80 (1.94)	0.010°
	Dose	Median (IQR)	95.36 (110.79)	135.23 (116.40)	0.034°
Neuroendocrine metastases n= 30 (26.1%)	T/NL	Median (IQR)	1.88 (1.30)	2.97 (4.34)	<0.001°
	Dose	Median (IQR)	80.89 (63.52)	125.16 (127.07)	0.009°
Colorectal metastases n= 48 (41.7%)	T/NL	Median (IQR)	1.57 (1.01)	1.80 (1.18)	0.162
	Dose	Median (IQR)	62.22 (62.93)	70.26 (72.97)	0.039°

IQR: interquartile range. T/NL : tumor to normal liver uptake. ° Indicates a significant result at a 5% type I error.

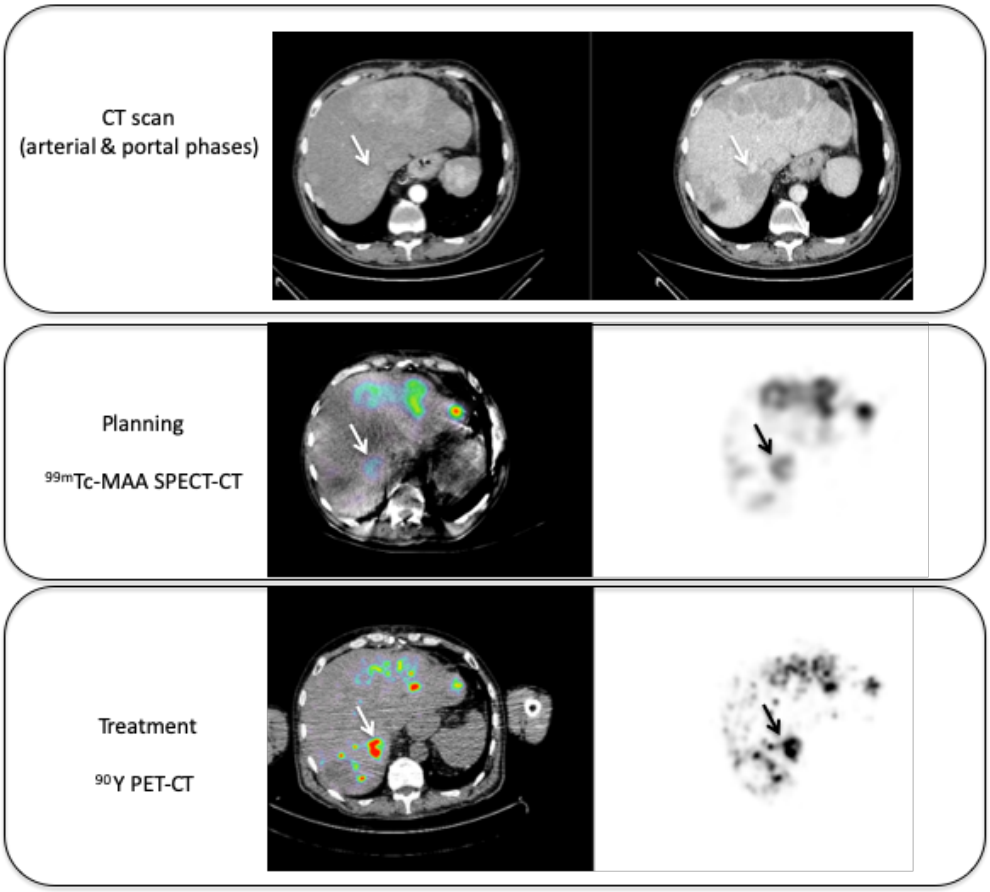

Figure 2: Example of a patient treated by liver radioembolization for high hypervascular neuroendocrine metastases demonstrated on CT scan (upper panel). The planning was performed with a classic end-hole catheter and followed by MAA SPECT-CT (middle panel). The treatment was performed with a antireflux catheter and followed by ^{90}Y PET-CT (lower panel). T/NL and tumor dose were respectively 2.9 and 69 Gy in the tumor located in segment 7 (arrow) with MAA imaging (planning). T/NL and tumor dose were respectively 8.4 and 172 Gy in this same tumor with ^{90}Y imaging (treatment).

7.4 Discussion

This study demonstrates that, using an ARC, an improvement of the T/NL of 36, 58 and 15% is obtained in HCC, NEM and CRM, respectively (median differences, table 4). In all radiation therapy applications, improving the absorbed dose to tumors, without increasing the dose to non-target tissues (which is expressed by the T/NL ratio), is a goal that cannot be overlooked. Better tumor targeting leads to higher doses to tumors and a higher probability of tumor control (11). Furthermore, the tumor control probability (TCP) as a function of the dose has a sigmoid shape (1, 12), resulting in the fact that little increases or decreases of tumor doses, close to the therapeutic window, may result in a major effect on clinical response or progression, respectively. Besides these scientific considerations, international authorities (e.g. Euratom 2013/59 and ICRP 140) strongly encourage all efforts towards dose optimization (13, 14).

Interestingly, a recent secondary analysis of the SARAH prospective study demonstrated a significant improvement in disease control and overall survival in radioembolization of HCC with a tumor dose above 100 Gy (15). Very recently, another study demonstrated that adding pre-therapeutic dosimetry as a tool for optimization results in better outcome results (16).

Why ARC improves tumor targeting is not totally understood. The downstream blood flow distribution is modified when the catheter tip is deployed. The occlusion level of this tip is dynamic, occlusive during the diastole. Similarly, if a retrograde flow appears, the expandable tip stays open and precludes reflux. A study by Rose et al. demonstrated a significant decrease of the blood pressure in the downstream arterial compartment (4). To maintain an antegrade flow in the downstream compartment, the pressure in the downstream vascular bed must be lower than the pressure near the catheter tip. Resistance in the downstream compartment may decline more and more in the distality by opening or recruiting new arteries. Arepally et al. illustrate this effect in an ex vivo study: in a swine model, the penetration of tantalum microspheres in the renal parenchyma was deeper with an ARC as compared with standard catheters. The microsphere distribution was visually more homogeneous and more extended to distal vessels (3). The distal pressure reduction induced by the deployment of this expandable tip is similar to what is demonstrated with the use of a microballoon catheter in transarterial chemoembolization (17). Pasciak et al. proposed another interpretation: the reduction of the downstream pressure may be induced by vasoconstriction of normal liver arteries, delivering more microspheres to tumor arteries (6). Moreover, in contrast with a conventional catheter, ARC allows an optimized centering of the catheter tip in the vessel lumen and generates a turbulent-like flow during the microsphere administration (18, 19). These effects

are responsible for a more homogeneous distribution in the downstream network. With a computer model of the hepatic artery and tumor vessels, Kennedy et al. demonstrated an increase in the tumor microsphere deposition when the flow was more homogeneous (20).

This study confirms some previous data. In a small prospective trial (n=9), Pasciak et al. performed for each patient two procedures of lobar infusions of ^{99}Tc-MAA in a nonrandomized 2 by 2 crossover design one-day protocol (6). One infusion was performed with an ARC and the other with an EHC. Tumor deposition increased between 33.0% to 90.0% with the ARC. In this study, lesions were mostly HCC (n=6). In a controlled trial conducted with 25 patients treated for CRM with holmium-166 (^{166}Ho) microspheres, the ARC was randomly allocated to the left or right liver artery and the standard catheter to the contralateral artery (5). The mean T/NL ratio was increased by 25.0% when lesions were treated using an ARC.

The current study also highlights other findings. In the ARC group, increases in tumor uptake and tumor dose between the planning arteriography (with an EHC) and the treatment arteriography (with an ARC) were variable in function of the tumor type: highly significant for NEM and HCC, modest for CRM. These differences could be explained by changes in tumor perfusion. Indeed, tumor targeting in ^{90}Y radioembolization depends on tumor arterial vascularization because microspheres are deposited preferentially in the terminal arterioles. NEM are often hypervascular with higher enhancement during a dynamic enhanced-

contrast CT scan compared to others types of metastases (21). To the contrary, CRM are often less perfused (22). Tumor arterial perfusion assessed by ^{99m}Tc MAA SPECT/CT confirmed in our study a higher tumor uptake for NEM and HCC as compared to CRM (table 4). Using computational models, Aramburu et al. demonstrated an important deceleration of the blood flow in the upstream compartment with ARC, resulting in a more homogeneous distribution of microspheres (23). In contrast, the flow velocity generated by an EHC is higher than twice the normal artery flow velocity (19, 24). Therefore, ARC could achieve a more physiological distribution of microspheres in the arterial flow, targeting better hypervascular tumors with high arterial blood supply.

This study has some limitations. First, although being an intra-patient comparison, our analysis is based on a comparison between two different radiolabeled vectors (^{99m}Tc-MAA and ^{90}Y microspheres) and the assumption of a good correlation between their respective behaviors. This consideration is questionable mainly due to physical differences between ^{99m}Tc-MAA particles and ^{90}Y-microspheres, including differences in size and number (25). A good reproducibility between ^{99m}Tc-MAA and ^{90}Y-microspheres requires also similar angiographic conditions and especially similar catheter positions (26). Minor differences in catheter tip positions could induce important differences in particle distributions (27, 28). With regards to ^{90}Y-PET-CT, previous studies confirmed a good accuracy of the technique to assess tumor uptake and absorbed doses after ^{90}Y-radioembolization

(29, 30). Some previous studies also demonstrated a good correlation between ^{99m}Tc-MAA SPECT/CT and ^{90}Y PET dosimetry (31-34). However, the reproducibility of dosimetry based on ^{99m}Tc-MAA SPECT/CT as compared with the ^{90}Y-PET/CT is not fully established and individual variations in tumor dose estimation can occur. To cope with this problem, we introduced a conventional (conv.) group where ^{99m}Tc-MAA and ^{90}Y microspheres injections were performed with the same type of microcatheter. This group confirmed that there were no significant differences between ^{99m}Tc-MAA and ^{90}Y microspheres in tumor deposition.

Secondly, this study is retrospective and the use of the ARC instead of a standard microcatheter was not randomized but left to the decision of the interventional radiologist.

In the future, controlled prospective trials are needed to investigate the effect of ARC in tumor response and survival after ^{90}Y radioembolization. Moreover, the changes in tumor targeting using ARC are not clearly understood and require more experiments with fluid particle models, using either ex vivo or mathematical models.

In conclusion, our results support the use of ARC to improve tumor targeting in ^{90}Y- radioembolization using resin microspheres. ARC impacts the risk-benefit ratio during a procedure of ^{90}Y microspheres infusion, by decreasing the risk of extrahepatic deposition as previously known, but also by improving the targeting efficiency. In addition, In addition, as shown by Morshedi et al., ARC may be a

cost-effective alternative to standard end–hole catheter, reducing the time of the procedure and the use of coil-embolization (35).

References

1. Strigari L, Sciuto R, Rea S, Carpanese L, Pizzi G, Soriani A, et al. Efficacy and toxicity related to treatment of hepatocellular carcinoma with 90Y-SIR spheres: radiobiologic considerations. J Nucl Med. 2010;51(9):1377-85.
2. van den Hoven AF, Prince JF, Samim M, Arepally A, Zonnenberg BA, Lam MG, et al. Posttreatment PET-CT-confirmed intrahepatic radioembolization performed without coil embolization, by using the antireflux Surefire Infusion System. Cardiovasc Intervent Radiol. 2014;37(2):523-8.
3. Arepally A, Chomas J, Kraitchman D, Hong K. Quantification and reduction of reflux during embolotherapy using an antireflux catheter and tantalum microspheres: ex vivo analysis. J Vasc Interv Radiol. 2013;24(4):575-80.
4. Rose SC, Kikolski SG, Chomas JE. Downstream hepatic arterial blood pressure changes caused by deployment of the surefire antireflux expandable tip. Cardiovasc Intervent Radiol. 2013;36(5):1262-9.
5. van den Hoven AF, Prince JF, Bruijnen RC, Verkooijen HM, Krijger GC, Lam MG, et al. Surefire infusion system versus standard microcatheter use during holmium-166 radioembolization: study protocol for a randomized controlled trial. Trials. 2016;17(1):520.
6. Pasciak AS, McElmurray JH, Bourgeois AC, Heidel RE, Bradley YC. The impact of an antireflux catheter on target volume particulate distribution in liver-directed embolotherapy: a pilot study. J Vasc Interv Radiol. 2015;26(5):660-9.
7. van Roekel C, van den Hoven AF, Bastiaannet R, Bruijnen RCG, Braat A, de Keizer B, et al. Use of an anti-reflux catheter to improve tumor targeting for holmium-166 radioembolization-a prospective, within-patient randomized study. Eur J Nucl Med Mol Imaging. 2021;48(5):1658-68.
8. Padia SA, Lewandowski RJ, Johnson GE, Sze DY, Ward TJ, Gaba RC, et al. Radioembolization of Hepatic Malignancies: Background, Quality Improvement Guidelines, and Future Directions. J Vasc Interv Radiol. 2017;28(1):1-15.
9. Giammarile F, Bodei L, Chiesa C, Flux G, Forrer F, Kraeber-Bodere F, et al. EANM procedure guideline for the treatment of liver cancer and liver metastases with intra-arterial radioactive compounds. Eur J Nucl Med Mol Imaging. 2011;38(7):1393-406.

10. Spahr N, Schilling P, Thoduka S, Abolmaali N, Schenk A. Predictive SIRT dosimetry based on a territorial model. EJNMMI Phys. 2017;4(1):25.
11. Cremonesi M, Chiesa C, Strigari L, Ferrari M, Botta F, Guerriero F, et al. Radioembolization of hepatic lesions from a radiobiology and dosimetric perspective. Front Oncol. 2014;4:210.
12. Dewaraja YK, Devasia T, Kaza RK, Mikell JK, Owen D, Roberson PL, et al. Prediction of Tumor Control in (90)Y Radioembolization by Logit Models with PET/CT-Based Dose Metrics. J Nucl Med. 2020;61(1):104-11.
13. euratom Ecd. Basic safety standards for protection against the dangers arising from exposure to ionising radiation and repealing Directives 89/618/Euratom, 90/641/Euratom, 96/29/Euratom, 97/43/Euratom and 2003/122/Euratom. OJ of the EU 2014;L53;57:1-73.
14. ICRP. Radiological protection in therapy wuth radiopharmaceuticals. Ann ICRP 48. 2019;Publication 140.
15. Hermann AL, Dieudonne A, Ronot M, Sanchez M, Pereira H, Chatellier G, et al. Relationship of Tumor Radiation-absorbed Dose to Survival and Response in Hepatocellular Carcinoma Treated with Transarterial Radioembolization with (90)Y in the SARAH Study. Radiology. 2020;296(3):673-84.
16. Garin E, Tselikas L, Guiu B, Chalaye J, Edeline J, de Baere T, et al. Personalised versus standard dosimetry approach of selective internal radiation therapy in patients with locally advanced hepatocellular carcinoma (DOSISPHERE-01): a randomised, multicentre, open-label phase 2 trial. Lancet Gastroenterol Hepatol. 2020.
17. Irie T, Kuramochi M, Takahashi N. Dense accumulation of lipiodol emulsion in hepatocellular carcinoma nodule during selective balloon-occluded transarterial chemoembolization: measurement of balloon-occluded arterial stump pressure. Cardiovasc Intervent Radiol. 2013;36(3):706-13.
18. van den Hoven AF, Lam MG, Jernigan S, van den Bosch MA, Buckner GD. Innovation in catheter design for intra-arterial liver cancer treatments results in favorable particle-fluid dynamics. J Exp Clin Cancer Res. 2015;34:74.
19. Aramburu J, Anton R, Rivas A, Ramos JC, Sangro B, Bilbao JI. Computational assessment of the effects of the catheter type on particle-hemodynamics during liver radioembolization. J Biomech. 2016;49(15):3705-13.
20. Kennedy AS, Kleinstreuer C, Basciano CA, Dezarn WA. Computer modeling of yttrium-90-microsphere transport in the hepatic arterial tree to improve clinical outcomes. Int J Radiat Oncol Biol Phys. 2010;76(2):631-7.
21. Namasivayam S, Martin DR, Saini S. Imaging of liver metastases: MRI. Cancer Imaging. 2007;7:2-9.
22. Schima W, Kulinna C, Langenberger H, Ba-Ssalamah A. Liver metastases of colorectal cancer: US, CT or MR? Cancer Imaging. 2005;5 Spec No A:S149-56.

23. Aramburu J, Anton R, Rodriguez-Fraile M, Sangro B, Bilbao JI. Computational Fluid Dynamics Modeling of Liver Radioembolization: A Review. Cardiovasc Intervent Radiol. 2021.
24. Kleinstreuer C, Basciano CA, Childress EM, Kennedy AS. A new catheter for tumor targeting with radioactive microspheres in representative hepatic artery systems. Part I: impact of catheter presence on local blood flow and microsphere delivery. J Biomech Eng. 2012;134(5):051004.
25. Van de Wiele C, Maes A, Brugman E, D'Asseler Y, De Spiegeleer B, Mees G, et al. SIRT of liver metastases: physiological and pathophysiological considerations. Eur J Nucl Med Mol Imaging. 2012;39(10):1646-55.
26. Garin E, Rolland Y, Laffont S, Edeline J. Clinical impact of (99m)Tc-MAA SPECT/CT-based dosimetry in the radioembolization of liver malignancies with (90)Y-loaded microspheres. Eur J Nucl Med Mol Imaging. 2016;43(3):559-75.
27. Aramburu J, Anton R, Rivas A, Ramos JC, Sangro B, Bilbao JI. Computational particle-haemodynamics analysis of liver radioembolization pretreatment as an actual treatment surrogate. Int J Numer Method Biomed Eng. 2017;33(2).
28. Aramburu J, Anton R, Rivas A, Ramos JC, Sangro B, Bilbao JI. Liver Radioembolization: An Analysis of Parameters that Influence the Catheter-Based Particle-Delivery via CFD. Curr Med Chem. 2020;27(10):1600-15.
29. Lhommel R, van Elmbt L, Goffette P, Van den Eynde M, Jamar F, Pauwels S, et al. Feasibility of 90Y TOF PET-based dosimetry in liver metastasis therapy using SIR-Spheres. Eur J Nucl Med Mol Imaging. 2010;37(9):1654-62.
30. Gates VL, Esmail AA, Marshall K, Spies S, Salem R. Internal pair production of 90Y permits hepatic localization of microspheres using routine PET: proof of concept. J Nucl Med. 2011;52(1):72-6.
31. Jadoul A, Bernard C, Lovinfosse P, Gerard L, Lilet H, Cornet O, et al. Comparative dosimetry between (99m)Tc-MAA SPECT/CT and (90)Y PET/CT in primary and metastatic liver tumors. Eur J Nucl Med Mol Imaging. 2019.
32. Gnesin S, Canetti L, Adib S, Cherbuin N, Silva Monteiro M, Bize P, et al. Partition Model-Based 99mTc-MAA SPECT/CT Predictive Dosimetry Compared with 90Y TOF PET/CT Posttreatment Dosimetry in Radioembolization of Hepatocellular Carcinoma: A Quantitative Agreement Comparison. J Nucl Med. 2016;57(11):1672-8.
33. Knesaurek K, Tuli A, Pasik SD, Heiba S, Kostakoglu L. Quantitative comparison of pre-therapy (99m)Tc-macroaggregated albumin SPECT/CT and post-therapy PET/MR studies of patients who have received intra-arterial radioembolization therapy with (90)Y microspheres. Eur J Radiol. 2018;109:57-61.
34. Kafrouni M, Allimant C, Fourcade M, Vauclin S, Guiu B, Mariano-Goulart D, et al. Analysis of differences between (99m)Tc-MAA SPECT- and (90)Y-

microsphere PET-based dosimetry for hepatocellular carcinoma selective internal radiation therapy. EJNMMI Res. 2019;9(1):62.
35. Morshedi MM, Bauman M, Rose SC, Kikolski SG. Yttrium-90 resin microsphere radioembolization using an antireflux catheter: an alternative to traditional coil embolization for nontarget protection. Cardiovasc Intervent Radiol. 2015;38(2):381-8.

8- Perspectives

8.1 Personalized dosimetry in SIRT: activity planning optimization with MAA SPECT/CT

Tumor dosimetry is a predictive tool of SIRT efficiency. Previous data have demonstrated a correlation between tumor absorbed dose and radiological response (1-3); indeed, a high tumor absorbed dose is associated with a high probability of tumor control. In addition, a multitude of clinical data demonstrating strong correlation between tumor absorbed dose, radiological response and survival of HCC patients are currently available. Table 1 summarizes the main studies reporting a tumor absorbed dose threshold associated with SIRT efficiency in HCC. Studies comparing glass to resin microspheres have indicated that the tumor absorbed dose cut-off is usually two-fold, which is explained by their different physical and radioactive properties (4, 5).

To improve the clinical results of RE, the activity prescription can be more personalized and optimized to reach higher tumor absorbed doses. As previously described, the recommended activity prescription is calculated using semi-empirical methods. While these methods are safe, they can induce suboptimal absorbed doses to tumors(15). A recent prospective study confirmed the clinical benefits of performing multi-compartmental dosimetry (known as 'the partition model') (16). In the partition model, activity planning is based upon the MAA distribution in the different compartments (Figure 1), simulating an absorbed

dose under the threshold of toxicity for the healthy liver and above the efficacy threshold for the tumor(s).

Table 1: Main studies reporting threshold absorbed doses correlated with clinical outcome in HCC.

Study	SIRT (type)	Nb of patients	Nb of tumors	Dosimetry performed with	Criteria for radiological response assessment	TD threshold for radiological response	Median PFS above and under the TD threshold	Median OS above and under the TD threshold
Garin et al. 2011 (6)	glass	36	58	MAA SPECT/CT	EASL	205 Gy (Se: 100%, Sp : 75%)	14 mo *vs* 5.2 mo*	18 mo *vs* 9 mo*
Chiesa et al. 2011 (7)	glass	46	91	MAA SPECT/CT	EASL	257 Gy (Se: 85%, Sp: 70%)	NA	NA
Garin et al. 2017 (8)	glass	85	132	MAA SPECT/CT	EASL	205 Gy (Se: 98%, Sp NA)	NA	21 mo *vs* 6.5 mo*
Kappadath et al. 2018 (9)	glass	34	53	^{90}Y SPECT/CT	modified RECIST 1.1	160 Gy (50% response)	NA	NA
Chan et al. 2018 (10)	glass	27	38	^{90}Y PET/CT	modified RECIST 1.1	200 Gy (Se : 66%, Sp: 100%)	NA	NA
d'Abadie et al. 2021 (11)	glass	26	73	^{90}Y PET/CT	modified RECIST 1.1	118 Gy (Se: 93%, Sp : 75%)	5.5 mo *vs* 1.8 mo*	14.6 mo *vs* 5.5 mo*
Nodari et al. 2021 (12)	glass	23	NA	^{90}Y PET/CT	NA	156 Gy (Se & Sp NA)	NA	23 mo *vs* 14 mo*
Allimant et	resin	38	42	^{90}Y PET/CT	modified RECIST 1.1	61 Gy (Se: 76%,	12.1 mo *vs* 6.3	NA

al 2018 (13)						Sp : 75%)	mo*+	
Hermann et al. 2020 (2)	resin	121	NA	MAA SPECT/CT	RECIST 1.1	100 Gy (72% response)	NA	14.1 mo *vs* 6.1 mo*
d'Abadie et al. 2021 (11)	resin	19	60	^{90}Y PET/CT	modified RECIST 1.1	61 Gy (Se: 87%, Sp : 64%)	4.6 mo *vs* 1.6 mo*	16 mo *vs* 5.3 mo*
Son et al. 2021 (14)	resin	34	45	MAA SPECT/CT	modified RECIST 1.1	125 Gy (Se: 86%, Sp: 75%)	NA	NA
Nodari et al. 2021 (12)	resin	25	NA	^{90}Y PET/CT	NA	98 Gy (Se & Sp NA)	NA	23 mo *vs* 14 mo*

Nb: number; SIRT: selective internal radiation therapy; EASL: European association for the study of the liver; NA: Not available; TD : Tumor absorbed dose ; Se : sensibility ; Sp : specificity, * statistically significant ; + reported for complete tumor targeting (25 patients)

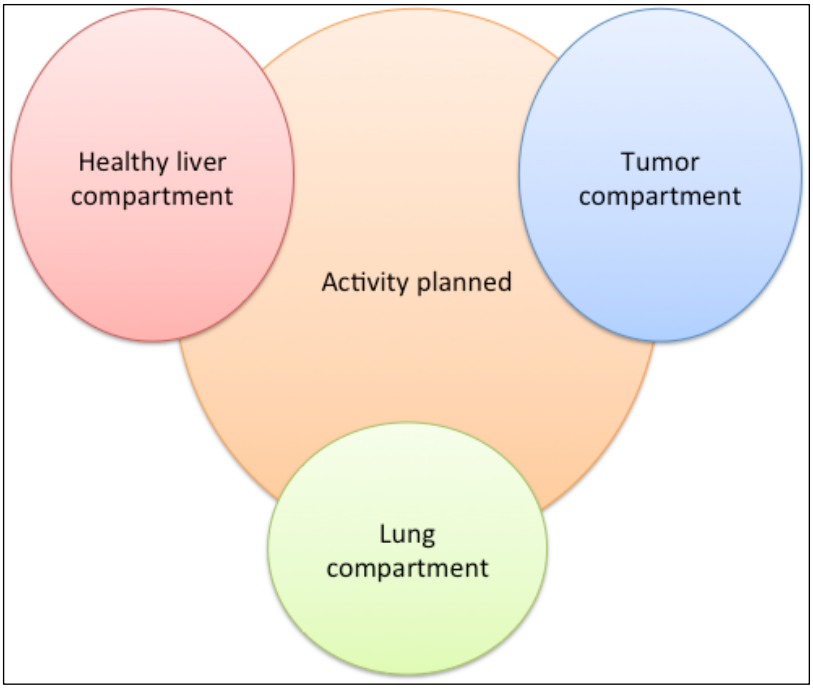

Figure 1: Multi-compartment dosimetry (partition model) using MAA SPECT/CT for activity planning. The absorbed doses in these different compartments can be simulated before treatment and this enables to optimize the activity planned.

The dose to the healthy liver can be accurately predicted with MAA SPECT/CT, controlling the risk of liver toxicity (17). Indeed, an excess of liver radiation can induce liver damage (*i.e*. RE-induced liver disease). The toxicity threshold doses have been well-demonstrated through non-tumoral whole liver dose (reaching 90 Gy for glass microspheres and 40-50 Gy for resin microspheres) (18, 19). As such, with MAA SPECT/CT dosimetry simulating an absorbed dose to the healthy liver under these thresholds, the activity can be planned safely. Moreover, the external beam radiotherapy models have shown that no liver damage can occur if the treated liver volume does not exceed 40% (20). When a small part of the liver volume is targeted by the treatment, the planned activity can be increased for performing a safe radiation segmentectomy. For treatments applied to most of the liver (> 60%), the planned activity can be adjusted to reach the maximal tolerable liver absorbed dose. With this method, the planned activity would be the highest possible and would therefore increase the activity in the tumor compartment to maximize the tumor control probability (Figure 2).

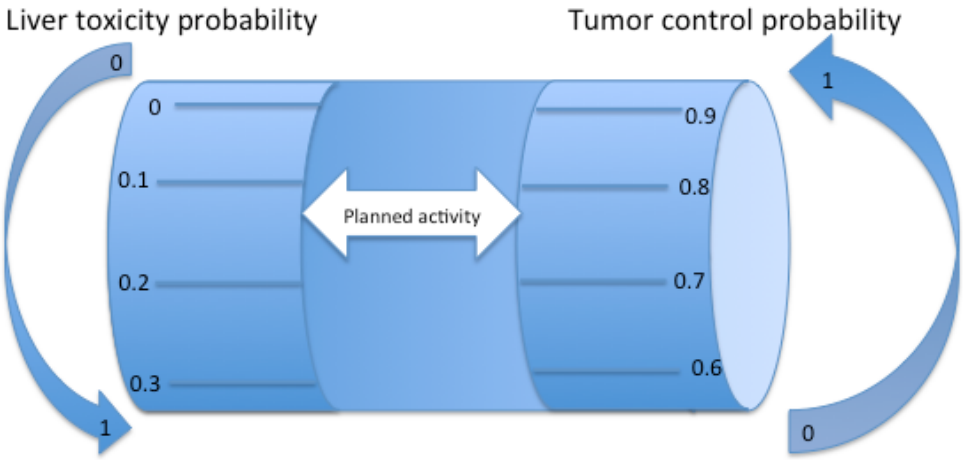

Figure 2: Probability of tumor control and liver toxicity depending on the planned activity.

A recent prospective trial performed using glass microspheres in patients with HCC, mostly with advanced stage disease, demonstrated better outcome achieved with personalized dosimetry and MAA imaging (16). When an approach reaching a maximum dose of 120 Gy to the targeted healthy liver and at least 205 Gy to tumors (> 250 Gy, if possible) was used, the clinical outcome was highly improved, as compared to patients treated with the standard (120 Gy to the targeted liver) dosimetric approach. The main results of this trial are summarized in Table 2. The median activity was increased by 38%, as shown upon comparison of the standard method to this personalized method of activity planning.

Table 2: Main results of the DOSISPHERE- 01 randomized trial (16)

	Personalized dosimetry	Standard dosimetry
Number of patients	28	28
Activity planned (median)	3.6 GBq*	2.6 GBq
Response rate at 3 months (EASL criteria)	71%*	36%
Curative surgery intent after SIRT	36%*	4%
REILD	9%	10%
Overall survival (median)	26.6 mo*	10.7 mo

EASL: European association for the study of the liver; SIRT: selective internal radiation therapy, REILD: radioembolization induced liver disease; * statistically significant

Similarly, in a retrospective study using personalized dosimetry with a whole normal liver dose reaching 40 to 70 Gy (glass microspheres), the median survival was 14.1 mo in HCC patients with portal vein invasion (95% confidence interval (CI): 10.7-17.5 mo) (21). These results were better than expected from previously published data in a similar population treated with a standard dosimetric approach (median: 10.4 mo, 95%CI: 7.2-16.6) (22).

However, using this optimized method of activity planning, patients with risk factors for RE-induced liver disease must be carefully evaluated before treatment

to limit the probability of liver toxicity. For this purpose, ^{99m}Tc–mebrofenin scintigraphy with SPECT/CT can evaluate and quantify the global and regional liver functions and predict the risk of post-radiation liver damage. In patients who undergo major liver resection, the remnant liver uptake of mebrofenin correlated well with the risk of postoperative liver failure (cut-off value: 2.69%/min/m^2) (23). Although this technique is not widely used, it could also be applied to SIRT for evaluating liver function in patients with risk factors (*e.g.*, advanced cirrhosis, large tumor involvement, *etc*.). Indeed, the mebrofenin liver uptake of the non-treated liver was also predictive of RE-induced liver disease in some case series (24-25).

8.2 Personalized dosimetry in SIRT: activity planning optimization with a scout dose

A scout dose consists in simulating the treatment using the radioactive microspheres but with a small activity to avoid a radiation induced organ damage. Regarding ^{166}Ho-PLLA microspheres, a scout dose (maximal activity of 250 MBq) is a safe and interesting alternative to ^{99m} Tc-MAA particles (26). In a multi-compartment dosimetry purpose (Figure 1), this scout dose could be more predictive than MAA dosimetry. Especially, the lung dose (due to hepatopulmonary shunting) was more precisely evaluated with this scout dose

(27). ^{99m} Tc MAA particles overestimate the lung shunt because some small particles (i.e. 10 µm) can pass through the liver capillaries and reach the lungs (28). Conversely, the size of ^{166}Ho-PLLA microspheres is larger on average (chapter 1, Figure 2). Moreover, the intrahepatic liver distribution could also be more accurately predicted with this scout dose using specific SPECT reconstructions (29). In a cohort of patients treated for liver metastases, compared to the real tumor absorbed dose evaluated after therapy, the simulate tumor absorbed dose was more accurately predicted with the ^{166}Ho scout dose (95% C.I, -90 Gy, +105 Gy) as compared to the MAA dose (95% C.I. – 164 Gy, + 197 Gy). However, the feasibility of this liver dosimetry in clinical practice remains questionable. ^{166}Ho radionuclide emits a low abundance of direct gamma photons used for the detection by SPECT systems (7%, window 81 keV). However, multiple gamma radiation of high energy (MeV range) are also emitted, interacting with the patient body and mainly with the lead collimator of the gamma camera (30). Secondary lead x-rays are formed (photoelectric effect) in the 81 keV photopeak detection of the gamma camera, limiting significantly the spatial resolution and the accuracy of a quantitative dosimetry. Moreover, the beta emissions of ^{166}Ho radionuclide interact with the patient and form a high amount of secondary bremsstrahlung x-rays (range 0-1.85 MeV) limiting as well as the spatial resolution and the quantification. Besides, a loss of the spatial resolution is also due to the use of a medium energy collimator during the SPECT acquisition (31). This poor

spatial resolution, using standard reconstruction parameters, could also raise problems for evaluating the extra hepatic deposition during the workup (illustrated in Figure 3).

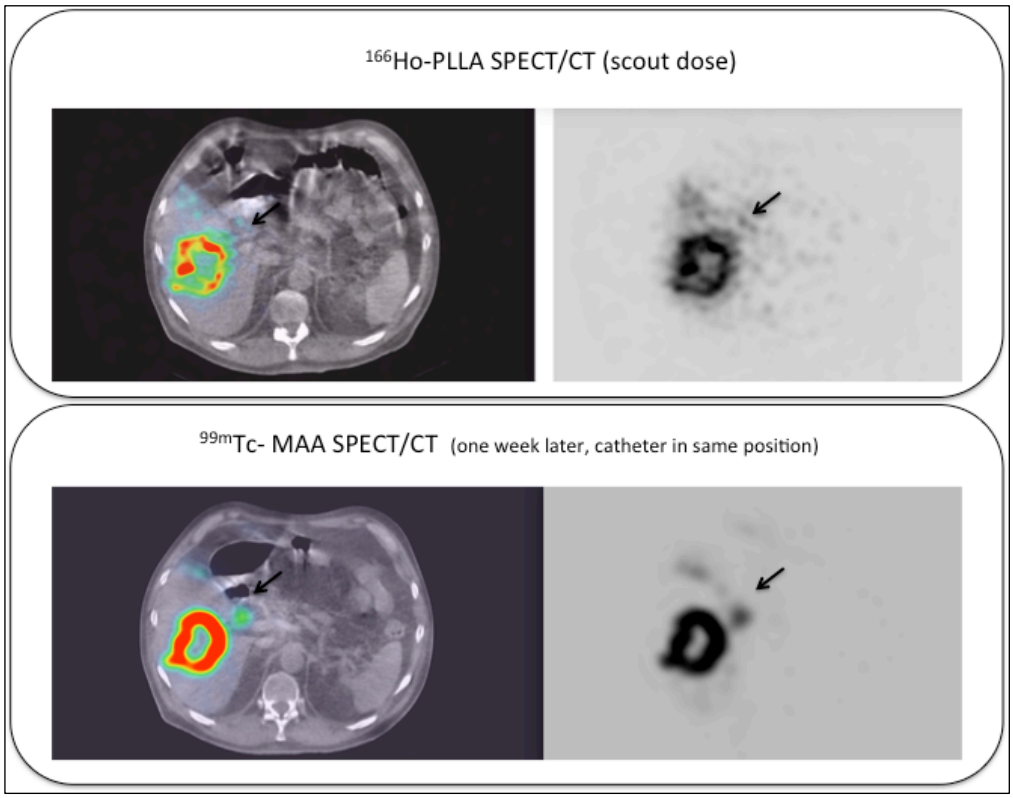

Figure 3: ^{166}Ho SPECT/CT scout dose and ^{99m}Tc MAA SPECT/CT in the same patient (unpublished data). A duodenal uptake (black arrow) was well defined with MAA imaging but hardly visible with ^{166}Ho SPECT/CT due to the lower spatial resolution.

Specific reconstructions algorithms using Monte Carlo simulation were developed to improve the resolution of the SPECT images, and hence the accuracy of

dosimetry estimates (30). However, these reconstruction algorithms involve important computer processing resources and are highly time consuming, not adapted for a routine clinical use.

Very recently, the scout dose concept was also applied to (^{90}Y) resin microspheres using an activity of 0.55 GBq. Preliminary results demonstrated that the tumor to normal liver uptake was better predicted using this scout activity as compared to MAA imaging (32). However, no data are available regarding the safety of this ^{90}Y scout dose.

8.3 Optimization of tumor targeting

Better tumor targeting is highly valuable because it will improve the tumor absorbed dose and effectiveness of the treatment. New microcatheters used in interventional radiology allow for more selective angiography, delivering higher activities in the vicinity of tumors and sparing the healthy liver. Interventional radiologists are able to perform this kind of selective approach more and more, splitting the activity among multiple injections for the different arterial branches of the tumor (33). For this purpose, a cone beam CT can be performed during the liver arteriography for precisely identifying the feeding artery (ies) of a tumor (34). Moreover, the innovative new antireflux catheters can also improve tumor targeting. In our retrospective analysis of neuroendocrine and HCC tumors (chapter 5), the antireflux catheters were found to provide significantly better

tumor targeting than the classic end-hole catheters (35). Some drugs infused during the treatment can also increase the tumor-to-normal liver ratio (i.e. the tumor targeting). The co-infusion of angiotensin II during SIRT was also shown to significantly increase tumor targeting (tumor-to-normal liver ratio × 3) by decreasing the healthy liver arterial flow, while the tumor arterial flow increased (36). However, this effect was short-lived (a few minutes) and rapidly reversed despite the continuous infusion of angiotensin II, due to liver arterial vasodilation triggered by the low arterial flow (*i.e*. a vascular escape mechanism) (37).

For clinical application of SIRT, the arterial vasoconstriction needs to be longer, to facilitate injection of all radioactive microspheres before activation of this opposing effect. Alternative drugs, such as sodium acetate and dopexamine, can induce a longer vasoconstrictive effect in the liver artery (38). These mesenteric vasodilators induce an increase in portal blood flow, resulting in a reflex vasoconstriction of the liver artery (i.e. the hepatic arterial buffer response) (39), an effect that tumors are not susceptible to due to their anarchic vascularization. Hence, the arterial flow would be redirected in tumors preferentially, and the tumor-to-normal liver ratio would be increased. For this purpose, dopexamine seems to be a good candidate. This analogue of dopamine is responsible for vasodilation of the mesenteric arteries, inducing a reduction of the liver arterial flow by a factor four in an animal model (40). Moreover, this drug has a short half-

life and is well tolerated at low infusion rates (41). Future investigations are needed to evaluate this effect more thoroughly.

8.4 Patient selection: good candidates for SIRT

The collective research efforts have provided a good understanding of the factors responsible for treatment ineffectiveness in HCC, helping clinicians to select the best candidates for SIRT. Currently, using tumor dosimetry, MAA imaging can generally select patients who will respond well to SIRT (high tumor uptake and high absorbed dose), or those who will not respond (low tumor uptake, low absorbed dose) (42). The interest of this dosimetry applied to MAA SPECT/CT was confirmed in the recent DOSISPHERE randomized controlled trial (16) and was also well illustrated in a retrospective study of 41 patients treated for advanced HCC with portal vein thrombosis. The overall survival was only 4.3 mo when the tumor absorbed dose was less than 205 Gy and 18.2 mo when at least 205 Gy (glass microspheres) (43). Moreover, patients with portal vein thrombosis and poor targeting *via* MAA imaging had a very poor prognosis.

HCC is a heterogeneous group of tumors with different behaviors; some can be very aggressive, with a tumor doubling time ranging from 3 mo to 1 year (44). [^{18}F]-FDG PET/CT has low sensibility, with a significant uptake in less than 50%-65% of the cases (45). However, data have indicated that HCC tumors with high

FDG uptake are more aggressive, with patients at higher risk of recurrence and shorter survival (46). SIRT is less effective in this population, with a significant reduction of the local control, progression-free survival (PFS) and overall survival (OS) (47, 48). In our study of 22 patients assessed with dual isotope PET/CT (chapter 6), FDG-avid tumors responded as well as others to radiation (chapter 6, graph 1). However, a trend (not statistically significant) to worse PFS and OS was also shown in our patients with FDG-avid tumors (Figure 4).

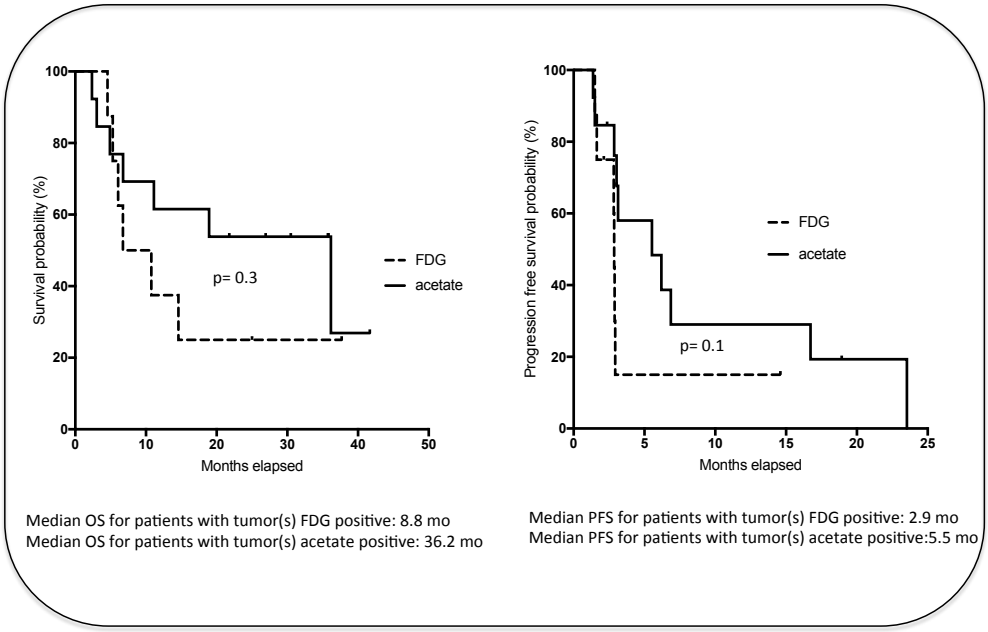

Figure 4: Median overall survival (OS) and progression free survival (PFS) in 22 HCC patients treated by SIRT and assessed at baseline with ^{18}F-FDG and ^{11}C-acetate PET/CT (data of chapter 6).

In advanced HCC, randomized trials have failed to demonstrate a superior PFS and OS in patients treated by RE compared to sorafenib, despite a significant increase of the tumor response rate in the RE arm (Table 1). Loco-regional therapies such as SIRT may be less effective in patients with aggressive HCC tumors, and [^{18}F]-FDG PET/CT could be useful to identify these patients.

Decompensated liver function is also a strong predictor of poor survival. The baseline bilirubin level, the Child-Pugh score and the albumin-bilirubin grade were independent predictors of poor survival in patients treated with SIRT (21, 49, 50). The median overall survival rates reported for advanced HCC patients treated with sorafenib range from 6.5 mo to 14.7 mo (51-54). By comparison, some markers of poor prognosis have been identified in large retrospective studies of advanced HCC patients treated with SIRT (Table 4). Patients with poor performance status (ECOG 2 or more), extrahepatic metastases, portal vein thrombosis extending to the main left/right branch, tumor burden > 50% of the liver volume, and a baseline alteration of the liver function (albumin-bilirubin score of 3 or bilirubin level of 2-3 mg/dL) have reported median survival rates that fall between 4.3 and 8.2 mo (Table 3).

Table 3: Studies reporting factors of poor prognosis in advanced HCC treated by SIRT.

Study	Number of patients	Parameter related to worse prognosis	Median survival (95% CI interval)
Ali et al. (55)	547	ECOG 2	4.3 mo (2.5-7.8)
		Extrahepatic metastases	7.4 mo (6.0-9.0)
		PVT	7.3 mo (6.3-8.0)
Spreafico et al. (21)	120	Bilirubin > 1.2 mg/dl	9.5 mo (8.8-10.2)
		PVT extended to right/left main branch	8.2 mo (5.7-10.8)
		Tumor burden >50% liver volume	6.4 mo (5.2-7.6)
Abouchaleh et al. (56)	185	ECOG 2	2.5 mo (2- 4.6)
		Bilirubin 2-3 mg /dl	5 mo (2.2-9.7)
		PVT extended to right/left main branch	7.7 mo (5.3-10.4)
Antkowiak et al. (49)	541	Bilirubin 2-3 mg/dl	8 mo (6.7-21)
		ALBI grade 3	6.7 mo (5.7-8.8)
Zu et al. (57)	91	CHILD B7	6 mo (4.4-7.6)

PVT: Portal vein thrombosis

Similarly, in patients with colorectal metastases, the clinical factors strongly correlated with worse prognostic after SIRT were evaluated in a large cohort of

patients and included a poor performance status (ECOG 2-3), a large liver involvement (>50%), extra hepatic metastases, prior multiple lines of chemotherapy (2nd line or more) and a baseline alteration of the liver function (58).

In this population of patients, RE will likely be ineffective and potentially toxic and alternative systemic therapies should be suggested.

Conclusion

SIRT is an effective therapy and can significantly improve the outcome of patients. Dosimetry plays a key role in predicting its effectiveness and can be optimized using a personalized method of activity planning (i.e. multi-compartmental dosimetry). Selection of patients based on performance status, liver function, tumor characteristics and tumor targeting as assessed by MAA imaging can also improve the clinical benefit of SIRT. Moreover, if the post-therapy 90Y PET/CT shows poor dosimetric results, the information should be available in real time to the clinician. This would allow to adapt the treatment, for instance to shift to a systemic therapy, before the classical radiological assessment.

References

1. Strigari L, Sciuto R, Rea S, Carpanese L, Pizzi G, Soriani A, et al. Efficacy and toxicity related to treatment of hepatocellular carcinoma with 90Y-SIR spheres: radiobiologic considerations. J Nucl Med. 2010;51(9):1377-85.
2. Hermann AL, Dieudonne A, Ronot M, Sanchez M, Pereira H, Chatellier G, et al. Relationship of Tumor Radiation-absorbed Dose to Survival and Response in Hepatocellular Carcinoma Treated with Transarterial Radioembolization with (90)Y in the SARAH Study. Radiology. 2020;296(3):673-84.
3. Dewaraja YK, Devasia T, Kaza RK, Mikell JK, Owen D, Roberson PL, et al. Prediction of Tumor Control in (90)Y Radioembolization by Logit Models with PET/CT-Based Dose Metrics. J Nucl Med. 2020;61(1):104-11.
4. d'Abadie P, Hesse M, Jamar F, Lhommel R, Walrand S. (90)Y TOF-PET based EUD reunifies patient survival prediction in resin and glass microspheres radioembolization of HCC tumours. Phys Med Biol. 2018;63(24):245010.
5. d'Abadie P, Hesse M, Louppe A, Lhommel R, Walrand S, Jamar F. Microspheres Used in Liver Radioembolization: From Conception to Clinical Effects. Molecules. 2021;26(13).
6. Garin E, Lenoir L, Rolland Y, Edeline J, Mesbah H, Laffont S, et al. Dosimetry based on 99mTc-macroaggregated albumin SPECT/CT accurately predicts tumor response and survival in hepatocellular carcinoma patients treated with 90Y-loaded glass microspheres: preliminary results. J Nucl Med. 2012;53(2):255-63.
7. Chiesa C, Maccauro M, Romito R, Spreafico C, Pellizzari S, Negri A, et al. Need, feasibility and convenience of dosimetric treatment planning in liver selective internal radiation therapy with (90)Y microspheres: the experience of the National Tumor Institute of Milan. Q J Nucl Med Mol Imaging. 2011;55(2):168-97.
8. Garin E, Rolland Y, Pracht M, Le Sourd S, Laffont S, Mesbah H, et al. High impact of macroaggregated albumin-based tumour dose on response and overall survival in hepatocellular carcinoma patients treated with (90) Y-loaded glass microsphere radioembolization. Liver Int. 2017;37(1):101-10.
9. Kappadath SC, Mikell J, Balagopal A, Baladandayuthapani V, Kaseb A, Mahvash A. Hepatocellular Carcinoma Tumor Dose Response After (90)Y-radioembolization With Glass Microspheres Using (90)Y-SPECT/CT-Based Voxel Dosimetry. Int J Radiat Oncol Biol Phys. 2018;102(2):451-61.
10. Chan KT, Alessio AM, Johnson GE, Vaidya S, Kwan SW, Monsky W, et al. Prospective Trial Using Internal Pair-Production Positron Emission Tomography to Establish the Yttrium-90 Radioembolization Dose Required for Response of Hepatocellular Carcinoma. Int J Radiat Oncol Biol Phys. 2018;101(2):358-65.
11. d'Abadie P, Walrand S, Hesse M, Annet L, Borbath I, Van den Eynde M, et al. Prediction of tumor response and patient outcome after radioembolization of

hepatocellular carcinoma using 90Y-PET-computed tomography dosimetry. Nucl Med Commun. 2021.
12. Nodari G, Popoff R, Riedinger JM, Lopez O, Pellegrinelli J, Dygai-Cochet I, et al. Impact of contouring methods on pre-treatment and post-treatment dosimetry for the prediction of tumor control and survival in HCC patients treated with selective internal radiation therapy. EJNMMI Res. 2021;11(1):24.
13. Allimant C, Kafrouni M, Delicque J, Ilonca D, Cassinotto C, Assenat E, et al. Tumor Targeting and Three-Dimensional Voxel-Based Dosimetry to Predict Tumor Response, Toxicity, and Survival after Yttrium-90 Resin Microsphere Radioembolization in Hepatocellular Carcinoma. J Vasc Interv Radiol. 2018;29(12):1662-70 e4.
14. Son MH, Ha LN, Bang MH, Bae S, Giang DT, Thinh NT, et al. Diagnostic and prognostic value of (99m)Tc-MAA SPECT/CT for treatment planning of (90)Y-resin microsphere radioembolization for hepatocellular carcinoma: comparison with planar image. Sci Rep. 2021;11(1):3207.
15. Kafrouni M, Allimant C, Fourcade M, Vauclin S, Delicque J, Ilonca AD, et al. Retrospective Voxel-Based Dosimetry for Assessing the Ability of the Body-Surface-Area Model to Predict Delivered Dose and Radioembolization Outcome. J Nucl Med. 2018;59(8):1289-95.
16. Garin E, Tselikas L, Guiu B, Chalaye J, Edeline J, de Baere T, et al. Personalised versus standard dosimetry approach of selective internal radiation therapy in patients with locally advanced hepatocellular carcinoma (DOSISPHERE-01): a randomised, multicentre, open-label phase 2 trial. Lancet Gastroenterol Hepatol. 2021;6(1):17-29.
17. d'Abadie P, Walrand S, Hesse M, Amini N, Lhommel R, Sawadogo K, et al. Accurate non-tumoral 99mTc-MAA absorbed dose prediction to plan optimized activities in liver radioembolization using resin microspheres. Phys Med. 2021;89:250-7.
18. Garin E, Palard X, Rolland Y. Personalised Dosimetry in Radioembolisation for HCC: Impact on Clinical Outcome and on Trial Design. Cancers (Basel). 2020;12(6).
19. Chiesa C, Mira M, Bhoori S, Bormolini G, Maccauro M, Spreafico C, et al. Radioembolization of hepatocarcinoma with (90)Y glass microspheres: treatment optimization using the dose-toxicity relationship. Eur J Nucl Med Mol Imaging. 2020;47(13):3018-32.
20. Chiesa C, Sjogreen-Gleisner K, Walrand S, Strigari L, Flux G, Gear J, et al. EANM dosimetry committee series on standard operational procedures: a unified methodology for (99m)Tc-MAA pre- and (90)Y peri-therapy dosimetry in liver radioembolization with (90)Y microspheres. EJNMMI Phys. 2021;8(1):77.
21. Spreafico C, Sposito C, Vaiani M, Cascella T, Bhoori S, Morosi C, et al. Development of a prognostic score to predict response to Yttrium-90

radioembolization for hepatocellular carcinoma with portal vein invasion. J Hepatol. 2018;68(4):724-32.
22. Salem R, Lewandowski RJ, Mulcahy MF, Riaz A, Ryu RK, Ibrahim S, et al. Radioembolization for hepatocellular carcinoma using Yttrium-90 microspheres: a comprehensive report of long-term outcomes. Gastroenterology. 2010;138(1):52-64.
23. de Graaf W, van Lienden KP, Dinant S, Roelofs JJ, Busch OR, Gouma DJ, et al. Assessment of future remnant liver function using hepatobiliary scintigraphy in patients undergoing major liver resection. J Gastrointest Surg. 2010;14(2):369-78.
24. Braat M, de Jong HW, Seinstra BA, Scholten MV, van den Bosch M, Lam M. Hepatobiliary scintigraphy may improve radioembolization treatment planning in HCC patients. EJNMMI Res. 2017;7(1):2.
25. Bennink RJ, Cieslak KP, van Delden OM, van Lienden KP, Klumpen HJ, Jansen PL, et al. Monitoring of Total and Regional Liver Function after SIRT. Front Oncol. 2014;4:152.
26. Braat A, Prince JF, van Rooij R, Bruijnen RCG, van den Bosch M, Lam M. Safety analysis of holmium-166 microsphere scout dose imaging during radioembolisation work-up: A cohort study. Eur Radiol. 2018;28(3):920-8.
27. Prince JF, van Rooij R, Bol GH, de Jong HW, van den Bosch MA, Lam MG. Safety of a Scout Dose Preceding Hepatic Radioembolization with 166Ho Microspheres. J Nucl Med. 2015;56(6):817-23.
28. Chiesa C, Maccauro M. (166)Ho microsphere scout dose for more accurate radioembolization treatment planning. Eur J Nucl Med Mol Imaging. 2020;47(4):744-7.
29. Smits MLJ, Dassen MG, Prince JF, Braat A, Beijst C, Bruijnen RCG, et al. The superior predictive value of (166)Ho-scout compared with (99m)Tc-macroaggregated albumin prior to (166)Ho-microspheres radioembolization in patients with liver metastases. Eur J Nucl Med Mol Imaging. 2020;47(4):798-806.
30. Elschot M, Smits ML, Nijsen JF, Lam MG, Zonnenberg BA, van den Bosch MA, et al. Quantitative Monte Carlo-based holmium-166 SPECT reconstruction. Med Phys. 2013;40(11):112502.
31. Elschot M, Nijsen JF, Dam AJ, de Jong HW. Quantitative evaluation of scintillation camera imaging characteristics of isotopes used in liver radioembolization. PLoS One. 2011;6(11):e26174.
32. kokabi N. CB, Brandon D., Bercu A., Sethi I., Mircea C. Accuracy of scout dose Y90 liver biodistribution for personalized treatment planning of Y90 radioembolization of hepatocellular carcinoma: interim analysis of a prospective clinical trial. SIR 2021 annual scientific meeting, abstract book, Abstract No 4
. 2021.

33. Tong AK, Kao YH, Too CW, Chin KF, Ng DC, Chow PK. Yttrium-90 hepatic radioembolization: clinical review and current techniques in interventional radiology and personalized dosimetry. Br J Radiol. 2016;89(1062):20150943.
34. Louie JD, Kothary N, Kuo WT, Hwang GL, Hofmann LV, Goris ML, et al. Incorporating cone-beam CT into the treatment planning for yttrium-90 radioembolization. J Vasc Interv Radiol. 2009;20(5):606-13.
35. d'Abadie P, Walrand S, Goffette P, Amini N, Maanen AV, Lhommel R, et al. Antireflux catheter improves tumor targeting in liver radioembolization with resin microspheres. Diagn Interv Radiol. 2021;27(6):768-73.
36. Sasaki Y, Imaoka S, Hasegawa Y, Nakano S, Ishikawa O, Ohigashi H, et al. Changes in distribution of hepatic blood flow induced by intra-arterial infusion of angiotensin II in human hepatic cancer. Cancer. 1985;55(2):311-6.
37. Macedo MP, Lautt WW. Shear-induced modulation of vasoconstriction in the hepatic artery and portal vein by nitric oxide. Am J Physiol. 1998;274(2):G253-60.
38. Walrand S, Hesse M, d'Abadie P, Jamar F. Hepatic Arterial Buffer Response in Liver Radioembolization and Potential Use for Improved Cancer Therapy. Cancers (Basel). 2021;13(7).
39. Lautt WW. Hepatic Circulation: Physiology and Pathophysiology. Colloquium Series on Integrated Systems Physiology: From Molecule to Function to Disease. San Rafael (CA)2009.
40. Biro GP, Douglas JR, Keon WJ, Taichman GC. Changes in regional blood flow distribution induced by infusions of dopexamine hydrochloride or dobutamine in anesthetized dogs. Am J Cardiol. 1988;62(5):30C-6C.
41. Fitton A, Benfield P. Dopexamine hydrochloride. A review of its pharmacodynamic and pharmacokinetic properties and therapeutic potential in acute cardiac insufficiency. Drugs. 1990;39(2):308-30.
42. Levillain H, Bagni O, Deroose CM, Dieudonne A, Gnesin S, Grosser OS, et al. International recommendations for personalised selective internal radiation therapy of primary and metastatic liver diseases with yttrium-90 resin microspheres. Eur J Nucl Med Mol Imaging. 2021.
43. Garin E, Rolland Y, Edeline J, Icard N, Lenoir L, Laffont S, et al. Personalized dosimetry with intensification using 90Y-loaded glass microsphere radioembolization induces prolonged overall survival in hepatocellular carcinoma patients with portal vein thrombosis. J Nucl Med. 2015;56(3):339-46.
44. Rich NE, John BV, Parikh ND, Rowe I, Mehta N, Khatri G, et al. Hepatocellular Carcinoma Demonstrates Heterogeneous Growth Patterns in a Multicenter Cohort of Patients With Cirrhosis. Hepatology. 2020;72(5):1654-65.
45. Sacks A, Peller PJ, Surasi DS, Chatburn L, Mercier G, Subramaniam RM. Value of PET/CT in the management of primary hepatobiliary tumors, part 2. AJR Am J Roentgenol. 2011;197(2):W260-5.

46. Sun DW, An L, Wei F, Mu L, Shi XJ, Wang CL, et al. Prognostic significance of parameters from pretreatment (18)F-FDG PET in hepatocellular carcinoma: a meta-analysis. Abdom Radiol (NY). 2016;41(1):33-41.
47. Abuodeh Y, Naghavi AO, Ahmed KA, Venkat PS, Kim Y, Kis B, et al. Prognostic value of pre-treatment F-18-FDG PET-CT in patients with hepatocellular carcinoma undergoing radioembolization. World J Gastroenterol. 2016;22(47):10406-14.
48. Jreige M, Mitsakis P, Van Der Gucht A, Pomoni A, Silva-Monteiro M, Gnesin S, et al. (18)F-FDG PET/CT predicts survival after (90)Y transarterial radioembolization in unresectable hepatocellular carcinoma. Eur J Nucl Med Mol Imaging. 2017;44(7):1215-22.
49. Antkowiak M, Gabr A, Das A, Ali R, Kulik L, Ganger D, et al. Prognostic Role of Albumin, Bilirubin, and ALBI Scores: Analysis of 1000 Patients with Hepatocellular Carcinoma Undergoing Radioembolization. Cancers (Basel). 2019;11(6).
50. Mohammadi H, Abuodeh Y, Jin W, Frakes J, Friedman M, Biebel B, et al. Using the Albumin-Bilirubin (ALBI) grade as a prognostic marker for radioembolization of hepatocellular carcinoma. J Gastrointest Oncol. 2018;9(5):840-6.
51. Llovet JM, Ricci S, Mazzaferro V, Hilgard P, Gane E, Blanc JF, et al. Sorafenib in advanced hepatocellular carcinoma. N Engl J Med. 2008;359(4):378-90.
52. Cheng AL, Kang YK, Chen Z, Tsao CJ, Qin S, Kim JS, et al. Efficacy and safety of sorafenib in patients in the Asia-Pacific region with advanced hepatocellular carcinoma: a phase III randomised, double-blind, placebo-controlled trial. Lancet Oncol. 2009;10(1):25-34.
53. Yau T, Park JW, Finn RS, Cheng AL, Mathurin P, Edeline J, et al. Nivolumab versus sorafenib in advanced hepatocellular carcinoma (CheckMate 459): a randomised, multicentre, open-label, phase 3 trial. Lancet Oncol. 2022;23(1):77-90.
54. Cheng AL, Qin S, Ikeda M, Galle PR, Ducreux M, Kim TY, et al. Updated efficacy and safety data from IMbrave150: atezolizumab plus bevacizumab vs. sorafenib for unresectable hepatocellular carcinoma. J Hepatol. 2021.
55. Ali R, Gabr A, Abouchaleh N, Al Asadi A, Mora RA, Kulik L, et al. Survival Analysis of Advanced HCC Treated with Radioembolization: Comparing Impact of Clinical Performance Status Versus Vascular Invasion/Metastases. Cardiovasc Intervent Radiol. 2018;41(2):260-9.
56. Abouchaleh N, Gabr A, Ali R, Al Asadi A, Mora RA, Kallini JR, et al. (90)Y Radioembolization for Locally Advanced Hepatocellular Carcinoma with Portal Vein Thrombosis: Long-Term Outcomes in a 185-Patient Cohort. J Nucl Med. 2018;59(7):1042-8.

57. Zu Q, Schenning RC, Jahangiri Y, Tomozawa Y, Kolbeck KJ, Kaufman JA, et al. Yttrium-90 Radioembolization for BCLC Stage C Hepatocellular Carcinoma Comparing Child-Pugh A Versus B7 Patients: Are the Outcomes Equivalent? Cardiovasc Intervent Radiol. 2020;43(5):721-31.
58. Kennedy A, Cohn M, Coldwell DM, Drooz A, Ehrenwald E, Kaiser A, et al. Updated survival outcomes and analysis of long-term survivors from the MORE study on safety and efficacy of radioembolization in patients with unresectable colorectal cancer liver metastases. J Gastrointest Oncol. 2017;8(4):614-24.

9. Summary and practical applications

In this thesis, we demonstrated the strong correlation between tumor dose and SIRT efficacy. Two dosimetric factors are correlated with clinical efficacy: the mean absorbed dose and the homogeneous distribution of the microspheres in the tumor, as demonstrated by DVH.

First, our data confirmed that the level of absorbed dose was strongly correlated with radiological response, with tumor control and with the patient survival (1, 2). Besides, the correlation between the tumor dose and the response was exponentially asymptotic, meaning that the clinical response can be highly variable within limited differences of doses (complete response to progression). For higher doses, the response tends towards a plateau with a tumor control probability near 100% at the highest tumor absorbed doses (3-5).

Second, the distribution of the microspheres is an essential parameter to predict the clinical efficacy of SIRT. Voxel dosimetry assessed by ^{90}Y PET-CT provided a good analysis of the microsphere distribution at a subcentimetric level. The analysis of DVH allowed defining the intratumoral distribution of the absorbed dose at a voxel level. With a minimal absorbed dose of 40 Gy in 66% of the tumor voxels (D_{66}), we demonstrated an accurate prediction of the radiological response and of the outcome of HCC patients (1). The homogeneous distribution of the microspheres can be assessed more precisely using an other dosimetric

parameter named equivalent uniform dose (EUD). EUD takes into account the distribution of the dose in each voxel, converting the dose into an uniform distribution in the tumor (6). The probability of survival after SIRT was strongly correlated with EUD, using a cutoff of 40 Gy in HCC (7).

This thesis highlighted also the dosimetric differences between resin microspheres (Sir-Sphere®) and glass microspheres (TheraSphere®). The two main differences between these devices are the activity per microsphere (2500 Bq for glass versus only 50 Bq for resin) and the number of microspheres injected in the liver (a few millions for glass versus dozens of millions for resin) (8).Using the mean absorbed dose, the efficacy per gray is twofold for glass compared to resin microspheres (1). However, our data demonstrated a similar efficacy cutoff using the voxel based dose (i.e. D_{66}=40 Gy and EUD= 40 Gy) (1, 7).

Taking into account the heterogeneous distribution of the tumor dose, EUD reunified the efficacy per gray between resin and glass microspheres. Based on our data of 45 patients, EUD can also be estimated multiplying D by an efficacy factor. This efficacy factor was estimated 0.73 for resin microsphere (EUD≈ 0.73D) and 0.36 for glass microspheres (EUD≈ 0.36D). More this efficacy factor tends towards 1 and more the tumor dose distribution is homogeneous. In our data, the efficacy factor for glass microspheres was very low, half less than resin microspheres, meaning that the microsphere distribution was very

heterogeneous. Nevertheless, TheraSphere® stays a very effective treatment as well as Sir-Sphere® (2).

Both treatments can irradiate tumor cells with an efficient homogeneous dose of 40 Gy at minimum, considered also as an efficient dose in EBRT (9). Interestingly, we demonstrated the same efficacy per gray comparing SIRT to EBRT using a voxel dosimetry (5). Besides, a parallel with EBRT can be performed using the linear quadratic model. The survival fraction (SF) to a homogeneous irradiation can be estimated using the HCC cell radiosensitivity (with α= 0.4)(10). With a dose above 40 Gy the survival fraction is almost to 0, i.e. about 10^{-7} (Figure 1). Due to the huge number of cells present in tumor ($\approx 10^{9}$), this corresponds to a TCP of 50% explaining why the 40 Gy cutoff clearly separated responding and not responding patient. However the therapeutic intent cannot be limited to this cutoff, indeed EUD of about 100 Gy is needed to ensure 90% probability to control the tumor. Then, the more important when we analyze DVH is the portion of the tumor volume receiving less than 40Gy, at risk of regrowth.

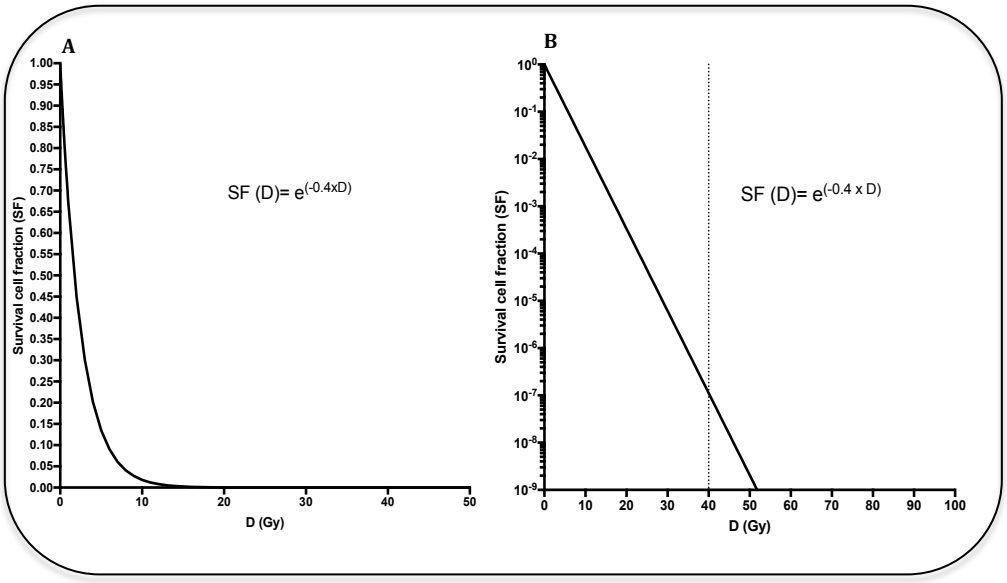

Figure 1 Linear quadratic model demonstrating the survival cell fraction following a dose of radiation (D) using a linear scale (A) and a logarithmic scale (B). $\mathrm{SF}\,(40\ \mathrm{Gy}) \approx 10^{-7}$ meaning that 40 Gy kills 99.99999% of the tumor cells.

Figure 2 illustrates the distribution of the dose in a tumor treated by TheraSphere® where D was calculated to 186 Gy and EUD to 66 Gy. The analysis of the distribution of the voxel dose (Figure 2) demonstrated that some areas of the tumor were covered by a very high absorbed dose (up to 1000 Gy), increasing mechanically the mean absorbed dose. In this tumor, a largest part was covered by an efficient dose (84% of the tumor volume received at least 40 Gy). In comparison, Figure 3 demonstrated an example of DVH of a tumor treated with Sir-Sphere®, having a similar EUD (62 Gy). Compared to figure 2, a similar portion

of the tumor was covered by an efficient dose (77% of the tumor volume received at least 40 Gy) but the voxel dose reached only 288 Gy in maximum.

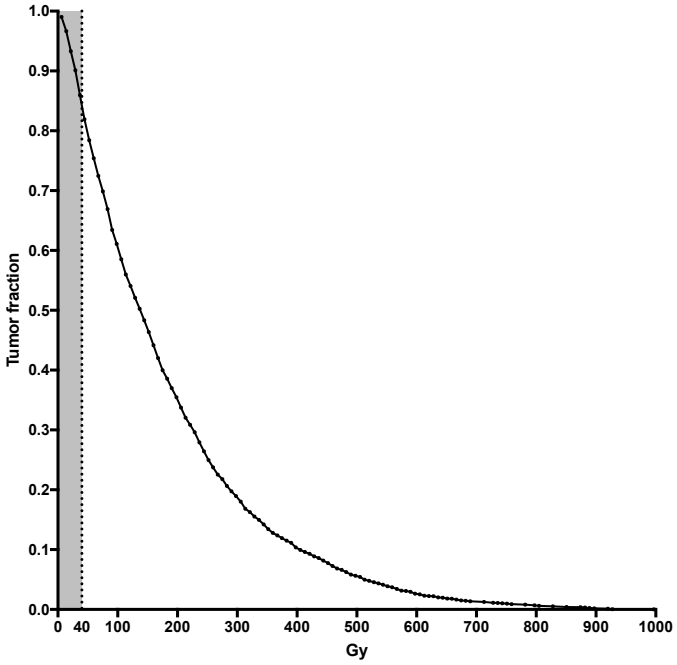

Figure 2: Dose volume histogram for a tumor treated by glass microspheres (D= 186 Gy, EUD= 66 Gy). The area under the curve corresponds to the distribution of the dose in the entire tumor volume. Only a very small part of the tumor volume received a suboptimal dose inferior to 40 Gy (area under the curve colored in grey). Note also that a portion of the tumor received a very high dose (for example, 10% received at least 400 Gy), explaining why the mean absorbed dose is high (i.e. 186 Gy).

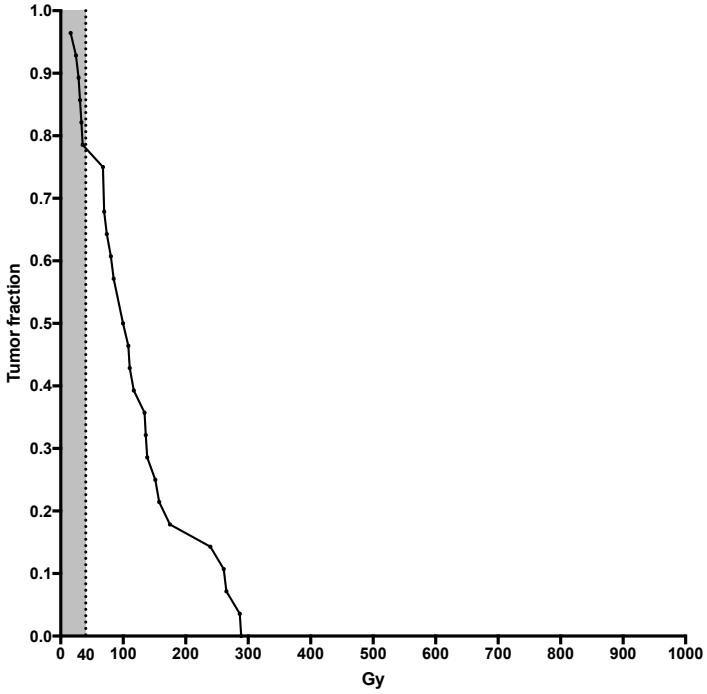

Figure 3: Dose volume histogram for a tumor treated by resin microspheres (D= 121 Gy, EUD= 62 Gy). Only a small part of the tumor volume received a suboptimal dose under 40 Gy (area under the curve colored in grey). Note that the range of voxel doses was limited to a maximum of 286 Gy.

Analyzing the TCP curve previously defined (chapter 5), the cutoff doses for SIRT efficacy can be approximated (Table 1), using TCP 50 (dose for 50% of tumor control) and TCP 100 (dose for 100% of tumor control) (5). Then, the cutoff doses for predicting efficacy (using ^{90}Y PET) must be at minimum 68 Gy for resin microspheres and 137 Gy for glass microspheres (TCP 50). To maximize the probability of tumor control, the tumor absorbed dose must reach 137 Gy for resin and 278 Gy for glass microspheres.

Using glass microspheres, the main limiting factor is the small number of radioactive microspheres injected during the treatment. For small tumors, the heterogeneous distribution of the microspheres is compensated by the very high activity per sphere (2500 Bq) and by the range of the energy deposition of the beta radiation (11 mm in maximum). For large tumors, some cold areas can appear and limit the efficacy of the treatment.

Using resin microspheres, the main limiting factor is the small activity per sphere (50 Bq), limiting the levels of dose in the tumor. Tumors with a low tumor to normal liver uptake can receive an absorbed dose bellow the efficacy cutoffs.

Table 1: Cutoffs for predicting tumor control in HCC using post therapy ^{90}Y PET/CT

TCP	EUD	D_{resin*}	D_{glass*}
50%	40 Gy	55 Gy	110 Gy
90%	100 Gy	137 Gy	278 Gy

* Using an average efficacy factor of 0.73 for resin and 0.36 for glass microspheres.

In addition, this thesis demonstrated how the treatment planning could be optimized. The treatment is simulated using MAA as surrogate to radioactive microspheres. Using the partition model, MAA SPECT/CT can be used for calculating the activity needed for the treatment, simulating tumor and healthy liver absorbed doses. However, a dosimetry based on MAA imaging is questionable because microspheres and MAA particles have different

physicochemical characteristics and because some modifications of the hemodynamic can occur between the arteriographies of simulation and treatment. Our data demonstrated that the tumor dose is not accurately predicted with MAA dosimetry (11). Indeed, the median absolute deviation (difference between estimated MAA dose and ^{90}Y dose) was 49 Gy with a similar under or overestimation of the tumor dose. Nevertheless, MAA dosimetry stays predictive using a cutoff of high tumor absorbed dose. In our data of 47 HCC tumors, a cutoff of minimum 100 Gy was achieved in 28 tumors with MAA imaging and in 31 tumors in realty (^{90}Y PET dosimetry), resulting in small differences (6%). Similarly, a high tumor uptake (T/NTL > 1.5), was accurately predicted in 85% of the treatments. Besides, these results can explain the correlation between the patient survival and the thresholds of tumor absorbed doses previously defined with MAA dosimetry(12, 13).

Our data demonstrated also a very accurate estimate of the healthy liver dose with MAA imaging with a median absolute deviation of only 2 Gy. Thus, the activity planning can be more accurate, performing a simulation on the healthy liver compartment, simulating a dose below the toxicity thresholds. Comparing this model to the classic BSA model, the activity planning can be significantly increased, controlling also the risk of toxicity (11).

In the practice, tumors with a higher MAA uptake than the healthy liver are suitable candidates for SIRT. Selective treatments can be planned reaching the

highest activity as possible to perform a radiation segmentectomy. Lobar or whole liver treatments can be planned using as reference the dose to the healthy liver considering the toxic thresholds doses (11, 14-16). Table 2 summarized the limiting dose to the healthy liver to avoid REILD (whole healthy liver dose) and to avoid a local toxicity such as cholangitis and liver fibrosis (targeted healthy liver dose). Note that the thresholds dose for local toxicity are hypothetical, not yet confirmed by clinical data.

Table 2: Toxicity thresholds for lobar or whole liver treatments

	Glass microspheres	Resin microspheres
Targeted healthy liver dose (30-40% of liver reserve)	120 Gy	70 Gy
Whole healthy liver dose	90 Gy*	40-50 Gy*

* Must be reduced for patient at risk for REILD

In patients with risk factors for liver failure (advanced cirrhosis, large tumor involvement…), ^{99m}Tc-mebrofenin scintigraphy can estimate the global and regional liver function and help to predict the risks (17, 18)

Finally, this thesis highlighted how a better tumor targeting can increase the SIRT efficacy. Using an innovative anti reflux catheter, tumor doses can be significantly increased in hypervascularized tumors, such as HCC and neuroendocrine tumors, hence increasing as well the probability of tumor control(19).

SIRT can be significantly optimized in the future using a personalized dosimetry. Pre-therapy MAA dosimetry can optimize the efficacy and the safety of the treatment. Post-therapy ^{90}Y PET dosimetry, by analyzing the aborbed dose, DVH and EUD, can predict the probability of response and the outcome for the patient. For the clinician, these parameters may be used to anticipate poor responders and propose an alternative therapy in due course.

References

1. d'Abadie P, Walrand S, Hesse M, Annet L, Borbath I, Van den Eynde M, et al. Prediction of tumor response and patient outcome after radioembolization of hepatocellular carcinoma using 90Y-PET-computed tomography dosimetry. Nucl Med Commun. 2021.

2. d’Abadie P. WS, Lhommel R., Hesse M., Borbath I., Jamar F. Optimization of the clinical effectiveness of radioembolization in hepatocellular carcinoma with dosimetry and patient-selection criteria
. Current Oncology. 2022;29:2422-34.
3. Romano C, Mazzaglia S, Maccauro M, Spreafico C, Gabutti A, Maffi G, et al. Radioembolization of Hepatocellular Carcinoma with (90)Y Glass Microspheres: No Advantage of Voxel Dosimetry with Respect to Mean Dose in Dose-Response Analysis with Two Radiological Methods. Cancers (Basel). 2022;14(4).
4. Levillain H, Duran Derijckere I, Marin G, Guiot T, Vouche M, Reynaert N, et al. (90)Y-PET/CT-based dosimetry after selective internal radiation therapy predicts outcome in patients with liver metastases from colorectal cancer. EJNMMI Res. 2018;8(1):60.
5. d’Abadie P WS, Hesse M., Borbath I., Lhommel R, Jamar F. EUD based 90Y-TOF-PET post selective internal radionuclide therapy provides a similar TCP in HCC than observed in EBRT. Preprint. 2022.
6. Jones LC, Hoban PW. Treatment plan comparison using equivalent uniform biologically effective dose (EUBED). Phys Med Biol. 2000;45(1):159-70.
7. d'Abadie P, Hesse M, Jamar F, Lhommel R, Walrand S. (90)Y TOF-PET based EUD reunifies patient survival prediction in resin and glass microspheres radioembolization of HCC tumours. Phys Med Biol. 2018;63(24):245010.
8. d'Abadie P, Hesse M, Louppe A, Lhommel R, Walrand S, Jamar F. Microspheres Used in Liver Radioembolization: From Conception to Clinical Effects. Molecules. 2021;26(13).
9. Hawkins MA, Dawson LA. Radiation therapy for hepatocellular carcinoma: from palliation to cure. Cancer. 2006;106(8):1653-63.
10. Wigg AJ, Palumbo K, Wigg DR. Radiotherapy for hepatocellular carcinoma: systematic review of radiobiology and modeling projections indicate reconsideration of its use. J Gastroenterol Hepatol. 2010;25(4):664-71.
11. d'Abadie P, Walrand S, Hesse M, Amini N, Lhommel R, Sawadogo K, et al. Accurate non-tumoral 99mTc-MAA absorbed dose prediction to plan optimized activities in liver radioembolization using resin microspheres. Phys Med. 2021;89:250-7.
12. Garin E, Rolland Y, Pracht M, Le Sourd S, Laffont S, Mesbah H, et al. High impact of macroaggregated albumin-based tumour dose on response and overall survival in hepatocellular carcinoma patients treated with (90) Y-loaded glass microsphere radioembolization. Liver Int. 2017;37(1):101-10.
13. Hermann AL, Dieudonne A, Ronot M, Sanchez M, Pereira H, Chatellier G, et al. Relationship of Tumor Radiation-absorbed Dose to Survival and Response in Hepatocellular Carcinoma Treated with Transarterial Radioembolization with (90)Y in the SARAH Study. Radiology. 2020;296(3):673-84.

14. Chiesa C, Mira M, Bhoori S, Bormolini G, Maccauro M, Spreafico C, et al. Radioembolization of hepatocarcinoma with (90)Y glass microspheres: treatment optimization using the dose-toxicity relationship. Eur J Nucl Med Mol Imaging. 2020;47(13):3018-32.
15. Levillain H, Bagni O, Deroose CM, Dieudonne A, Gnesin S, Grosser OS, et al. International recommendations for personalised selective internal radiation therapy of primary and metastatic liver diseases with yttrium-90 resin microspheres. Eur J Nucl Med Mol Imaging. 2021.
16. Garin E, Lenoir L, Edeline J, Laffont S, Mesbah H, Poree P, et al. Boosted selective internal radiation therapy with 90Y-loaded glass microspheres (B-SIRT) for hepatocellular carcinoma patients: a new personalized promising concept. Eur J Nucl Med Mol Imaging. 2013;40(7):1057-68.
17. Braat M, de Jong HW, Seinstra BA, Scholten MV, van den Bosch M, Lam M. Hepatobiliary scintigraphy may improve radioembolization treatment planning in HCC patients. EJNMMI Res. 2017;7(1):2.
18. de Graaf W, van Lienden KP, Dinant S, Roelofs JJ, Busch OR, Gouma DJ, et al. Assessment of future remnant liver function using hepatobiliary scintigraphy in patients undergoing major liver resection. J Gastrointest Surg. 2010;14(2):369-78.
19. d'Abadie P, Walrand S, Goffette P, Amini N, Maanen AV, Lhommel R, et al. Antireflux catheter improves tumor targeting in liver radioembolization with resin microspheres. Diagn Interv Radiol. 2021;27(6):768-73.